UNIVERSITY OF CAMBRIDGE

# Exploring Controls on the Flow Dynamics of Devon Ice Cap Using a Basal Friction Inversion

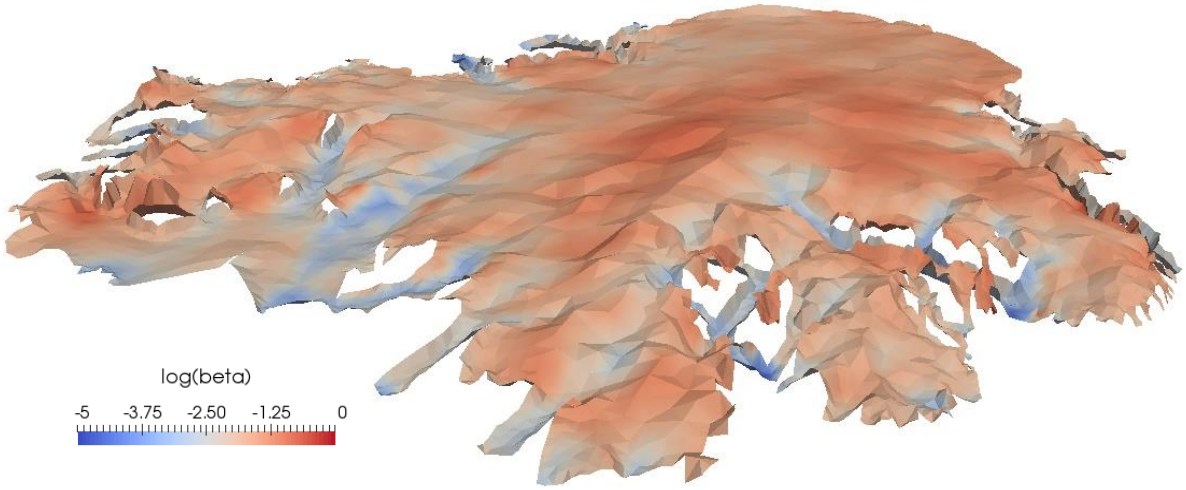


James Marschalek

Thesis submitted 9th June 2017 for the Degree of Master of Philosophy

Scott Polar Research Institute
University of Cambridge

# Abstract

Accurately predicting the future dynamic contribution to mass loss from the ice caps of the High Arctic requires an improved understanding of the basal conditions of these ice bodies. An adjoint method numerical inversion is therefore applied to elucidate the basal and englacial conditions of Devon Ice Cap in the Canadian Arctic Archipelago, which exhibits a variety of changes to flow dynamics in recent years. These include the surge of Southeast1 and Southeast2 Glaciers, which is suggested to be thermally-regulated. A cryo-hydraulic warming feedback may contribute to the acceleration during this surge as an additional source of heat or water is required for the base of sliding areas to reach pressure melting point. During the active phase of the surge, freezing rates increase as the basal temperature gradient increases dramatically, leading to enhanced conductive heat loss which is not countered by additional frictional heating as the weakened till provides less resistance to flow. The termination of this surge could therefore result from water withdrawal from the underlying till without the need for changes to geometry. Glaciers defined as pulsing consistently had lower basal shear stresses when velocities were higher, but different pulses produced different changes to the basal conditions, making it difficult to suggest a mechanism for these events. The cause of the unequal periods of faster and slower flow observed on the Croker Bay Glaciers also remains uncertain. However, changes to water storage in the till layer are far smaller than interannual variability in surface meltwater reaching the bed, suggesting this could play some role in modulating till strength, thus flow speeds. The bed of Belcher Glacier provides very little resistance to flow near the terminus, supporting the hypothesis that its acceleration is a result of the thinning and retreat of the terminus reducing resistive stresses.

# Acknowledgements

Completing this project would not have been possible without support from a number of people. Firstly, I would like to thank my supervisors, Julian Dowdeswell and Poul Christoffersen, for their continued guidance throughout the year. I am also grateful to Toby Benham, whose knowledge and assistance was invaluable when collating the datasets this project required, and Wesley Van Wychen, who kindly provided the velocity data. Thanks are also due to Emily Haggard for keeping me company in SPRI as all the other MPhils gradually disappeared….

Last but not least, I would like to thank Samuel Cook for his help with Elmer/Ice and putting up with me asking questions all year. From an 'unofficial supervisor', I could not have asked for more.

## Contents

## List of Figures

## List of Tables

## Nomenclature

| | |
|---|---|
| $\alpha$ | Surface slope |
| $\alpha_p$ | Power Formulation of $\beta$ |
| $\beta$ | Basal Friction Coefficient |
| $\gamma$ | Lapse Rate |
| $\Gamma$ | Model Domain |
| $\dot{\varepsilon}$ | Shear Strain Rate |
| $\varepsilon$ | Absolute Error |
| $\eta$ | Relative Error |
| $\theta_b$ | Vertical Basal Temperature Gradient |
| $\lambda$ | Regularisation Parameter |
| $\rho_i$ | Ice density |
| $\rho_w$ | Water Density |
| $\bar{\sigma}'_x$ | Longitudinal Deviatoric Stress |
| $\boldsymbol{\sigma}$ | Cauchy Stress Tensor |
| $\tau_d$ | Driving Stress |
| $\tau_b$ | Basal Shear Stress |
| $\tau_f$ | Sediment Shear Strength |
| $\bar{\tau}_{xy}$ | Lateral Shear Stress |
| $\varphi$ | Angle of Internal Friction |
| $A$ | Creep parameter |
| $A_0$ | Prefactor Coefficient |
| $c$ | Apparent Cohesion |
| $C$ | Coefficient of Compressibility |
| $e$ | Void Ratio |
| $e_0$ | Reference Void Ratio |
| $g$ | Gravitational Acceleration |
| $G$ | Geothermal Heat Flux |
| $H$ | Ice Thickness |
| $h_w$ | Water Level Elevation |
| $J_0$ | Cost Function |
| $J_{\mathrm{reg}}$ | Regularisation Function |
| $J_{tot}$ | Total Cost Function |
| $K$ | Conductivity of Ice |

| | |
|---|---|
| $L$ | Specific Latent Heat of Fusion |
| $\dot{m}$ | Basal Melt Rate |
| $m$ | Stress Exponent |
| $n_t$ | Total Porosity |
| $n$ | Creep Exponent |
| $\boldsymbol{n}$ | Normal Unit Vector |
| $N_0$ | Reference Effective Stress |
| $N$ | Effective Normal Stress |
| $P_i$ | Ice Overburden Pressure |
| $P_w$ | Water Pressure |
| $P_0$ | Compressive Normal Stress |
| $Q$ | Activation Energy for Ice Creep |
| $R$ | Universal Gas Constant |
| $S(x)$ | Elevation at Point $x$ |
| $T_i$ | Ice temperature |
| $T_0$ | Ice Melting Point |
| $T_{surf}$ | Mean Surface Air Temperature |
| $T_{sea}$ | Mean Annual Sea-Level Temperature |
| $u_b$ | Basal Velocity |
| $u_H$ | Modelled Horizontal Velocity |
| $u_H^{obs}$ | Observed Horizontal Velocity |
| $\bar{U}$ | Theoretical Centreline Velocity |
| $z_x$ | Ice Depth Below Water Line |

## Values of Constants

| **Constant** | **Symbol** | **Value** |
|---|---|---|
| Ice Density | $\rho_i$ | 917 kg $m^{-3}$ |
| Gravitational Acceleration | $g$ | 9.81 m $s^{-1}$ |
| Creep Exponent | $n$ | 3 |
| Prefactor Coefficient | $A_0$ | 0.09302 $Pa^{-3}$ $a^{-1}$ |
| Universal Gas Constant | $R$ | 8.314 J $mol^{-1}$ $K^{-1}$ |
| Activation Energy for Ice Creep | $Q$ | $7.88\times10^{-4}$ J $mol^{-1}$ |
| Reference Void Ratio | $e_0$ | 0.3 |
| Reference Effective Stress | $N_0$ | 500 kPa |
| Coefficient of Compressibility | $C$ | 0.07 |
| Mean Annual Sea-Level Temperature | $T_{sea}$ | -13.6 °C |
| Lapse Rate | $\gamma$ | 0.0045 K $m^{-1}$ |
| Geothermal Heat Flux | $G$ | 40 mW $m^{-2}$ |
| Angle of Internal Friction | $\varphi$ | 30° |

# 1. Introduction

## 1.1 The Canadian Arctic and Environmental Change

The Arctic is warming at a rate almost twice the global average (Cohen et al., 2014), with surface air temperatures recently increasing at a rate of 1.35 $^{o}$C per decade (Bekryaev et al., 2010). This has led to accelerating mass loss from Arctic glaciers and ice caps, which have contributed nearly one third of recent eustatic sea-level rise (Gardner et al., 2013). The Canadian Arctic Archipelago contains approximately one third of the land ice outside the Greenland and Antarctic ice sheets (Radic and Hock, 2010), and has provided a significant portion of this mass loss. The region lost 61±7 Gt $a^{-1}$ between 2004 and 2009 (Gardner et al., 2011) and this trend seems to have continued until at least 2014 (Millan et al., 2017). The low sensitivity of the Canadian Arctic Archipelago's ice masses to precipitation levels and high sensitivity to air temperatures is likely to result in the region continuing to contribute to sea-level rise in the coming decades and centuries (Gardener et al., 2011), with estimated additions of between 27±12 mm (Radic and Hock, 2011) and 35±24 mm (Lenaerts et al., 2013) by 2100.

However, as with many studies seeking to model the mass balance of ice bodies outside the major ice sheets (e.g. Raper and Braithwaite, 2006; Hock et al., 2009), the estimates of both Lenaerts et al. (2013) and Radic and Hock (2011) neglect the impact that changing ice dynamics may have on mass loss. Although surface mass balance currently dominates mass loss in the Canadian Arctic Archipelago (Gardner et al., 2011; Millan et al., 2017), changes to dynamics should not be overlooked; iceberg calving could account for 30 to 40% of recent mass loss from some ice caps (Dowdeswell et al., 2002; Burgess et al., 2005; Van Wychen et al., 2016, 2017) and the rapid mobilisation of previously slow-flowing ice is possible (McMillan et al., 2014).

Furthermore, measurements of surface velocity suggest that changes to the dynamics of the ice caps of the Canadian Arctic Archipelago are occurring (Van Wychen et al., 2016, 2017). The potential impact of changing flow dynamics on sea-level rise is highly uncertain (Pfeffer et al., 2008); thus, to better constrain estimates of sea-level rise, there is a need to understand the controls on ice dynamics. This will not only improve estimates of future

mass loss from the Canadian Arctic Archipelago, but could provide useful analogies for changes expected to occur on continental-scale ice sheets (McMillan et al., 2014).

The basal conditions of ice bodies influence flow dynamics greatly, but the inherent difficulty of accessing the subglacial environment inhibits direct observations of the processes occurring. Numerical inversion modelling can help overcome this issue by inferring englacial and basal conditions from observed surface velocities. In this project, a numerical inversion using the adjoint method is applied Devon Ice Cap, one of the largest ice caps outside the great ice sheets at ~14,400 $km^2$.

## 1.2 Aims of the Thesis

Despite Devon Ice Cap being one of the most intensively studied ice masses in the circum-polar Arctic (Boon et al., 2010), it has received little attention from the modelling community and its flow dynamics are therefore poorly understood. This thesis addresses that gap, with the overall aim of improving knowledge of how the englacial and basal conditions of the ice cap have changed over the last two decades, and how these changes have impacted ice flow. As the glaciers draining Devon Ice Cap exhibit a variety of changes to flow in recent years, to achieve this aim each behaviour described in the surface velocity mapping of Van Wychen et al. (2017) will be investigated. The specific objectives of this project are therefore to:

- Identify a physically-based mechanism for the recent surge of Southeast1 and Southeast2 Glaciers.
- Determine the basal conditions during the behaviour classified as 'pulsing' by Van Wychen et al. (2017).
- Explain the recent acceleration of Belcher Glacier.
- Investigate the cause of the variable periods of faster and slower flow of the Croker Bay Glaciers.

This improved understanding will ultimately help to separate the contributions of internally driven processes from climatically forced ones, enabling better predictions of how the Devon Ice Cap and similar ice bodies might respond in the future.

## 1.3 Structure of the Thesis

This study will first introduce the changes to the flow of Devon Ice Cap that are known to have taken place (Chapter 2), and the mechanisms of ice flow (Chapter 3). The results of the numerical modelling are then presented in Chapter 5. Chapter 6 discusses the results and considers the insights the work has given into the causes of the changes to dynamics on Devon Ice Cap, before these are summarised in Chapter 7.

# 2. Devon Ice Cap

This chapter introduces the form, mass balance and flow of the Devon Ice Cap, before examining the changes to the ice cap since monitoring began in the 1960s.

## 2.1 Introduction to Devon Island

Devon Island is found in the Qikiqtaaluk region of Nunavut, Canada (Fig. 2.1A). It covers an area of 55,247 $km^2$, making it the fifth largest island in the Canadian Arctic Archipelago. Devon Island is also part of the northern-most subset of the Canadian Arctic Archipelago known as the Queen Elizabeth Islands.

The island was first sighted by Europeans during Robert Bylot and William Baffin's 1616 voyage (Markham, 1881). However, it was not until the 1819-1820 expedition led by William Parry that it was named 'North Devon' after the English county - a name which later evolved into Devon Island. A settlement was present in Dundas Harbour for part of the early $20^{th}$ century, but this was abandoned in 1951 making Devon Island the largest uninhabited island in the world (Mills, 2003).

Geologically, most of Devon Island is comprised of Palaeozoic carbonates overlying the igneous and metamorphic Precambrian bedrock that forms the Canadian Shield (Zhang et al., 2016). In the east of the island where the ~14,400 $km^2$ ice cap is located (Fig. 2.1), glacial erosion has exposed much of this older rock. Biologically, Devon Island is dominated by sparse vegetation and limited wildlife (Bliss, 1977), although there are some more biodiverse areas such as the Truelove Lowlands to the north east of the ice cap (Fig 2.1 B).

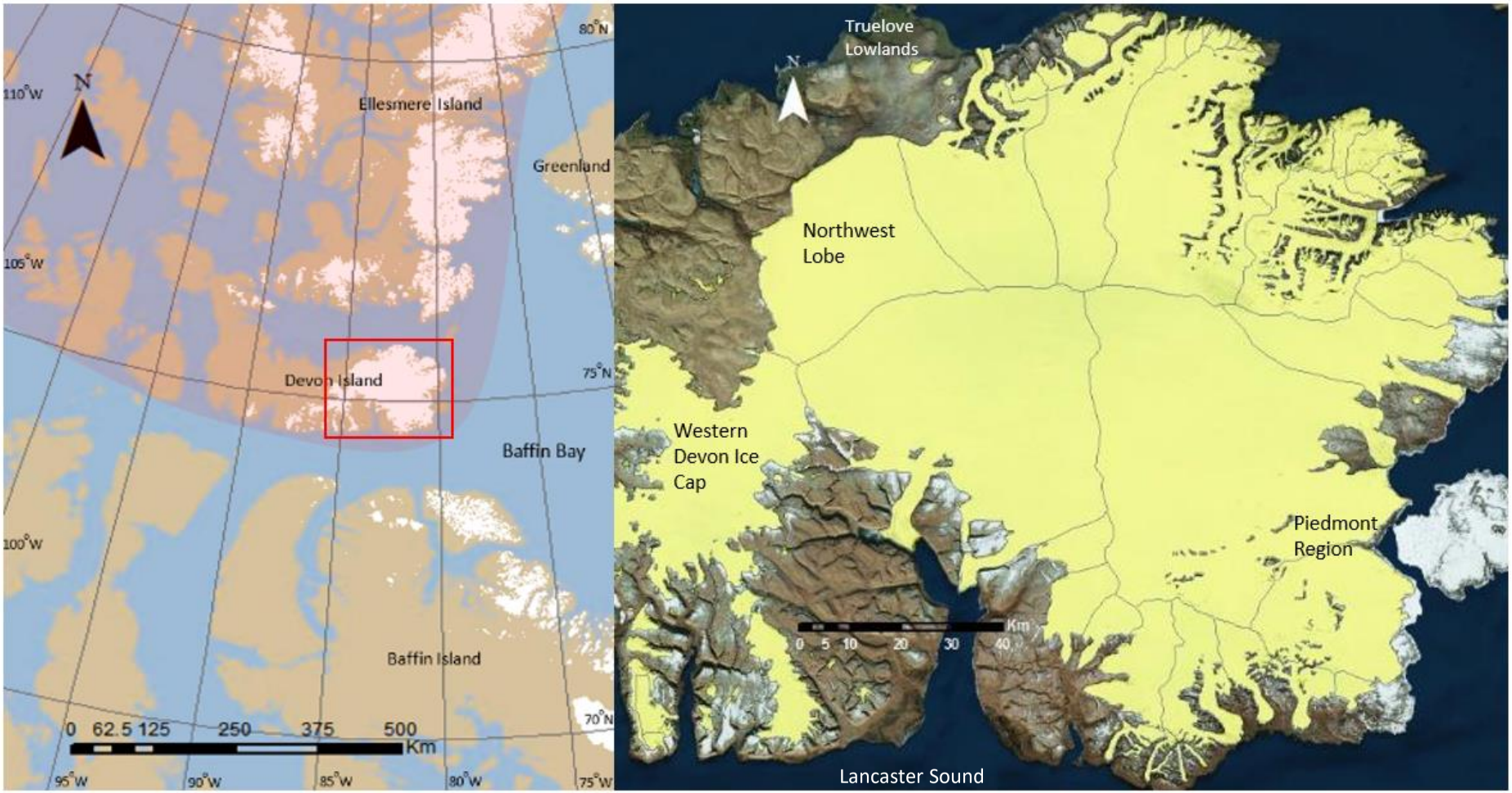


*Figure 2.1. A) Location of Devon Island within northern Nunavut. The shaded region indicates the position of the Queen Elizabeth Islands. The red box corresponds to the area shown in B), which displays the major drainage basins of Devon Ice Cap. The base maps were accessed from ArcGIS online (2017), and the ice extent from the Randolf Glacier Inventory (Pfeffer et al., 2014).*

## 2.2 Climate and Surface Mass Balance

On Devon Island, precipitation levels are very low (<200 mm $a^{-1}$); the island is classed as a polar desert (Gardner and Sharp, 2007). Accumulation rates are highest in the summer and early autumn, and are closely linked to sea ice extent around the QEI and the trajectory of moisture-bearing air masses (Colgan and Sharp, 2008). There is substantial spatial variability in precipitation (Mair et al., 2005), with up to 40 cm water equivalent per year (w.e. $a^{-1}$) in the southeast versus around 11 cm w.e. $a^{-1}$ to the northwest (Koerner, 1966). Much of this additional precipitation in the southeast originates from evaporation in Baffin Bay (Koerner and Russel, 1979). Devon Ice Cap's melt season begins in June or July, with mean monthly temperatures peaking in July and not exceeding 0 $^{o}$C (Boon et al., 2010). Like precipitation, ablation is spatially variable, with greater amounts at lower elevations (Boon et al., 2010) and towards the east due to a lower mean altitude (Burgess et al., 2005).

The mass balance of the ice cap has been relatively well monitored since the 1960s, especially in the northwest sector (Koerner, 2005). The record shows little long-term trend for the first 25 years, but, after 1985, the mass balance is increasingly negative (Koerner, 2005; Sharp et al., 2011; Lenaerts et al., 2013). This has been attributed to rising summer air temperatures (Koerner, 2005; Sharp et al., 2011), as the relatively small ablation and accumulation rates make the mass balance of the ice cap especially sensitive to days when a high degree of melting takes place (Boon et al., 2010). This has resulted in a −0.09 ± 0.29 m $a^{-1}$ average elevation change between 2002 and 2008 (Rinne et al., 2011).

However, it should be noted that elevation changes on Devon Ice Cap are not uniform; although many areas are thinning, some are thickening (Burgess and Sharp, 2008; Rinne et al., 2011). Mass loss also appears to be linked to ice-cap drainage basin size and mean elevation, with smaller, lower basins reducing in extent the most (Burgess and Sharp, 2004). Surface mass balance is currently dominating the overall mass loss from Devon Ice Cap (Boon et al., 2010). However, up to 30% of the volume loss between the 1960s and 2005 may have been lost by iceberg calving, thus this component should not be ignored (Burgess et al., 2005).

## 2.3 Ice Cap Geometry and Velocity Structure

The ice cap reaches a maximum elevation of 1921 m above sea level (m a.s.l.). Ice thicknesses are greatest towards the centre of the ice cap and beneath the major marine-terminating glaciers, reaching a maximum of 880 m (Dowdeswell et al., 2004). As with other large High Arctic ice caps (e.g. Academy of Sciences in Severnaya Zemlya; Dowdeswell et al., 2002), Devon Ice Cap is split into regions of fast and slow-flowing ice (Burgess et al., 2005). The western portion is generally slower-flowing, and slopes gently down to terminate on land in a lobe-like structure (Fig. 2.1B, labelled Northwest Lobe) displaying radial flow (Dowdeswell et al., 2004). In contrast, to the east and north of the major ice divides, mountain ranges and deep, steep-sided valleys constrain the flow of the large tidewater glaciers that drain these regions. The largest of these include Belcher Glacier, Fitzroy Glacier, East5 Glacier and Eastern Glacier (Fig. 2.2).

The southeast of the ice cap also has large tidewater glaciers, primarily Southeast1 Glacier (SE1) and Southeast2 Glacier (SE2) which have a shared terminus and extend inland almost to the ice divide (Burgess et al., 2005). However, unlike their counterparts to the north, the lack of topographic constraint in their lower 20-30 km has resulted in a gently sloping piedmont region with ice thicknesses of <350 m (Dowdeswell et al., 2004). Also of note is the 1960 $km^2$ ice-covered area - sometimes referred to as the southwest arm, the western arm or western Devon Ice Cap - that extends westwards from main ice cap (Fig. 2.1B). Satellite imagery has revealed this to be entirely land-terminating and dynamically separate from the main ice cap (Dowdeswell et al., 2004).

The varying flow behaviours in different regions are likely to be partially a result of the precipitation gradient mentioned in Section 2.2, as the rate of mass turnover in the east is greater than elsewhere on the ice cap (Dowdeswell et al., 2004). Bedrock topography is also likely to contribute to this discrepancy between drainage basins, as the west is underlain by a plateau-like bed which towards the east is cut by steep-sided troughs. These troughs will result in thicker ice (Dowdeswell et al., 2004), thus increased insulation favouring basal melting (Dowdeswell et al., 2004; Van Wychen et al., 2016), alongside accumulations of water due to the lower elevation head (Bennet, 2003). Bedrock topography may also influence the position of the onset of fast flow (Boon et al., 2010), as the ice depth and surface gradient can dramatically increase moving over a bedrock step (Dowdeswell et al.,

2004). Where significant steps are absent, such as for SE1 and SE2 (hereafter collectively referred to as SE1/2), fast flow can extend much further inland.

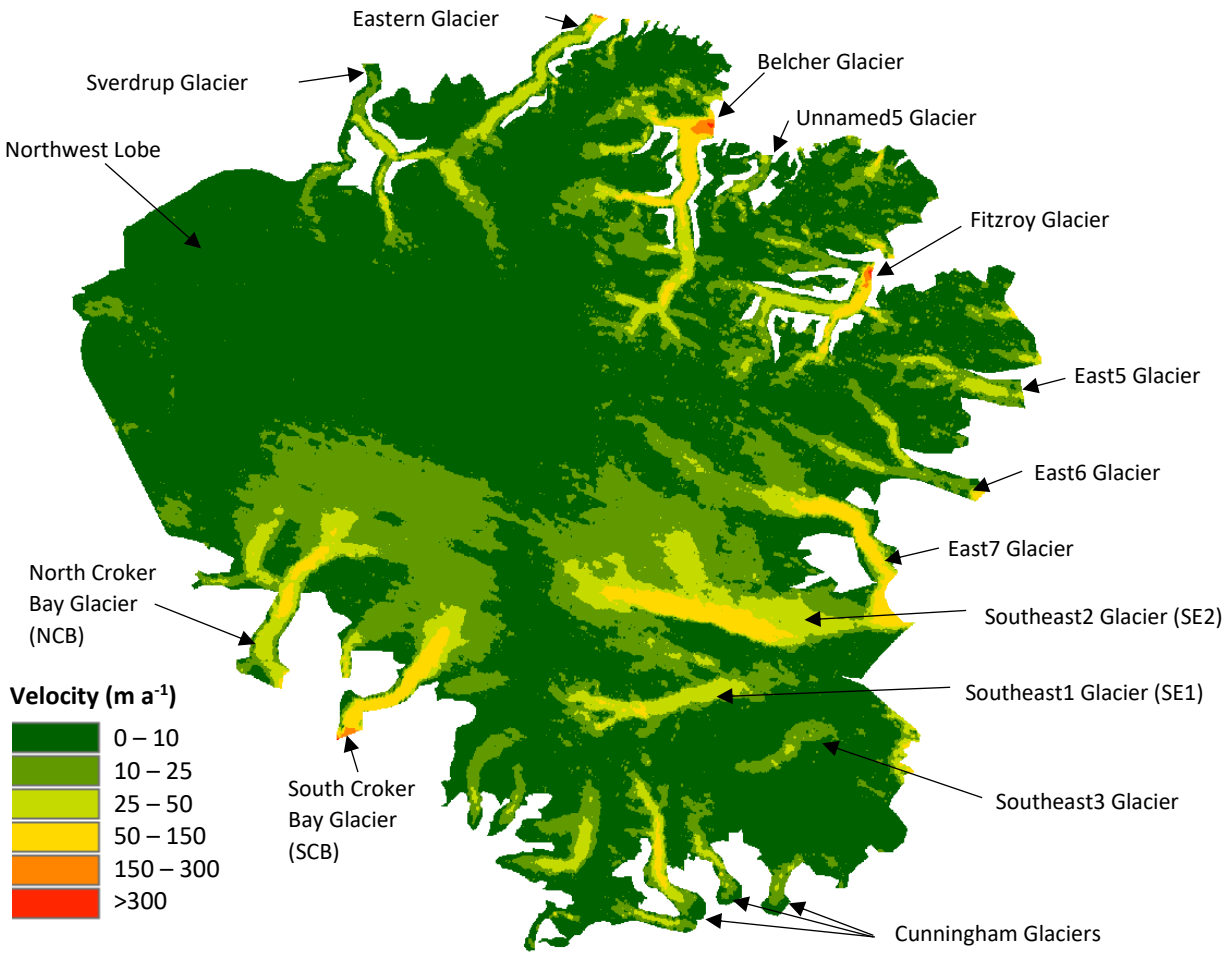


*Figure 2.2. Surface velocities of Devon Ice Cap from January 2013. Major outlet glaciers are labelled (with their corresponding acronyms when applicable). Data from Van Wychen et al., 2017.*

## 2.4 Calving Flux

Estimates for Devon Ice Cap's total calving flux average 0.41 ± 0.11 Gt $a^{-1}$ (Table 2.1), with relatively little interannual variability as fluctuations in the discharge from different glaciers appear to approximately cancel each other out (Van Wychen et al., 2017). Of this total calving flux, nearly a third stems from Belcher Glacier, with significant contributions from Fitzroy Glacier and SE1/2 (Table 2.1). In total, more than 90% of the mass lost through calving is from the major tidewater glaciers listed in Table 2.1, with the remaining 10% lost from small alpine glaciers (Burgess et al., 2005).

| Glacier | Dynamic discharge (Gt $a^{-1}$) | | | | | | | | |
|---|---|---|---|---|---|---|---|---|---|
| | 2009 | 2010 | 2011 | 2012 | 2013 | 2014 | 2015 | Mean | SD |
| Belcher (NA) | $0.01^{0.01}$ | $0.01^{0.01}$ | $0.01^{0.01}$ | $0.01^{0.01}$ | $0.00^{0.01}$ | $0.00^{0.01}$ | $0.01^{0.01}$ | $0.01^{0.01}$ | 0.01 |
| Belcher (SA) | $0.11^{0.01}$ | $0.12^{0.01}$ | $0.11^{0.02}$ | $0.13^{0.01}$ | $0.14^{0.01}$ | $0.14^{0.01}$ | $0.17^{0.01}$ | $0.13^{0.01}$ | 0.02 |
| Sverdrup | $0.01^{0.00}$ | $0.00^{0.00}$ | $0.01^{0.00}$ | $0.01^{0.01}$ | $0.01^{0.00}$ | $0.01^{0.00}$ | $0.01^{0.01}$ | $0.01^{0.00}$ | 0.00 |
| N. Croker Bay | $0.06^{0.01}$ | $0.06^{0.01}$ | $0.02^{0.01}$ | $0.01^{0.01}$ | $0.01^{0.00}$ | $0.02^{0.00}$ | $0.01^{0.01}$ | $0.03^{0.01}$ | 0.02 |
| S. Croker Bay | $0.03^{0.01}$ | $0.02^{0.01}$ | $0.02^{0.01}$ | $0.02^{0.01}$ | $0.02^{0.01}$ | $0.03^{0.01}$ | $0.02^{0.01}$ | $0.02^{0.01}$ | 0.01 |
| Eastern | $0.03^{0.00}$ | | $0.03^{0.01}$ | $0.03^{0.01}$ | $0.01^{0.01}$ | $0.02^{0.01}$ | $0.01^{0.01}$ | $0.02^{0.01}$ | 0.01 |
| Fitzroy (NA) | $0.00^{0.01}$ | | $0.01^{0.01}$ | $0.00^{0.01}$ | $0.00^{0.01}$ | $0.00^{0.01}$ | $0.00^{0.01}$ | $0.00^{0.01}$ | 0.00 |
| Fitzroy (SA) | $0.08^{0.01}$ | | $0.09^{0.01}$ | $0.09^{0.01}$ | $0.08^{0.01}$ | $0.09^{0.01}$ | $0.08^{0.01}$ | $0.09^{0.01}$ | 0.01 |
| East 5 | $0.05^{0.01}$ | | $0.03^{0.01}$ | | $0.01^{0.00}$ | $0.01^{0.01}$ | $0.00^{0.00}$ | $0.02^{0.01}$ | 0.02 |
| East 6 | $0.00^{0.00}$ | | $0.01^{0.00}$ | $0.00^{0.01}$ | $0.01^{0.00}$ | $0.00^{0.00}$ | $0.00^{0.00}$ | $0.00^{0.00}$ | 0.00 |
| East 7 | $0.04^{0.00}$ | $0.04^{0.01}$ | $0.03^{0.01}$ | $0.02^{0.01}$ | $0.02^{0.00}$ | $0.02^{0.01}$ | $0.02^{0.01}$ | $0.05^{0.02}$ | 0.01 |
| Southeast 1/2 | $0.04^{0.02}$ | $0.03^{0.02}$ | $0.05^{0.02}$ | $0.05^{0.02}$ | $0.04^{0.01}$ | $0.05^{0.02}$ | $0.06^{0.02}$ | $0.05^{0.07}$ | 0.01 |
| Southeast 3 | $0.02^{0.01}$ | | $0.02^{0.01}$ | $0.02^{0.01}$ | $0.01^{0.01}$ | $0.01^{0.01}$ | $0.01^{0.01}$ | $0.02^{0.01}$ | 0.01 |
| Devon Ice Cap | $0.48^{0.10}$ | | $0.44^{0.13}$ | $0.39^{0.13}$ | $0.36^{0.08}$ | $0.40^{0.11}$ | $0.40^{0.12}$ | $0.41^{0.11}$ | 0.04 |

*Table 2.1. Mean calving flux from the largest glaciers draining Devon Ice Cap estimated based on Radarsat-2 derived surface velocities. Superscripts indicate uncertainties. Belcher and Fitzroy glaciers have been separated into the southern arms (SA) and northern arms (NA). SE1 and 2 are grouped as they share a terminus. From Van Wychen et al. (2017).*

## 2.5 Changes to Flow Dynamics

### *2.5.1 Surging Glaciers*

Clear changes to the velocities of many of the major outlet glaciers draining Devon Ice Cap have been identified from velocity observations spanning the last two decades (Burgess et al., 2005; Van Wychen et al., 2012, 2017). For example, SE1 and SE2 entered the active phase of a surge (Van Wychen et al., 2012, 2017). Prior to measurements of velocity change, SE1 and SE2 were already suspected to be surge-type due to the presence of indicative features such as looped medial moraines (Burgess et al., 2005) and the terminus region not reaching the modelled balance velocity (Burgess and Sharp, 2008).

The mid-1990s data show the pre-surge state of SE1/2, with velocities up to ~50 m $a^{-1}$ in the fast-flowing areas in the upper portions of both glaciers and very slow velocities near the terminus (Fig. 2.3A). Redistribution of mass was occurring, as using an indirect method Burgess and Sharp (2008) record thickening in the portions of the glaciers at the lower end of the spatially confined fast flow units where the two glaciers join, with thinning above and below this region. This trend can be seen to continue in operation IceBridge data (Fig. 2.3A) and is visible in ICESat data collected between 2003 and 2009 (Gardner et al., 2011). The surge of these glaciers occurred simultaneously, implying this region of thickening acts as the reservoir area. Thinning near the terminus at this stage is a result of a negative SMB (Burgess and Sharp, 2008).

Since the mid-1990s, the area of fast flow has extended downstream and the terminus region has accelerated (Fig. 2.3B). The active phase is therefore suggested to have begun in ~2009, when the terminus was activated and began to reach velocities four to seven times those in the quiescent phase (Van Wychen et al., 2012, 2017). The terminus region continues to flow rapidly until at least 2015 and presumably beyond (Van Wychen et al., 2017), making the duration of the active phase of the surge of SE1/2 at least 6 years. However, instead of advancing, the terminus has retreated by ~1800 m between 2000 and 2016 (Van Wychen et al., 2017); the cause of this remains uncertain.

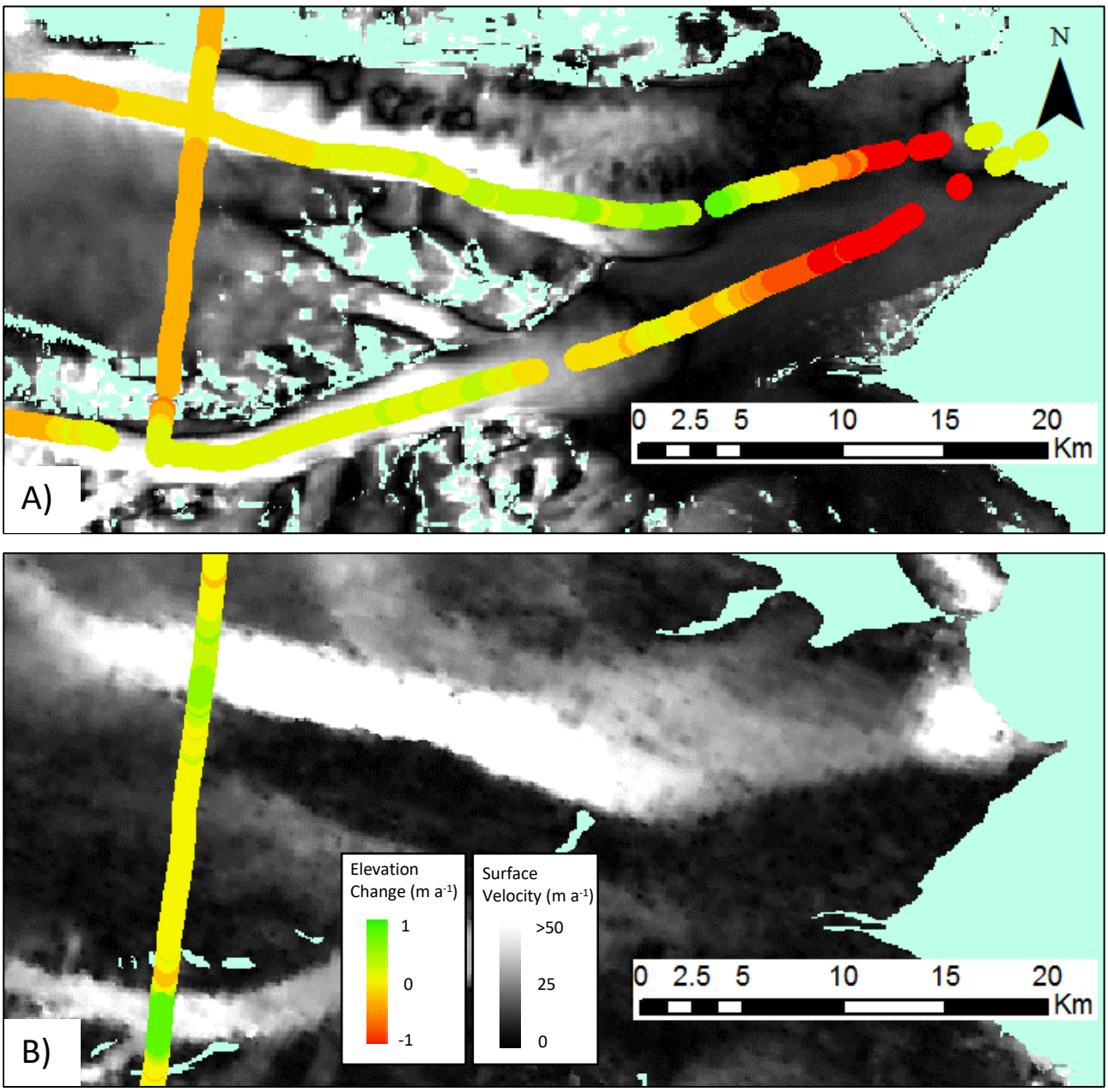


*Figure 2.3. Changes elevation and velocity on SE1/2. A) Elevation change between 2005 and 2012 overlain on a map showing the pre-surge (mid-1990s) velocities. B) Elevation change between 2012 and 2015 overlain on velocities from during the surge (2013). The elevation data is from Operation IceBridge (Krabill et al., 2014) and the velocity data is from Burgess et al. (2005) and Van Wychen et al. (2017) for A) and B) respectively.*

### *2.5.2 Pulsing Glaciers*

Other tidewater glaciers draining Devon Ice Cap undergo multiannual periods of acceleration then deceleration, but cannot easily be classified as surging (Van Wychen et al., 2017). Van Wychen et al. (2017) refer to these glaciers as 'pulse-type'; different definitions of pulsing exist (e.g. Turrin et al., 2014), but Van Wychen et al. (2017) use the scheme outlined in Van Wychen et al. (2016), so for continuity this is also used here. Following this classification, pulsing behaviour is distinct from surging as the velocity variability initiates from near the terminus and propagates upstream, and because it is largely limited to areas of the glacier that are grounded below sea level (Van Wychen et al., 2016). Bedrock bumps also appear to play an important role, with velocity variability greater downstream of such features. For these reasons, East5 Glacier, East7 Glacier and Fitzroy Glacier have been classed as pulsing (Van Wychen et al., 2017; Fig. 2.4).

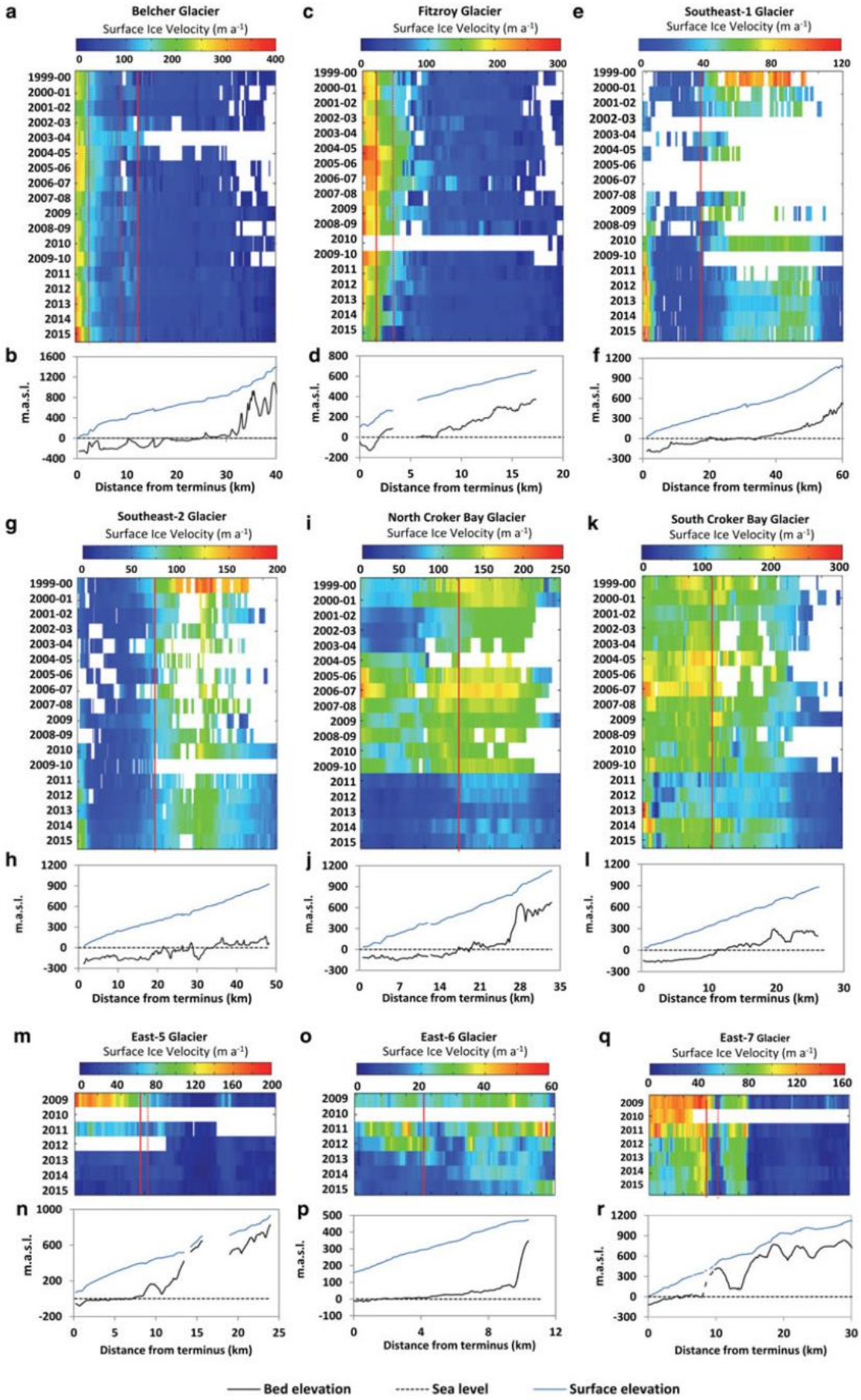


*Figure 2.4. Velocities derived from feature tracking in summer (1999-2010) and speckle tracking in winter (2009-2015) for the centrelines of the glaciers of interest (a to q). Solid red lines indicate where the bed drops below sea level, and dashed red lines prominent bedrock bumps. Figure is from Van Wychen et al. (2017), with figure 1 in this paper displaying the transect locations.*

### *2.5.3 Other Velocity Variability*

Alongside glaciers displaying cyclic velocity fluctuations, Belcher Glacier has only been observed to speed up (Fig. 2.4). This glacier is therefore classified as accelerating (Van Wychen et al., 2017). For glaciers such as this, Van Wychen et al. (2016) propose a mechanism equivalent to accelerating marine-terminating glaciers in Greenland, where thinning and retreat of the glacier front leads to a reduction in longitudinal resistive stresses, causing acceleration (Joughin et al., 2012). Belcher Glacier's calving rates appear to be linked to sea-ice concentration (Herdes et al., 2012), demonstrating further the importance of marine influences. Nevertheless, as supraglacial meltwater channels often terminate in the major crevasse field near the terminus of Belcher Glacier, surface meltwater could also be playing a role in the acceleration (Burgess et al., 2005; Wyatt and Sharp, 2015). It should also be noted that Operation IceBridge data (Krabill et al., 2014) suggests part of the trunk is thickening between 2012 and 2015, and the upper half has slowed since 2009 (Van Wychen et al., 2017). It is unknown why these changes are occurring.

Other velocity variations on Devon Ice Cap that are potentially climatically forced are the multi-annual periods of faster and slower flow of the Croker Bay Glaciers (Van Wychen et al., 2017). Since 2011, both glaciers have seen a substantial slow down (Fig. 2.4), although this is most pronounced in the two to three-fold decrease in the velocities of NCB (Van Wychen et al., 2017). These periods are not on the same timescales as surging glaciers in the Canadian Arctic Archipelago, and neither glacier completely stagnated at any point in the last ~20 years, making them unlikely to be surge-type (Fig. 2.4). Furthermore, changes in velocity seem to be uniform over the entire main trunk and not limited to areas grounded below sea level, making a classification as pulsing unsuitable (Van Wychen et al, 2017). Observations from 2006 saw enhanced velocities on both these glaciers (Van Wychen et al., 2017) accompanied by an almost threefold increase in meltwater delivery to the bed compared to 2004 (Clason et al., 2012) and a 2 m drop in elevation (Rinne et al., 2011). This suggests climatic conditions are involved, although the data required to elucidate this relationship are not available.

## 2.6 Flow Regimes

To identify whether surface motion is most likely dominated by basal sliding or by internal deformation at a given point, Burgess et al. (2005) calculated the ratio of the driving stress ($\tau_d$) to the surface velocity divided by the ice thickness ($v/h$) for Devon Ice Cap. From this analysis, the ice cap was split into four flow regimes: 1 ($v/h$ < 0.075 $a^{-1}$), where the ice cap is frozen to the bed; 2 (0.075 $a^{-1}$ < $v/h$ < 0.28 $a^{-1}$), where basal temperature is approaching pressure melting point (PMP) and sliding begins to take effect; 3 ($v/h$ > 0.28 $a^{-1}$ & $\tau_d$ > 0.075 MPa), where basal motion has a greater contribution; and 4 ($v/h$ > 0.28 $a^{-1}$ & $\tau_d$ < 0.075 MPa), where basal friction is low, basal motion high and sediment deformation is likely to be occurring. Van Wychen et al. (2017) repeated this analysis for more recent years, highlighting changes in flow regime (FR). These include the main two tributaries to Belcher Glacier changing from FR3 to FR2, the Cunningham Glaciers changing from FR3/4 to FR2, NCB from FR3/4 to FR2 and the terminus region of SE1/2 from FR1 to FR2.

# 3. Mechanisms Controlling Ice Flow

To understand what is driving the changes to the dynamics of Devon Ice Cap discussed in the previous chapter, an understanding of the processes that govern ice flow and the dynamics of ice bodies is needed. The factors that influence the flow of ice are therefore described, before the mechanisms thought to result in fluctuations in velocity are introduced.

## 3.1 Introduction to Ice Motion

Processes controlling the flow of ice can be broadly split into internal deformation purely resulting from the mass of the ice itself (known as ice creep), sliding over the bed and deformation of the bed (Cuffey and Paterson, 2010). The latter two processes are often grouped and referred to as basal slip. Surface velocities can be influenced by all of these mechanisms, and will comprise of the integrated displacement of all the points below (Fig. 3.1).

Creep, often a few metres per year, dominates in areas where the base of the glacier is frozen to the bed, although a very limited amount of basal motion is possible even under frozen bed conditions (Echelmeyer and Zhongxiang, 1987). However, creep alone cannot explain velocities exceeding a few metres per year; motion resulting from basal slip is also required (Dowdeswell and Collin, 1990; Schafer et al., 2014). On Devon Ice Cap, this supposition is supported by the presence of flow stripes in fast-flowing areas, which are indicative of basal sliding (Burgess et al., 2005). The controls on basal motion are complex, but all require the presence of water, with temperatures above the pressure melting point (Schafer et al., 2014).

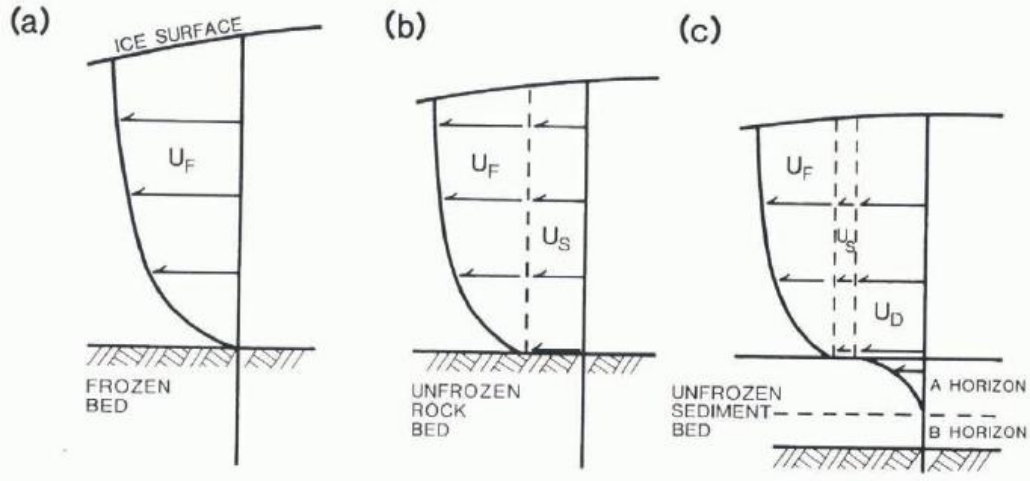


*Fig. 3.1. Contributions of different processes to ice flow, with a very large horizontal exaggeration. (a) represents pure ice creep, (b) includes sliding over the bed and (c) deformation of a soft bed. From Boulton (1996).*

The motion of an ice mass can be understood by considering the force balance of the system. As glacial motion is relatively slow, it can be assumed that the forces instigating motion (driving stresses) will approximately equal those opposing it (resistive stresses). The driving stress ($\tau_d$) is driven by gravity and is calculated from:

$$\tau_d = \rho_i g H \sin(\alpha) \tag{3.1}$$

where $\alpha$ is surface slope, $H$ is ice thickness, $\rho_i$ is ice density and $g$ is the acceleration due to gravity. However, the resistive stresses - the sum of basal drag ($\tau_b$), lateral drag and longitudinal drag - are far harder to quantify (van der Veen and Whillans, 1989). Nevertheless, a force-balance approach provides a useful framework with which to understand the flow of ice. The overall force balance in the direction of flow can be represented as:

$$\rho_i g H \sin(\alpha) = \tau_b - \frac{\partial(H\bar{\tau}_{xy})}{\partial y} - \frac{\partial(H\bar{\sigma}'_x)}{\partial x} \tag{3.2}$$

where $\bar{\tau}_{xy}$ is the shear stress acting parallel to the sides of the glacier and $\bar{\sigma}'_x$ is the longitudinal deviatoric stress acting in the direction of flow (Benn and Evans, 2014). In the centre of ice sheets and on most mountain glaciers, basal drag dominates, but beneath ice shelves and fast-flowing ice, the driving stress can greatly exceed basal drag. In these regions, flow will be faster so that lateral and longitudinal drag are high enough to balance the driving stress (Benn and Evans, 2014).

## 3.2 Ice Creep

### *3.2.1 Grain-Scale Processes*

When modelling ice flow on a broad scale, the bulk properties of ice are generally of interest. However, as motion occurs at a grain-scale level, these finer-scale processes should also be considered. For example, if the cleavage planes found within ice crystals align, this is likely to substantially weaken the ice (Benn and Evans, 2014). The rheology will also be influenced by the presence of impurities including solutes, bubbles and rock fragments. Bubbles will result in weakening as they create stress concentrations, whereas rock fragments will tend to strengthen ice unless the debris content is greater than ~75% (Nickling and Bennett, 1984). The concentration of impurities is often higher in ice from the Pleistocene, making it softer (Paterson, 1977), but this effect is generally ignored when modelling ice flow.

### *3.2.2 Bulk Properties of Ice*

Ice will deform in three phases – termed primary, secondary and tertiary creep - as a stress is applied, but secondary creep is often the only phase considered (Cuffey and Paterson, 2010). This is generally because it is the easiest to identify, but Cuffey and Patterson (2010) suggest that typical driving stresses would most likely lead to a response like secondary creep, making the assumption valid. Consequently, the strain resulting from the driving stress is given by Nye's generalisation of Glens' flow law (Glen, 1955; Nye, 1957). Where there is only one component of applied stress, this flow law can be approximated as:

$$\dot{\varepsilon} = A\tau^n \tag{3.3}$$

where $\dot{\varepsilon}$ is the shear strain rate and $A$ (the creep parameter) and $n$ (the creep exponent) are constants. Selecting the correct values for these constants is crucial to modelling the flow of ice accurately. Studies conducted on a range of samples have measured creep exponents between 1.5 and 4.2 (Weertman, 1973; 1983), but a value of $n$ = 3 is typically used as this is most consistent with field data (Cuffey and Paterson, 2010). As $n$ > 1, ice is considered a non-linear viscous fluid; the strain rate will increase non-linearly with the applied stress

(Benn and Evans, 2014). A consequence of equation 3.3 is that the higher shear stresses near the bed result in more deformation lower in the ice column (Fig. 3.1).

Unlike *n*, $A$ can vary by several orders of magnitude and no conceptual frameworks have been developed to understand it (Cuffey and Paterson, 2010). However, the relationship with temperature is the most important influence, and this can be approximated by a simple Arrhenius relation adapted for ice (Hooke, 1981):

$$A = A_0 \exp\left(-\frac{Q}{RT_i} + \frac{0.49836}{(T_0 - T_i)^{1.17}}\right) \quad (3.4)$$

where $A_0$ is the prefactor coefficient (effected by impurities and pressure, taken as 0.09302 $Pa^{-3}$ $a^{-1}$), $R$ is the universal gas constant (8.314 J $mol^{-1}$ $K^{-1}$), $Q$ is the activation energy for ice creep ($7.88\times10^{-4}$ J $mol^{-1}$), $T_i$ is the ice temperature (K) and $T_0$ is the melting point of ice (273.39 K).

Combining equations 3 and 4 and integrating over the ice thickness ($H$) will therefore give an expression for surface motion in the glacier's centreline ($\overline{U}$):

$$\overline{U} = \frac{2A}{n+1}(\rho_i\, g\, \sin\alpha)^n H^{n+1} \quad (3.5).$$

When typical parameters are input into this equation, the velocities produce are usually on the scale of metres per year (Cuffey and Paterson, 2010). However, when basal slip begins to influence velocities and basal drag no longer dominates the force balance (Equation 3.2), the velocities produced by equation 3.5 will become increasingly inaccurate.

## 3.3 Basal Slip

### *3.3.1 Sliding Over a Hard Bed*

Two mechanisms that explain the sliding of ice over an uneven hard bed were proposed by Weertman (1957): regelation and enhanced creep. Enhanced creep is a result of the increased stresses upstream of a bump causing a far greater increase in the strain rate due to the non-linearity of Glen's Flow Law (Equation 3.3). This allows the ice to deform more readily around the obstacle, and means enhanced creep will operate more effectively over larger bumps. Regelation relies on the assumption that the whole bed is at the pressure

melting point (PMP), and occurs as pressures on the upstream side of an obstacle are greater than those on the downstream side. This locally lowers the PMP on the upstream side, resulting in the production of meltwater which flows as a film down the pressure gradient to the downstream side, where it refreezes as the PMP is raised. Regelation is more efficient over bumps less than ~1 m in length as heat cannot conduct as readily through the bump as dimensions increase. As each operates best on a different scale, a combination of these processes is required to explain the motion of a glacier over a hard bed.

Weertman's propositions assume a thin film of water is present at the bed but, in reality, water is likely to concentrate in cavities on the lee side of obstacles. To understand the mechanism of cavity formation, the concept of effective stress ($N$) must be introduced. This is defined as the normal stress exerted by the ice overburden ($P_i$) minus the local water pressure ($P_w$):

$$N = P_i - P_w \tag{3.6}$$

where $P_i = \rho_i g H$. Cavities will form in the lee side of bumps because the compressive normal stress exerted by the ice ($P_0$, the mean of which $= P_i$) will be lower, and when $P_0$ is less than the water pressure, separation can occur. The minimum value of $P_0$ required for cavity formation is known as the separation pressure, $P_s$ , thus separation begins when $P_s = P_w$ and increases as $P_w$ increases (Cuffey and Paterson, 2010). Cavities are important as they decrease the area of contact between ice and bed, therefore increasing stresses in other areas and increasing the sliding rate (Lliboutry, 1968). This mechanism can account for faster slip velocities than Weertman's theories, and implies basal drag cannot exceed a critical limit imposed by the bed geometry. Up to a certain velocity, this holds true; beyond this, however, the contribution of resistive forces other than basal drag increases, making broader-scale controls such as lateral drag more important (Cuffey and Paterson, 2010).

### *3.3.2 Sediment Deformation*

Since the paradigm shift following the discovery of widespread subglacial till beneath the Siple Coast ice streams in West Antarctica (Alley et al., 1986) and the work on Breidamerkurjokull in Iceland by Boulton and Hindmarsh (1987), it has become increasingly

apparent that sediment deformation influences the flow of ice bodies. It was demonstrated that till could have an extremely low shear strength (Boulton and Jones, 1979), facilitating fast ice motion even when driving stresses are very small (Blankenship et al., 1986). 8% of Devon Ice Cap's bed lies below sea level; in these areas, marine sediments deposited during previous interglacials are likely to be present (Dowdeswell et al., 2004) and will influence flow dynamics (Burgess et al., 2005).

Geomechanical tests (Kamb, 1991; Tulaczyk et al., 2000a; Kavanaugh and Clarke, 2006) have shown that a Coulomb-plastic rheology best describes the mechanical behaviour of subglacial till. Consequently, shear strength ($\tau_f$) is largely independent of strain rate and magnitude; instead, it increases roughly linearly with effective stress:

$$\tau_f = c + N \tan \varphi \tag{3.7}$$

where $c$ is apparent cohesion (≈ 0) and $\varphi$ is the angle of internal friction (Tulaczyk et al., 2000a). Once this shear strength is exceeded, the till will fail rapidly and become extremely weak. The void ratio ($e$) is also related to effective stress:

$$e = e_0 - C \log(N/N_0) \tag{3.8}$$

where $e_0$ is the void ration at a reference value of effective stress ($N_0$) and $C$ is the dimensionless coefficient of compressibility.

## 3.4 Basal Hydrology

Regardless of whether the bed is hard or soft, basal water pressure is clearly critical to controlling the rate of basal sliding, with small changes in water pressure able to greatly alter the basal friction parameter (Jay-Allemand et al., 2011). Basal water pressure is controlled by both the rate at which water is supplied to the ice-bed interface and the rate at which the subglacial drainage system can remove this water; thus, the potential sources of water available to the bed and how this water is likely to drain away are important.

Before introducing more recent findings, it should be noted that Llibourtry's (1968) distributed, cavity-based drainage system (Section 3.3.1) is only one potential structure for a subglacial hydrological network; a second type of drainage system with efficient,

distributed, arborescent channels can also exist (Röthlisberger, 1972; Nye, 1976). These two systems are thought to evolve into one another as a result of two opposing processes: ice creep and melting by liquid water. Creep will close channels, whereas the release of the latent heat stored in meltwater will widen them (Röthlisberger, 1972). As the surface area-to-volume ratio in a channelised system is relatively low, melting will tend to outpace closure by creep, growing the channels if the influx of water can keep pace. The opposite is true of a distributed system (Walder, 1986). This means that as discharge from a channelised system increases, water pressure is likely to drop, whereas for a distributed system, pressure will increase. This switching can explain why deceleration occurs before the end of the melt season, when meltwater supply is still high. The evolution of the subglacial drainage system, from a distributed system to a channelised one, is thought to increase the capacity of the drainage system, increasing basal drag (Bartholomew et al., 2010; Schoof, 2010).

Zwally et al. (2002) suggested that the delivery of surface meltwater to the bed of the Greenland Ice Sheet can greatly affect basal lubrication and cause faster flow. Observations support this, with increased summer melting linked to an increased summer mean velocity (Bartholomew et al., 2010). However, the switching between the drainage systems described above makes the relationship between increased meltwater supply and decreased effective pressure more complex than Zwally et al. (2002) initially proposed. Future warming may therefore have a limited influence on dynamics (Sundal et al., 2011; Shannon et al., 2013).

### 3.5 Cryo-Hydraulic Warming

Lubrication is not the only potential consequence of the penetration of surface meltwater to the bed; warming is also possible, both through heat transferred directly from the water to the basal ice and the refreezing of meltwater releasing latent heat. Known as cryo-hydraulic warming, this has the potential to substantially alter the thermal structure of an ice cap (Phillips et al., 2010; Dunse et al., 2015; Gilbert et al., 2016) and could raise more of the bed to PMP (Phillips et al., 2013). Warmer basal ice will also deform more readily as the ice is less viscous (Phillips et al., 2010).

## 3.6 Marine-Terminating Glaciers

The marine environment can be a very influential control on glacier dynamics, evidenced by the fact that the extent of significant velocity variability on Devon Ice Cap is in many cases limited to ice grounded below sea level (Van Wychen et al., 2017). Near the termini of tidewater glaciers, basal water pressure will generally be high and effective stress low, leading to very little basal drag as the glacier approaches flotation. The force balance is therefore maintained by increased stresses at the lateral margins due to higher flow velocities (van der Veen, 2002). These areas are therefore particularly sensitive to changes such as increasing ocean temperatures. The intrusion of warmer waters into fjords could interact with cold, low salinity meltwater to produce strong convection currents and increase the calving rates (O'Leary and Christoffersen, 2013). Furthermore, the buttressing of the calving front by ice melange during the winter could be reduced should warming waters weaken the sea ice (Todd and Christoffersen, 2014). These factors should therefore be considered when assessing changes to the dynamics of tidewater glaciers draining Devon Ice Cap.

## 3.7 Surging

The processes described so far in this chapter together help explain the flow of ice, and can provide an insight into the changes to the dynamics occurring on Devon Ice Cap. Although some of the changes are likely to be externally forced, an intrinsic process known as surging will also lead to velocity variability on some glaciers. To understand the surge mechanism on Devon Ice Cap, and perhaps provide some insight into the behaviour described as pulsing, the causes of and controls on this behaviour will be discussed.

### *3.7.1 Surge Mechanisms*

Surging glaciers are characterised by cyclic, orders-of-magnitude fluctuations in flow velocities between longer quiescent (slow-flowing) phases and briefer active (fast-flowing) phases (Meir and Post, 1969; Raymond, 1987). In temperate regions, active and quiescent phases generally last ~1-2 and ~20-40 years, respectively (Dowdeswell et al., 1991).

However, in colder regions such as Svalbard (Dowdeswell et al., 1991) and the Canadian High Arctic (Copland et al., 2003), these phases can be considerably longer, with active phases typically lasting ~3-10 years and quiescent phases ~50-500 years. The observed dynamics of these two types of surge are very different (Murray et al., 2003; Benn and Evans, 2014), leading to the development of two key mechanisms that explain surging: the hydrological switch mechanism (Kamb, 1985) and the thermal switch mechanism (Clarke et al., 1984; Fowler et al., 2001; Murray et al., 2003).

The hydrological-switch mechanism explains the observations seen on glaciers that surge on shorter timescales; Kamb et al. (1985) based his theory on the surge of Variegated Glacier in Alaska, which lasted only a few months. This mechanism suggests that, during the quiescent phase, an imbalance between accumulation and discharge results in thickening in the upper part of the glacier, increasing driving stresses. This would increase basal shear stress, thus the area of the bed where the effective stress is zero, eventually crossing a threshold. Eisen et al. (2005) suggest that as water pressure rises in winter, leakage of water to conduits on the lee-side cavities of bedrock bumps triggers a switch to a linked-cavity drainage system when this threshold is crossed, elevating basal water pressure and thus reducing effective pressure. This would lead to faster flow locally, raising creep closure rates enough to restrict the formation of a channelised drainage system and propagating the fast-flowing area down the glacier as a bulge. A consequence of this would be thinning in the upper region and thickening towards the terminus. Creep closure rates remain high under the bulge, causing the very low subglacial water velocities observed during a surge (Kamb, 1985). This type of surge generally terminates during the early summer, as the influx of meltwater causes the cavity system to open up, reducing basal water pressure (Sharp, 1988). The hydrological-switch mechanism is generally assumed to operate in temperate regions where the bed is always at the PMP.

However, this theory cannot explain velocity fluctuations in colder regions where the beds of many glaciers are known to be at least partially below PMP (Murray et al., 2003). This has led to the development of the soft-bedded thermal switch mechanism, which predicts many of the observations in regions with slower surge cycles and better fits glaciers suspected to be underlain by till. This theory suggests that, during the quiescent phase, thickening will both increase driving stresses and make the bed more likely to reach the PMP, the latter

through a combination of increasing amounts of insulation and an increase in pressure (Fowler et al., 2001; Murray et al., 2003). Basal meltwater would then weaken the underlying till, dilating it and weakening it further. This would increase frictional heating, forming a positive feedback between basal motion and meltwater production (Murray et al., 2003). As the meltwater would be unable to escape through the adjacent frozen till, water pressure would build and the surge would begin. As this would cause stresses to be transferred to the boundaries of the fast-flowing area, the surge would propagate outwards due to a positive feedback between strain rate and strain heating, although at a slower rate than the hydrological switch, consistent with observations (Benn and Evans, 2014; Cuffey and Paterson, 2010).

Dunse et al. (2015) proposed a modification to this mechanism, suggesting that a hydro-thermodynamic feedback linked to cryo-hydraulic warming may play a role. Following this theory, gradual thickening in the reservoir area would lead to spatially confined fast flow, allowing increased penetration of meltwater to the bed. Summer melting would then promote cryo-hydraulic warming and lubrication, enhancing fast flow and increasing longitudinal extension leading to more crevasse formation. This would further enhance meltwater penetration and expand the area of the bed subject to fast flow, until the cold-ice plug downstream failed, beginning the surge. Surface meltwater has been found to penetrate the ice to reach the bed in some areas of Devon Ice Cap (Clason et al., 2012). Furthermore, Wyatt and Sharp (2015) mapped the supraglacial drainage system on Devon Ice Cap and found a higher density of meltwater sink points in areas with the greatest velocity variability, suggesting the dynamics of Devon Ice Cap are influenced by surface meltwater in these regions. Dunse et al.'s (2015) cryo-hydraulic warming feedback could therefore play a role in driving the observed velocity variability.

These theories describe the initiation and propagation of a thermally driven surge well, but the mechanism behind the observed gradual termination of these surges is less clear. Early studies suggested that terminations are a result of dynamic thinning of the glacier and the convection of cold ice from inland, leading to basal cooling and a reduction in driving stress (Clarke, 1984; Murray et al., 2003). However, the timescales required for this form of heat loss are larger than the duration of a typical active phase (Gladstone et al., 2014; Gong et al. 2016). Fowler et al. (2001) suggested an alternative mechanism, where once all the bed

reaches the PMP, the water generated begins to drain freely, lowering water pressure. A 'leaky' surge front, where high pressure water escapes from fractures near the bulge, could also contribute in some cases (Murray et al., 2000). Another potential mechanism of termination was suggested by Cook (2016), who proposed that till failure during a surge would cause a reduction in frictional heating. This process would increase basal freezing rates, complementing the effects of enhanced conductive and advective heat loss and leading to strengthening of the till as water is withdrawn, terminating the surge.

Polythermal marine-terminating glaciers often behave differently to their land-terminating counterparts. Similarities include gradual surge termination, but the surges often initiate near the terminus and propagate upstream with no clear surge front (Murray et al., 2003; Mansell et al., 2012). This behaviour has been documented in Svalbard (Luckman et al., 2002; Dowdeswell and Benham, 2003; Murray et al., 2003) and Greenland (Pritchard et al., 2003, 2005), but the mechanism causing these differences in flow behaviour is not well understood. The similarities with pulsing behaviour (i.e. propagating from the near terminus up) suggest that there is potentially a link between these behaviours, but the lack of knowledge about pulsing makes this uncertain.

### *3.7.2 Controls on Surging Glacier Distributions*

To better understand surge mechanisms, it is important to understand what conditions are required for a glacier to surge. Surging glaciers are relatively rare and tend to be found in regional clusters (Jiskoot et al., 2000), thus statistical studies have aimed to understand what causes a glacier to be of surge-type. Sevestre and Benn (2015) proposed the concept of an enthalpy balance to explain the worldwide distribution of surge-type glaciers. This suggests that surging will occur if enthalpy gains, generated through accumulation adding potential energy, cannot be lost at an equal rate. This encompasses both the thermal and hydrological mechanisms, as enthalpy losses can result from both meltwater discharge or conductive cooling. Warm, humid environments can sustain high meltwater discharges and cold, dry environments with thin, low-flux glaciers can conduct heat away from the bed efficiently; intermediate states are therefore more likely to produce surging (Sevestre and Benn, 2015).

Consequently, climate can be considered a first-order control on surging despite the process being internally driven (Sevestre and Benn, 2015). It has therefore been suggested that, if the climate were to change, the balance between accumulation and discharge may be modified sufficiently to change the nature of a surge-type glacier, or even to prevent it surging all together (Dowdeswell et al., 1995). Many glaciers are currently unable to return to pre-surge geometries, suggesting that changes to a glaciers ability to surge are occurring (Dowdeswell et al., 1995; Murray et al., 2012; Murr et al., 2012). Other factors making a glacier more likely to surge include the presence of subglacial till. A till layer favours surging (Jiskoot et al., 2000), although Fowler et al. (2001) suggested that the hydraulic conductivity of the till must be sufficiently low to allow water pressures to rise. Furthermore, longer, more branching glaciers are more likely to surge. This could be a consequence of higher balance velocities and thicker ice reducing conductive heat losses (Sevestre and Benn, 2015). Overall, despite this progress a general theory of surging remains elusive, and the causes of the mass imbalance driving surges are still uncertain (Benn and Evans, 2014).

# 4. Data and Methods

In this chapter, the datasets used in the numerical model are introduced, including how they were sourced, prepared and a discussion of any limitations. This is followed by a brief description of both the forward model and the inverse method used.

## 4.1 Data Acquisition

### *4.1.1 Surface Velocity Data*

Data on the surface velocities of Devon Ice Cap during winter or early spring were acquired for years ranging from the mid-1990s to 2015 (Table 3.1). Most of these data were collected using a speckle tracking algorithm, where the displacement of ice-surface features in RADARSAT-2 imagery over a roughly one month period was measured, then interpolated to a 100m grid (Van Wychen et al., 2012, 2014, 2017).

*Table 4.1. Details of the velocity data used. Note that the data hereafter referred to as 2014 were collected in late 2013, but can be assumed to represent the 2013-14 winter period.*

| Year(s) | Dates of Image Collection | Publication | Data Acquisition Method |
|---|---|---|---|
| 1992 and 1996 | Northeast: 6/9$^{th}$ Feb. 1992<br>Southeast: 15-16$^{th}$ Mar. & 19-20$^{th}$ Apr. 1996<br>West: 25-26$^{th}$ Apr. 1996 | Burgess et al. (2005) | Majority InSAR, some speckle tracking |
| 2009 | West: 1$^{st}$-25$^{th}$, East: 2$^{nd}$-26$^{th}$ and Interior: 5$^{th}$-29$^{th}$ March. | Van Wychen et al. (2012) | Speckle tracking |
| 2012 | Majority 9$^{th}$ Apr.- 3$^{rd}$ May, but Eastern Glacier was imaged 31$^{st}$ Jan.- 24$^{th}$ Feb. and Sverdrup Glacier 7$^{th}$ Feb.- 2$^{nd}$ Mar. | Van Wychen et al. (2014) | Speckle tracking |
| 2013 | 31$^{st}$ Dec.-24$^{th}$ Jan. and 5$^{th}$-29$^{th}$ Jan. | Van Wychen et al. (2017) | Speckle tracking |
| 2014 | 2$^{nd}$-26$^{th}$ and 7$^{th}$-31$^{st}$ Dec. 2013 | | |
| 2015 | 26$^{th}$ Dec.-19$^{th}$ Jan. and 7$^{th}$ Feb.-3$^{rd}$ Mar. | | |

Burgess et al. (2005) also attempted some speckle tracking using RADARSAT-1 images acquired in 2000, but this was confined to the terminus of Belcher Glacier (Table 3.1). Instead, velocities were primarily derived using InSAR data obtained from the European Remote-sensing Satellites 1 and 2 (ERS-1/-2). Double-differencing, where the differences between two radar pairs are used to remove topographic effects, was applied where possible, but when only one radar pair was available, the Canadian Digital Elevation Dataset (CDED) was used instead. Three regions imaged at different dates during the 1990s were mosaiced together to create the velocity field used, hence the 9-year interval of these data. For simplicity, this velocity map will hereafter be referred to as the mid-1990s data.

Using data collected over a ~20-year period (Table 4.1) allowed temporal changes in the basal conditions to be examined, as differences in surface velocity were reflected in the inversions. However, variations in the velocity data could result from factors not linked to interannual changes in basal conditions. For example, when comparing data derived from InSAR and speckle tracking, some differences may arise because of the different measurement techniques; whereas speckle tracking is more efficient in fast-flowing regions, InSAR is more effective at detecting the small velocities in the ice cap interior (Van Wychen et al., 2012). Another factor leading to variations in the velocity data between the years is the date the images were taken, with seasonal fluctuations in glacier velocities estimated to average 11% (Van Wychen et al., 2017). However, as the melt season does not typically begin until June or early July (Boon et al., 2010) and the data used here were collected before June (Table 4.1), the effects of this will be small.

### *4.1.2 Topographic Data*

Surface Digital Elevation Model (DEM) data for Devon Ice Cap (Fig. 4.1A) were acquired at a 10-30 m horizontal resolution and 3-33 m vertical resolution from the 1:50000 Canadian Digital Elevation Data (CDED) dataset, which is accessible from: http://geogratis.gc.ca/api/en/nrcan-rncan/ess-sst/c40acfba-c722-4be1-862e-146b80be738e.html.

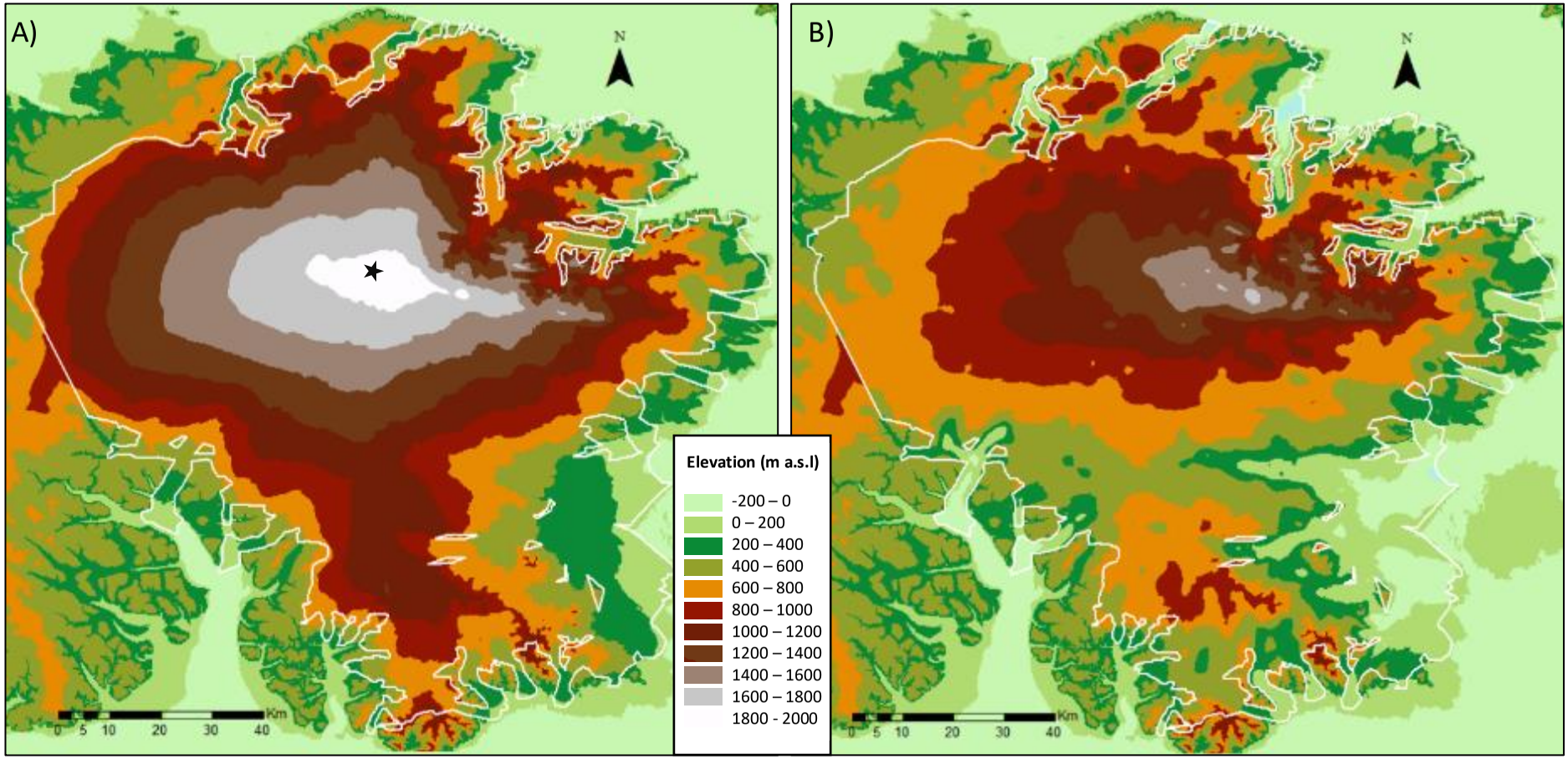


*Figure 4.1. Surface (A) and bed (B) DEMs plotted using the same colour ramp. Model domain is displayed as a white line, and the approximate location of the summit is indicated by the black star on the surface DEM.*

CDED is compiled from various surveys; for Devon Ice Cap, these were largely conducted in July 2010 and June 2011. However, towards the southern margin, some data are derived from aerial photography from 1959. Although this is not ideal, no other complete, high-resolution DEMs were available.

To obtain bed elevation data (Fig 4.1B), in April 2000 Dowdeswell et al. (2004) used a 100 MHz ice-penetrating radar system with an approximately 10 km spaced grid of flight lines to obtain ice thickness estimates. These data were subsequently interpolated using an inverse-distance weighted (IDW) algorithm to a 1 km grid, to produce ice thicknesses that could then be subtracted from the surface DEM to produce the bed DEM. Ice thicknesses were also set to zero outside the model domain – a reasonable assumption given that these areas can be seen to be ice free (Fig. 4.2).

### *4.1.3 Temperature Data*

Measurements of surface temperature on Devon Ice Cap are limited to a series of point measurements taken at automatic weather stations (Gardner et al., 2009; Sharp et al., 2011). As a map of surface temperature is required as a model input, data collected along two transects towards the west of the ice cap between 1992 and 2006 were used to estimate the temperature change with elevation for the entire ice cap (Gardner et al., 2009). Alongside this surface temperature data, temperature profiles from two deep boreholes drilled near the centre of Devon Ice Cap (Paterson and Clarke, 1978) and from a shallow borehole on Sverdrup Glacier (Keeler, 1964) were available to help validate model outputs.

## 4.2 Data Preparation

### *4.2.1 Domain Definition and Mesh Generation*

The boundaries of the ice cap (Fig. 4.2) were established manually using a combination of the outlines from the Randolph Glacier Inventory (RGI), accessed from http://www.glims.org/RGI/rgi50_dl.html (Pferrer et al., 2014), and Landsat imagery. As defining these boundaries to a high degree of accuracy would increase the computational load, they were simplified, with smaller features neglected.


*Figure 4.2. Red outline of the ice cap used for mesh generation and for clipping other datasets, superimposed on Landsat 7 imagery from summer 1999 (ArcGIS online, 2017). Nunataks too small to be accounted for in the mesh can be seen, and some areas not of interest, such as Western Devon Ice Cap, have been excluded.*

Defining the margin of the ice cap was straightforward for the smoother western side, but along the mountainous northern, eastern and southern edges it proved more problematic. This is a result of the steep-sided valleys draining these areas (Dowdeswell et al., 2004), leading to more nunataks and areas of exposed rock, thus a much more complex boundary (Fig. 4.2). Furthermore, Western Devon Ice Cap was excluded from the model domain entirely, as it is dynamically separate and completely frozen to the bed (Dowdeswell et al., 2004). Once created, the outline polygon was then used to produce the mesh and mask the velocity and temperature data to consistent sizes.

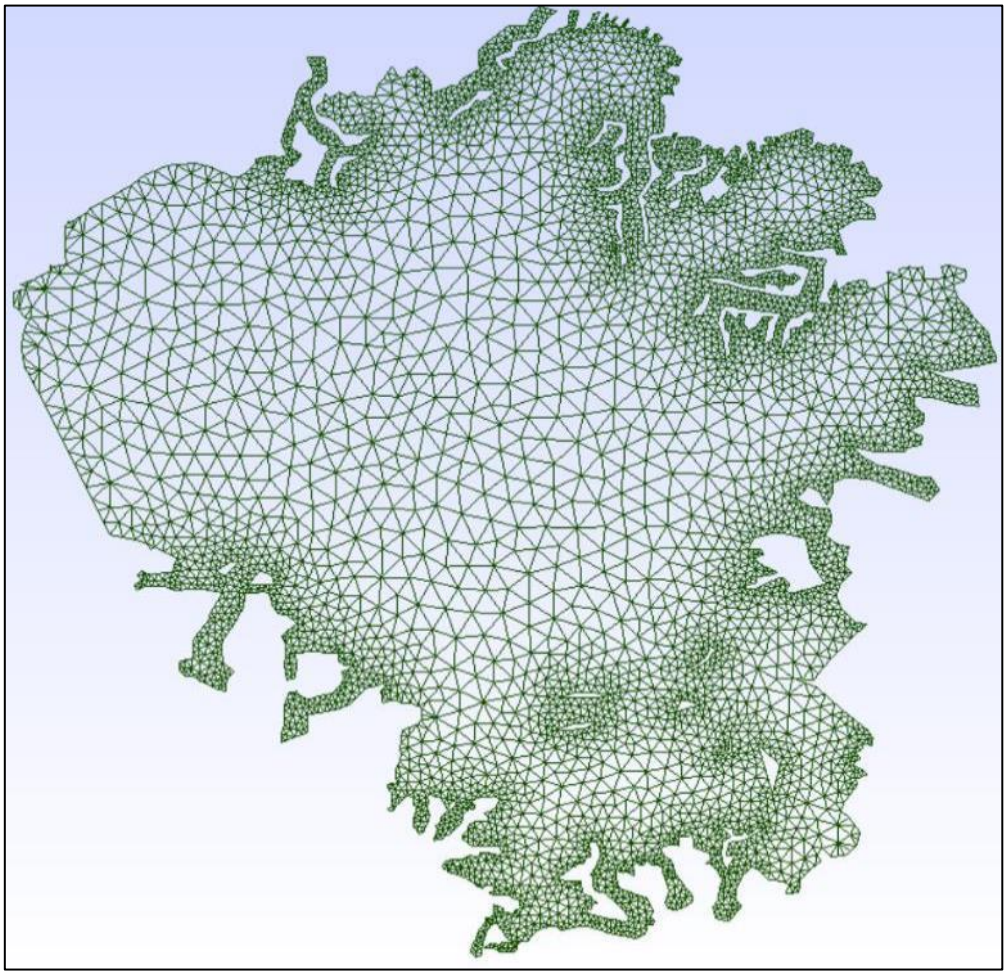

*Figure 4.3. 2D mesh created in gmsh before extrusion to 3D. Mesh resolution increases towards margins in fast-flowing areas and around nunataks.*

The mesh was first produced in 2D using the programme gmsh (Fig. 4.3). A variable element size was implemented to reduce the computational load, with the finest resolution (1 km) around nunataks and the fast-flowing outlet glaciers near the ice-cap margin. The mesh resolution decreased linearly towards the centre of the ice cap over 10 km, reaching a coarsest resolution of 4 km. Resolutions courser than this did not satisfactorily resolve all the features of interest, leading to difficulties in converging on a steady state.

The marine and land terminating regions of the ice cap were defined at this stage using both Landsat imagery (ArcGIS online, 2017) and previous studies (Dowdeswell et al., 2004; Burgess et al., 2005). To facilitate parallel computing, and thus considerably faster model run times, the mesh was subsequently split into seven parts using ElmerGrid. This simple mesh generating programme is based on the Serial Graph Partitioning and Fill-reducing Matrix

programme (METIS). Within model runs, the mesh was extruded into 3D with 10 equally-spaced vertical levels. To ensure ice flow was realistic in the small areas where ice thickness estimates were very small, a minimum ice thickness of 20 m was specified.

### *4.2.2 DEMs*

As it does not account for the fact that ice flux must be conserved, interpolating ice thicknesses from flight lines can potentially lead to unrealistic thickness estimates. This issue can lead to substantial flow divergence in high-resolution modelling (Seroussi et al., 2011). Several approaches have been proposed to overcome these problems, including: coarsening the mesh resolution to the flight line spacing (Seroussi et al., 2011); inverting for the bed topography (van Pelt et al., 2013); approaches based on mass conservation (Morlighem et al., 2011; Mosbeux et al., 2016); and relaxation of the surface DEM (Zwinger and Moore, 2009; Schafer et al., 2014). However, none of these approaches could be used in this study; coarsening the mesh to 10 km would not resolve the glaciers, inverting for the bed topography requires major assumptions about basal resistance (van Pelt et al., 2013) and time constraints prevented the application of mass conservation techniques and surface relaxation.

The decision was therefore made to adjust the thickness estimates only where they were clearly wrong. These anomalous thicknesses were largely limited to the margins of the topographically constrained outlet glaciers, where unrealistically high ice cliffs were present leading to the model producing rapid flow into the valley walls. Measures were therefore taken to reduce the size and number of these cliffs. At margins that remained problematic, it was also assumed that the velocity must equal zero - a reasonable assumption given that ice flow into a valley wall is not possible. Other anomalous flow patterns were seen inland to the south east, where the surface DEM and the presence of small nunataks indicated that mountains were present in an area between radar flight lines. Ice thicknesses were therefore manually reduced in these areas to achieve more realistic modelled velocities.

The surface DEM also presented some problems, as where datasets had been mosaiced together, tile edge artefacts produced anomalous slope estimates. Consequently, an attempt was made to reduce these artefacts; the surface for several hundred metres either

side of these boundaries was removed, and a smooth surface interpolated over the gap. Most interpolation techniques retained the rapid jump in heights between the tiles, thus linear interpolation, implemented using a MATLAB script, was applied. Although this approach did not completely remove the artefacts, they were substantially reduced. The adjusted surface and bed DEMs were then converted to an ASCII gridded XYZ (.xyz) files.

Another issue is that using just one surface DEM implies the ice cap has a fixed geometry. This is unlikely to be the case; the area covered by the ice cap declined by 338 ± 40 $km^2$ between 1959-1960 and 1999-2000 (Burgess and Sharp, 2004), and between 2000 and 2016, the termini of several outlet glaciers retreated 800-2200 m (Van Wychen et al., 2017). As well as changes in lateral extent, Devon Ice Cap has been found to be thickening slightly in the centre whilst thinning up to -0.23 ± 0.11 m $a^{-1}$ on some major outlet glaciers in the north and east (Colgan et al., 2008). This evidence suggests that the geometry of the ice cap will have evolved over the study period. However, changing the domain extent each year was not practical and only one complete, high-resolution surface DEM was available (Section 3.1.2). Furthermore, Schafer et al. (2012) found variations in the geometry of the 2,500 $km^2$ ice cap of Vestfonna, Svalbard, of a similar magnitude and over a similar timespan did not significantly affect obtained friction parameter fields. Changes to the ice cap geometry are therefore assumed to be small enough to not contribute substantially to error in the results.

### *4.2.3 Surface Temperature*

To approximate the annual mean surface temperature ($T_{surf}$) of the entire ice cap, a linear relationship between the surface elevation at any given location ($S(x)$) and temperature was assumed (Schafer et al., 2012; Gladstone et al., 2014; Gong et al., 2017):

$$T_{surf} = T_{sea} - \gamma S(x) \tag{4.1}$$

where $\gamma$ is the annual average lapse rate and $T_{sea}$ is the mean annual sea level temperature. Mair et al. (2005) and Shepherd et al. (2007) have estimated Devon Ice Cap's average lapse rate to be 0.0048 and 0.0046 K $m^{-1}$ respectively, but in this study $\gamma$ was assumed to be approximately 0.0045 K $m^{-1}$ based on Gardner et al.'s (2009) melt season value of 0.0049 K

$m^{-1}$ and a non-ablation season value of 0.0040 K $m^{-1}$. $T_{sea}$ around Devon Ice Cap is approximately -13.6 $^{o}$C (Mair et al., 2005). Once calculated, the map of surface temperature was converted to an ASCII gridded XYZ format. Although elevation will not be the only factor that influences mean annual temperatures, this approach is deemed sufficient as basal drag is not strongly dependant on surface temperature (Schafer et al., 2012).

### *4.2.4 Velocity*

The velocity data, provided in an ASCII format with a magnitude and orientation, were decomposed into x and y components using a MATLAB script and converted to TIFFs. Unfortunately, areas of no data existed in many of the velocity datasets. The majority of these holes were small, thus the application of an IDW algorithm was sufficient to fill them. However, for 2000, 2009 and 2012, more substantial areas were not covered. In these instances, large patches of no data were filled using data from the nearest available date, before the remaining, smaller holes were filled using IDW interpolation. Consequently, areas where these large patches of no data were found will not be analysed later in the thesis. Further issues arose with the mid-1990s data, as orientations were not available. The aspect of the surface DEM was therefore used to suggest the direction of flow. Once complete, the TIFFs produced were then converted to NetCDF (.nc) format, with one file for each year containing 3 variables specifying the magnitude, x component and y component.

### *4.2.5 Initial Estimate of Basal Friction*

To iterate towards more precise values of the basal friction coefficient ($\beta$), an initial estimate of $\beta$ is required. Although this guess does not have to be exact, appropriate values must be used as inverse methods are sensitive to initial estimates (Berger et al., 2016). For this reason, despite it assuming driving stress is entirely resisted by basal shear stress ($\tau_b$), the Shallow Ice Approximation (SIA) was used, where:

$$\tau_b = \rho_i g H sin(\alpha) \quad (4.2).$$

Surface slope ($\alpha$) and ice thickness ($H$) were estimated from the DEMs to generate the estimate of basal stress, which can be related to $\beta$ using a simple Weertman sliding law (Shapero et al., 2016):

$$\tau_b = \beta u_b^{\frac{1}{m}} \quad (4.3)$$

where $m$ is the stress exponent and $u_b$ is the basal velocity. Equation 4.3 was simplified further by assuming $m$ = 1 as, although more complex sliding laws have been formulated (e.g. Jay-Allemand et al., 2011), this achieves the most favourable convergence rates (Shapero et al., 2016), will converge on the same value of $\beta$ as alternative sliding laws (Morlighem et al., 2010; Minchew et al., 2016) and does not require the derivation of several parameters, which increases ambiguity (Arthern et al., 2015). As it was also assumed that surface and basal velocities are equal, an estimate of $\beta$ was easily obtained from the available data. To ensure the values of $\beta$ calculated by the model were always positive, its logarithm ($\alpha_p$) is used as the model input instead (Gillet-Chaulet et al., 2012):

$$\beta = 10^{\alpha_p} \quad (4.4).$$

Once prepared, this map of $\beta$ was also converted to an ASCII gridded XYZ format.

## 4.3 Inversion Modelling Principles

Before introducing the specificities of the model used in this study, the basic steps of the inversion process must be understood. These are as follows:

1. The required data are prepared and an initial estimate of the parameter being inverted for (in this case $\beta$) is made (Section 4.2).
2. A forward model of the ice cap is run, producing a surface velocity output.
3. The difference between the calculated and observed velocities is then assessed, and a minimisation procedure is used to adjust the parameter being inverted for to reduce the discrepancy.
4. Steps 2 and 3 are iterated to reduce this mismatch to a suitable level.

*4.3.1 The Forward Model*

The forward model component calculates the expected behaviour of the ice body given the input geometry, boundary conditions and estimate of the basal friction coefficient. The ice is modelled as an isotropic, incompressible, viscous fluid; thus, flow will depend on viscosity in accordance with Glen's Flow Law (Equation 3.3). The flow law exponent, $n$, is assumed to equal 3 and the rate factor, $A$, is calculated based on temperature using a version of the Arrhenius relation (Equation 3.4).

However, assuming the ice to be isotropic is perhaps unrealistic for Devon Ice Cap, as some parts are known to be underlain by patches of relatively soft Pleistocene ice (Koerner, 1977). Modelling of the nearby Barnes Ice Cap on Baffin Island accounting for areas of Pleistocene ice has suggested that some of the surface motion modelled to be sliding is instead a consequence of enhanced deformation of this ice (Gilbert et al., 2016). However, these effects do not appear to exceed ~30 m $a^{-1}$ and enhanced sliding will have little effect in areas where basal shear stress is low (Gilbert et al., 2016). For the fast-flowing glaciers of interest in this study, the effects are therefore likely to be minimal.

The 3D force balance is described by the Navier-Stokes equations. To determine all the components of the stress field, these equations must be solved by the forward component of the model. However, solving these partial differential equations in full is computationally expensive, thus approximations are frequently used (e.g. Greve, 1997). Simple approaches include the SIA, outlined in Section 4.2.5, and the Shallow Shelf (or Shelfy Stream) Approximation (SSA), which assumes basal shear stress is negligible. The SIA and SSA can be combined in 'hybrid' models to utilise either one where it is more appropriate, and this can produce useful results (Habermann et al., 2013; van Pelt et al., 2013; Bernales et al., 2017). Other approximations include 'higher-order' models, which incorporate more stress components (e.g. Pattyn, 2003). These approaches may be sufficient in many circumstances, leading to the development of models which automatically decide on which level of approximation is sufficient (Ahlkrona et al., 2016).

However, where ice thickness varies rapidly, bridging effects can lead to simplified models overestimating basal drag (Morlighem et al., 2010). If the computing power is available, problems arising from simplifications can be avoided by using 'full-Stokes' models, which

solve the Navier-Stokes equations in full. As the results from such models are often noticeably different from the results of even higher-order models (Pattyn et al., 2008), the full-Stokes modelling software Elmer/Ice (Gagliardini et al., 2013) was used in this study. Elmer/Ice is open-source, uses a 3D finite element approach and has been demonstrated to be well-suited to glaciological inversion modelling (Jay-Allemand et al., 2011; Gillet-Chaulet et al., 2012; Schafer et al., 2014).

Elmer/Ice also solves for temperature, which will strongly influence the value of $A$ (Equation 3.4). Instead of assuming a constant temperature, temperatures are calculated by iteratively solving the advection-diffusion equation, producing more accurate values of $A$. It should be noted that instead of imposing a maximum temperature equal to the PMP, a constant upper temperature limit (273 K) was used for the inversions to increase model stability and aid convergence. As ice thicknesses are only a few hundred metres, this was assumed to be a reasonable approximation.

To define the processes occurring at the edges of the ice cap, boundary conditions must be defined. At the ice cap edges, marine and land-terminating regions were defined at the meshing stage (Section 4.2.1). Whereas land-terminating margins were assumed to be stress-free and left to evolve freely, where the ice cap reaches the sea the backstress imposed by the ocean-water pressure on the calving front must be considered. This is given as:

$$P_w = \rho_w g (z_x - h_w) \tag{4.5}$$

where $P_w$ is water pressure, $\rho_w$ is water density, $z_x$ is the ice depth below the water line and $h_w$ is the water level elevation. The upper surface was considered stress-free, with the following Neumann boundary condition applied (Jay-Allemand et al., 2011):

$$\boldsymbol{\sigma} \cdot \boldsymbol{n} = 0 \tag{4.6}$$

where $\boldsymbol{\sigma}$ is the Cauchy stress tensor and $\boldsymbol{n}$ is the normal unit vector.

Surface temperature was set to the mean annual surface temperature based on elevation (Section 3.2.3). For the lower surface, a uniform geothermal heat flux was specified as well as a frictional heating component. Based on a study of the Canadian Arctic Archipelago (Majorowicz and Embry, 1998), the geothermal heat flux was estimated to be approximately

40 mW $m^{-2}$. Similar values were also derived by Paterson and Clarke (1978), who tuned parameters including the geothermal heat flux to measured borehole temperature profiles.

However, the basal temperature produced were often several degrees below PMP beneath the major outlet glaciers. This is unrealistic; these regions reach speeds that imply a warm bed must be present. A boundary condition specifying that the bed must reach the upper temperature limit when velocities exceed 30 m $a^{-1}$ was therefore applied.

### *3.3.2 The Inverse Model*

Once the forward model has been run, the inverse component of the model then seeks to minimise the difference between the observed and calculated surface velocities by altering the estimate of the parameter being inverted for. Many approaches to inversions exist, including the Robin inverse method (Arthern and Gudmundsson, 2010), the adjoint-based inexact Gauss-Newton method (Petra et al., 2012) and Bayesian methods (Raymond and Gudmundsson, 2009; Petra et al., 2014; Arthern et al., 2015). However, in this study the control method was selected. This method was applied in the pioneering works of MacAyeal (1992, 1993) and continues to be widely used (Gillet-Chaulet et al., 2012; Khazendar et al., 2015; Gong et al., 2017). The control method regularly involves adjoint equations, and is therefore often referred to as the adjoint method (Arthern et al., 2015).

Gillet-Chaulet et al. (2012) provide a detailed explanation of the equations used by the adjoint method, which are outlined here. This method assesses the difference between the modelled horizontal velocity ($u_H$) and the observed horizontal velocity ($u_H^{obs}$) using a cost function. The initial term measuring the square of the difference in velocities ($J_0$) is given by Gillet-Chaulet et al. (2012) as:

$$J_0 = \int_{\Gamma_s} \frac{1}{2} (|u_H| - |u_H^{obs}|)^2 \, d\Gamma \tag{4.7}$$

where $\Gamma$ is the model domain. However, the $J_0$ term alone is not sufficient to compute stable solutions to inverse problems; a regularisation method must be used (Golub et al., 1999). In this study, Tikhonov regularisation was applied (Tikhonov and Arsenin, 1977), which penalises dramatic oscillations by assessing the first spatial derivative (Furst et al., 2015). The regularisation term ($J_{\mathrm{reg}}$) therefore takes the form of:

$$J_{\mathrm{reg}} = \frac{1}{2}\int_{\Gamma_b}\left(\frac{\partial\alpha_p}{\partial \mathrm{x}}\right)^2 + \left(\frac{\partial\alpha_p}{\partial \mathrm{y}}\right)^2 d\Gamma \quad (4.8)$$

(Gillet-Chaulet et al., 2012). Note the use of $\alpha_p$ as opposed to $\beta$ (Equation 4.4), as the potential for the minimisation process to produce negative values of $\beta$ is avoided and the output is smoother (Cook, 2016). Following Gillet-Chaulet et al. (2012), the overall cost function ($J_{tot}$) is therefore:

$$J_{tot} = J_0 + \lambda J_{reg} \quad (4.9)$$

where $\lambda$ is the regularisation parameter, which controls the amount of regularisation applied. If this is too large, the regularisation term will dominate $J_{tot}$, producing a smoother result at the expense of potentially important detail and increased mismatch with observed velocities. Conversely, if $\lambda$ is too small, the result will match observations very well, but data errors will dominate and a level of detail higher than is physically possible to resolve will be produced (Konovalov and Nagornov, 2015; Shapero et al., 2016).

To select the optimal value of $\lambda$, it is common to plot the value of the initial cost function term ($J_0$) against the regularisation term ($J_{reg}$) and produce an L-curve, as the value of $\lambda$ nearest the inflection point will represent the best compromise (e.g. Habermann et al., 2013; Konovalov and Nagornov, 2015; Berger et al., 2016; Shapero et al., 2016). This optimal value is controlled by the mesh resolution and signal-to-noise ratio of the measurements constraining the model (Hansen, 1999; Shapero et al., 2016). The L-curve produced from this study (Fig. 4.4) led to $\lambda = 10^{8.5}$ being selected because for values above this, $J_{reg}$ increases rapidly with little appreciable decrease in $J_0$, whilst for lower values of $\lambda$ the opposite is true.

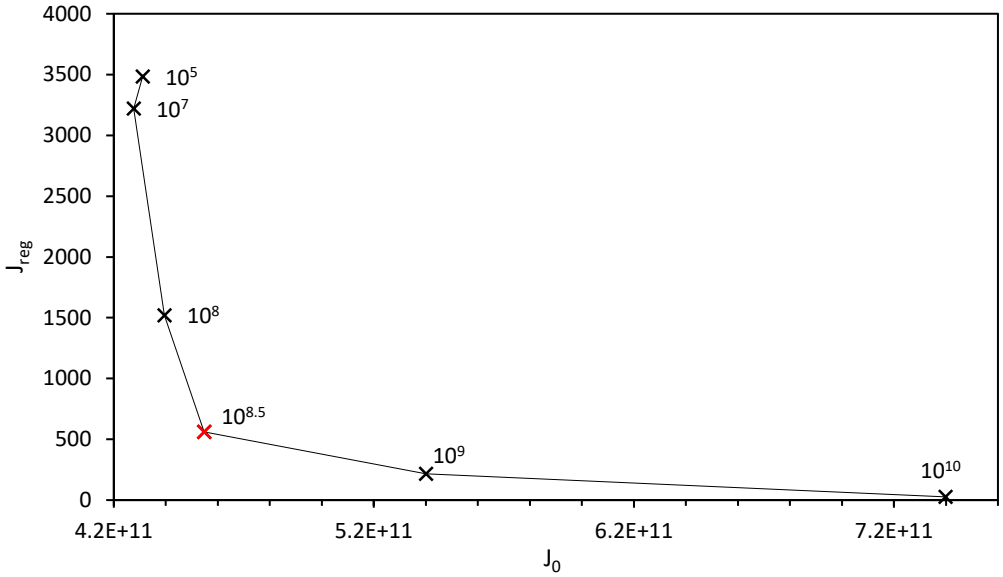


*Figure 4.4. L-curve produced by plotting the initial cost function value against the value of the regularisation term for different values of the regularisation parameter. The optimal value ($\lambda = 10^{8.5}$) is highlighted in red.*

Once the total cost function ($J_{tot}$) has been formulated, it is then minimised; in this study, Gilbert and Lemaréchal's (1989) M1QN3 routine was used. This is more efficient than a fixed-step minimisation process as it uses a limited-memory quasi-Newtonian iterative system based on the second derivatives of the cost function (Cook, 2016). The Biconjugate Gradient Stabilised Method (BicGStab) (van der Vorst, 1992), preconditioned through Incomplete LU factorisation, was implemented to accelerate the convergence process.

## 4.4 Basal Melting/Freezing and Till Water Storage

### *4.4.1 Basal Freezing/Melting Rates*

Following the calculation of the basal drag, an approximation of the rate of melting/freezing beneath many fast-flowing areas was also possible. Thermal energy is provided to the bed by geothermal heating, friction and the release of latent heat by freezing meltwater. These gains must be balanced by the removal of heat by conduction to the surface and the melting of ice. The basal melt rate ($\dot{m}$) can therefore be calculated using:

$$\dot{m} = \frac{\tau_b u_b + G - K\theta_b}{\rho_i L} \tag{4.10}$$

where $L$ is the specific latent heat of fusion (333.5 kJ kg$^{-1}$), $K$ is conductivity and $\theta_b$ is the vertical basal temperature gradient (Tulaczyk et al., 2000b; Christoffersen et al., 2014). Friction heating is the product of basal shear stress and basal velocity, and the geothermal heat flux ($G$) is given by the thermal boundary condition as 0.04 W m$^{-2}$. $K$ is dependent on the temperature of the ice, following (Cuffey and Paterson, 2010):

$$K = 9.828 \exp(-5.7 \times 10^{-3}\, T_i) \tag{4.11}$$

### *4.4.2 Till Water Content*

By combining equations (3.7) and (3.8) and assuming $\tau_f = \tau_b$, the void ratio can be calculated from the modelled basal traction (Bougamont et al., 2014):

$$\tau_f = N_0 \tan(\varphi)\, 10^{-\left(\frac{e-e_0}{C}\right)} \tag{4.12}$$

Clarke (1987) provides experimentally-derived values for the constants in this equation, which are relatively similar to those from tills in Svalbard (Murray, 1997). The porosity ($n_p$) can therefore be calculated from the model outputs as void ratio is related to porosity through:

$$n_p = \frac{e}{e+1} \tag{4.13}.$$

To estimate the water volume stored in the till layer, the porosity can be multiplied by the volume of till likely to be present, which requires an estimate of till thickness. Beneath a surging glacier in Svalbard, minimum estimates of till depth varied between 0.08 and 0.55 m, averaging 0.2 m (Murray and Porter, 2001). Consequently, a depth of 0.3 ± 0.2 m is used in this study as this encompasses all the likely values.

## 4.5 Error Analysis

A disadvantage of numerical inversions is the difficulty in quantifying error (Gillet-Chaulet et al., 2016). For this reason, instead of providing a direct indication of the uncertainty of the measurement, the standard deviations provided in the following analyses represent the spatial variability of the data. To give some idea of the degree of error in the inversion, the

difference between the observational ($u_{obs}$) and modelled ($u_{mod}$) flow velocities was assessed for 2013. Following the approach of Gong et al. (2016), the absolute ($\varepsilon$) and relative ($\eta$) errors are given by:

$$\varepsilon = |u_{mod}| - |u_{obs}| \tag{4.14}$$

$$\eta = \frac{|\varepsilon|}{|u_{obs}|} \times 100 \tag{4.15}.$$

Areas where the model failed to match the velocities accurately will produce high values for these errors. To exclude areas where errors are likely to dominate, areas with ice thicknesses of less than 30 m were excluded when analysing results. The calculations were also limited to areas with a modelled basal velocity of >20 $ma^{-1}$, as above this threshold it is reasonable to assume significant basal motion is occurring, making these the areas of interest when studying dynamics.

# 5. Results

This chapter presents the results of the numerical inversion modelling of Devon Ice Cap, including the temperature and basal shear stress outputs, before using these data to calculate further properties such as the rates of basal melting/freezing and changes to the quantity of water stored within the basal till layer.

## 5.1 Temperature

### *5.1.1 Englacial Temperature Profiles*

Modelled temperature profiles from the lower reaches of Sverdrup and Belcher Glaciers (Fig. 5.1A) and from slightly to the north west of the summit of the ice cap (Fig. 5.1B) were examined to investigate the predicted englacial temperatures. Both Sverdrup and Belcher Glacier's profiles show the effect of advection of cold ice from the interior, with temperatures slightly lower at depth than at the surface. Belcher Glacier also has a bed that reaches PMP, giving a steeper temperature gradient towards the base.

Sverdrup Glacier and the summit location were chosen as these are the sites of boreholes where englacial temperatures have been measured, allowing comparison between the model results and observational data. Temperatures from a shallow (15 m) borehole in the lower reaches of Sverdrup Glacier (Keeler, 1964) suggest an approximately one degree overestimation of modelled near surface temperatures in this location (~-16.0 $^{o}$C measured versus -15.3 $^{o}$C modelled at 10 m depth). The modelled summit temperatures were also approximately a degree warmer than those measured in the upper few metres of fully-penetrating boreholes (Paterson and Clarke, 1978), suggesting the input surface temperatures (see Section 4.2.3) are consistently approximately 1 $^{o}$C too warm.

However, modelled temperatures at depth are in very close agreement with those measured by Paterson and Clarke (1978); at 300 m, these were approximately -18.4 $^{o}$C and -18.2 $^{o}$C, respectively. Due to inaccuracies in the interpolated measurements, the modelled ice thickness was ~385 m opposed to the ~305 m measured (Paterson and Clarke, 1978), but it still seems likely that the modelled basal temperatures are accurate for the model geometry that was used.

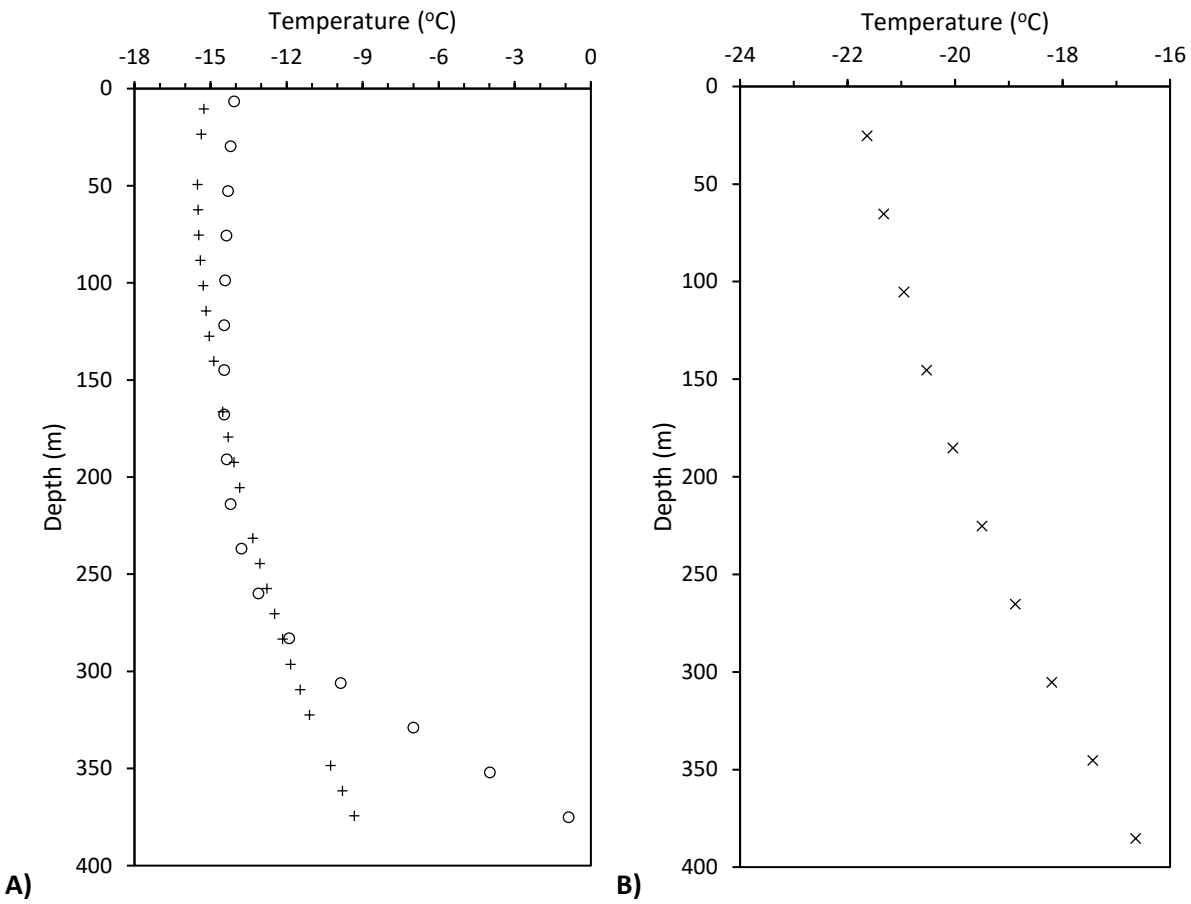


*Figure 5.1. Modelled temperature profiles for the lower reaches of Sverdrup (crosses) and Belcher (circles) Glaciers (A), as well as the summit region (B). Note the different temperature scales. The locations of the profiles are indicated in Fig. 5.2. The glacier bed is represented by the depth to the lowest point shown.*

### *5.1.2 Basal Temperatures*

There is relatively little change in the modelled basal temperatures between years for most of the ice cap, probably because of the constant geometry, surface temperatures and geothermal heat flux used. The majority of the ice cap is frozen to the bed, except for beneath the major glaciers which consistently reach pressure melting point (Fig. 5.2A). However, some changes are distinguishable. For example, from 2009 onwards, the shared terminus region of Southeast1 Glacier and Southeast2 Glacier (located in Fig. 2.2) reaches the PMP (Fig. 5.2). This is likely to be linked to the beginning of the active phase of the surge of SE1/2 in about 2009 (Section 2.5). Furthermore, the warm-bedded area beneath East5 Glacier expands substantially during the pulse in 2009, before returning to similar conditions to before the event (Fig. 5.2).

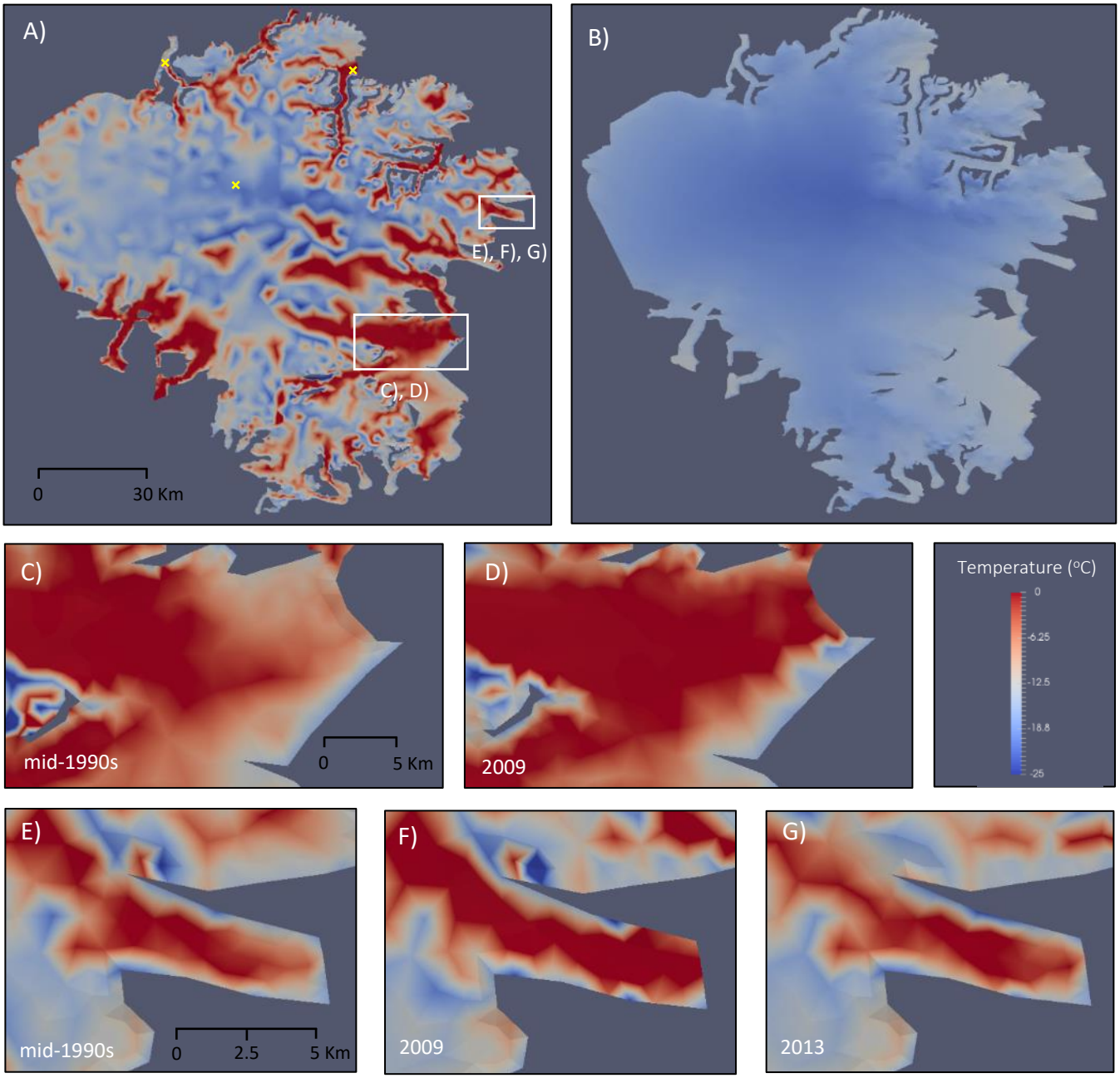


*Figure 5.2. The modelled basal temperature for the entire ice cap in 2014 (A) alongside the input surface temperature as described in Section 4.2.3 (B). The locations of the temperature profiles in Fig. 5.1 are displayed as yellow crosses in A). Data for all years are not displayed because modelled basal temperatures are largely consistent from year to year. Instead, the areas of notable change are highlighted in (C) to (F), which show the lower reaches of Southeast1 Glacier and Southeast2 Glacier (C and D) and East5 Glacier (E, F and G). Years that each image represents are indicated in the lower left-hand corner.*

## 5.2 Basal Shear Stress

### *5.2.1 Spatial Distribution*

In the frozen interior of the ice cap, the driving stress is expected to approximately equal the basal shear stress ($\tau_b$). This explains features such as the east-west strip of low $\tau_b$ near the centre of the ice cap and the patch of low $\tau_b$ towards the south west ((i) in Fig. 5.3E), as these areas are approximately located beneath the major ice divides (Dowdeswell et al., 2004). Low driving stresses also explain the consistently low $\tau_b$ in the piedmont region to the south east ((ii) in Fig. 5.3E). As expected, the majority of the beds of the marine-terminating glaciers have a low $\tau_b$, facilitating fast ice flow.

However, as surface slope increases further away from the ice divides but the bed is still frozen, most the ice cap interior has a relatively high $\tau_b$. This is particularly noticeable near the heads of some of the fast-flowing outlet glaciers (e.g. (iii) in Fig. 5.3E); in these regions, it is likely that the ice is still frozen to the bed, but there are steep surface slopes and increased longitudinal stress gradients as ice begins to be removed more efficiently downstream (Cook, 2016). There are also patches of high basal drag (or 'sticky spots') beneath some glaciers in all years (Fig. 5.3). The largest and most persistent of these is the spot of high basal drag on Belcher Glacier a few kilometres west of the terminus (Fig. 5.3F). Although this varies in magnitude and exact location, it is always present.

However, some small patches of high $\tau_b$ – especially those located in the south-eastern parts of the ice cap – are likely to be a result of anomalous ice thicknesses (e.g. (iv) in Fig. 5.3E). In these cases, it is probable that mountains are present in the surface DEM, but poorly resolved in the basal DEM as they were between flight lines, giving high surface slopes, large ice thicknesses and therefore very fast calculated surface velocities. As the observed surface velocities in these areas are low, the inversion procedure attempts to counter the fast flow by producing very high values of $\beta$. Nevertheless, the results in these areas will not affect modelled conditions beneath the major tidewater glaciers which are the areas of primary interest.

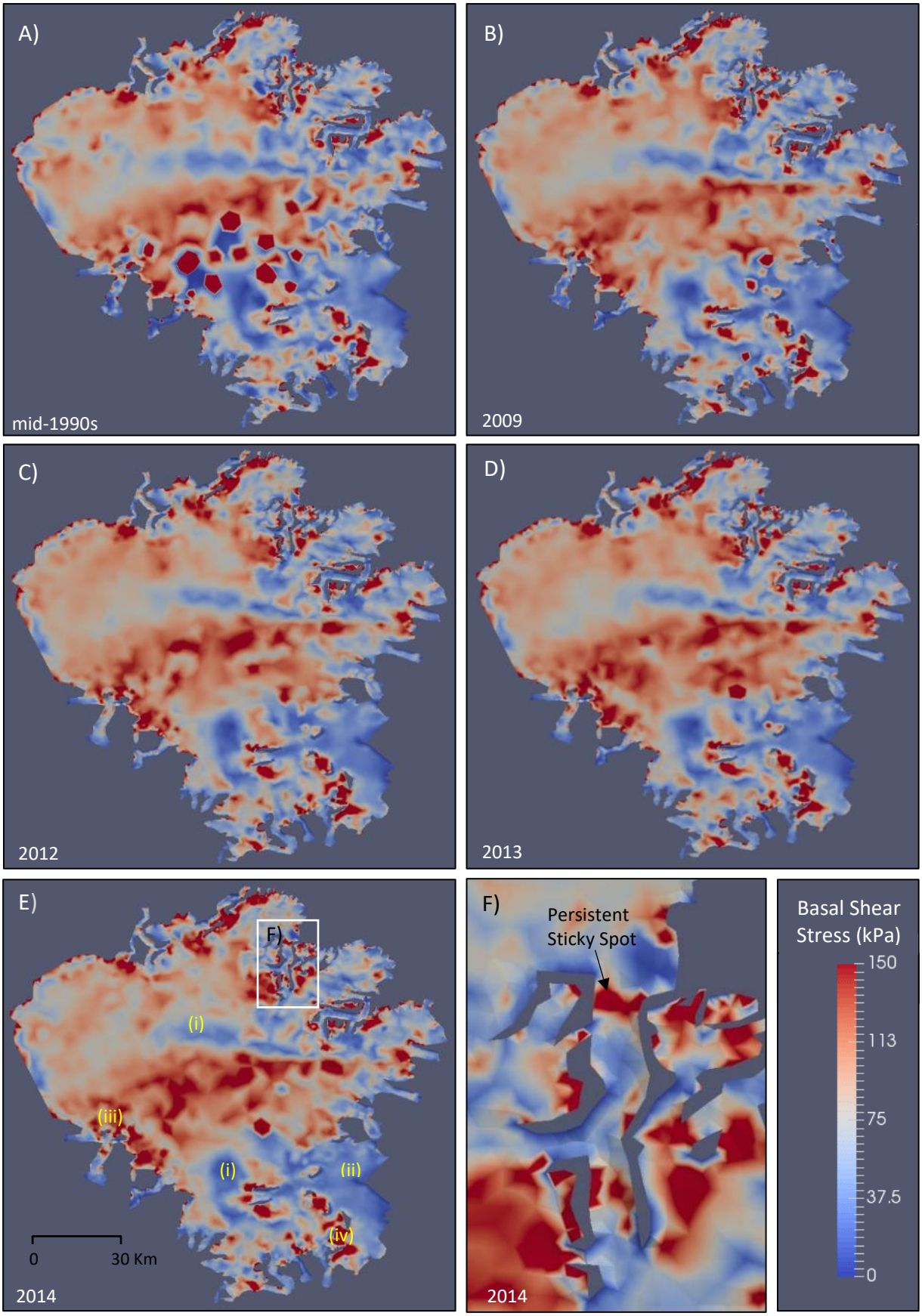


*Figure 5.3. Modelled basal shear stress distribution for the mid-1990s (A), 2009 (B), 2012 (C), 2013 (D) and 2014 (E). (i) to (iv) in E) correspond to descriptions in the text. Patches of high basal shear stress beneath Belcher Glacier in 2014 are shown in F).*

*5.2.2 Temporal Variations*

There are several clear changes to the distribution of basal shear stress beneath the major marine-terminating glaciers (Fig. 5.3, 5.4). Perhaps the most noticeable change is the increase in basal drag beneath the Croker Bay Glaciers between 2009 and 2012 (Fig. 5.4B) accompanying the fall in velocity (Table 5.1). Other years see fluctuations in $\tau_b$ on both these glaciers, but there is no clear overall trend (Fig. 5.3). The active phase of the pulsing glaciers East5 Glacier and East7 Glacier also had a clear effect on $\tau_b$. Both saw a significant drop between the mid-1990s and 2009 (Fig. 5.4C, E) which was completely reversed by 2012/3 (Fig. 5.4D, F). The terminus region of SE1/2 was also subject to a drop in basal shear stress following the beginning of the active phase (Fig. 5.4A).

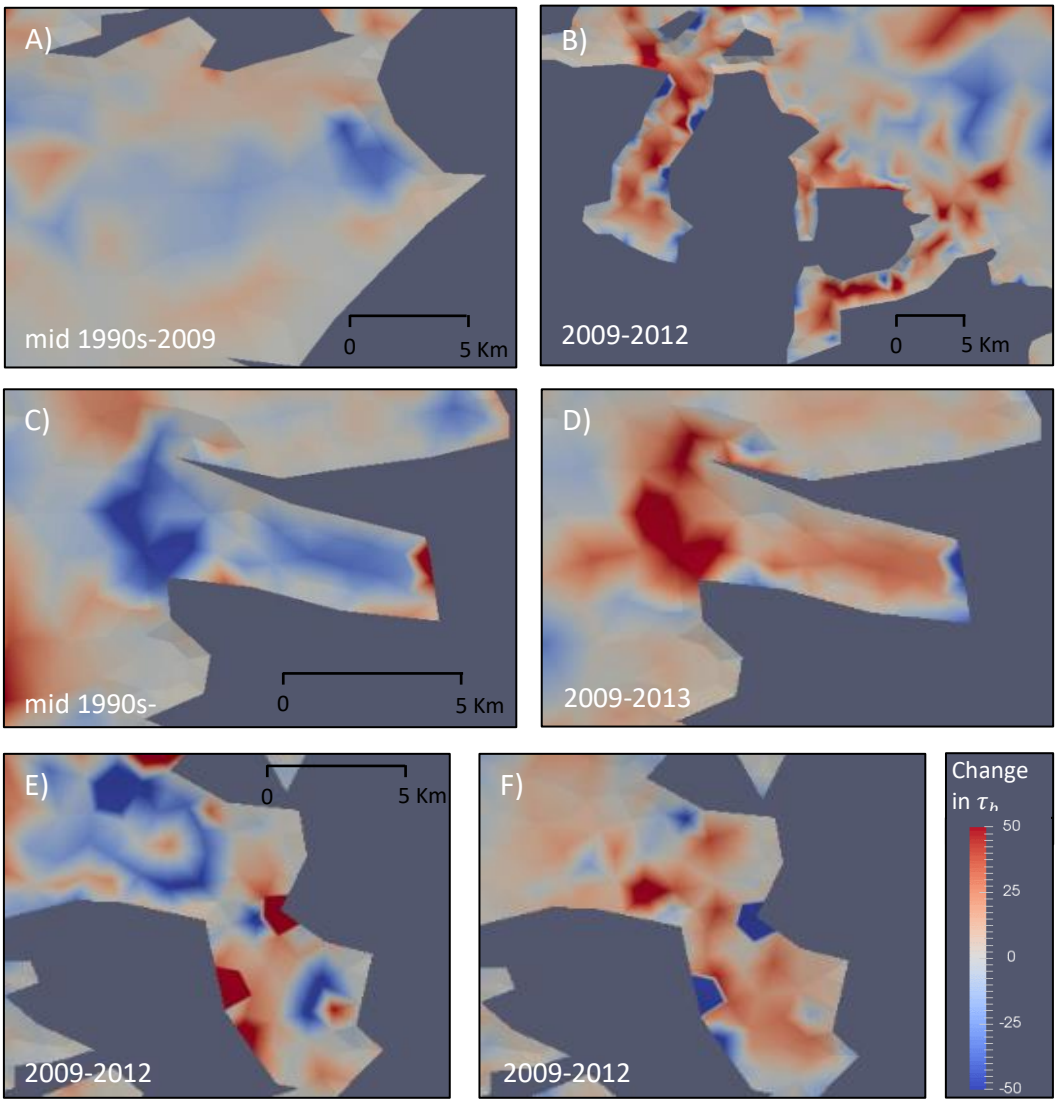


*Figure 5.4 Change in basal shear stress in areas of most interest. Dates over which the change took place are indicated in the bottom left corner of each image. A) shows the terminus of glaciers SE1/2 at the start of the surge, B) the slow-down of the Croker Bay Glaciers NCB and SCB, C) and D) The pulse of East5 Glacier, and E) and F) the pulse of East7 Glacier. All glaciers are located in Fig. 2.2.*

However, the pulse of Fitzroy Glacier is less clearly defined (Fig 5.3, Table 5.1). In 2009, mean velocities are the greatest and $\tau_b$ values the lowest, but this trend is not particularly obvious. This is perhaps because velocities peaked in 2005 (Van Wychen et al., 2017), so it was not possible to compare changes betwen the years of fastest and slowest flow with the velocity data used in this study. Additionally, the majority of this velocity variability was located in the 1.5 km section of the trunk nearest the terminus, but the sliding area of Fitzroy Glacier actually extends nearly 20 km inland (Van Wychen et al., 2017). As the model resolution was only 1 km, this large sliding area could therefore easily have obscured any trend in the means in Table 5.1.

The acceleration of Belcher Glacier is also indistinguishable in statistics for the entire glacier (Table 5.1), again probably due to the large sliding area and limited spatial extent of velocity change. The 3 km nearest the calving front was therefore considered separately (Table 5.1). Standard deviations remain large due to major discrepancies between areas near the lateral margins and the centre of the trunk, resulting in little trend in $\tau_b$. However, the mean velocity increases and peaks in 2013, consistent with Van Wychen et al. (2017).

Although there are marginally lower basal shear stresses and faster velocities in 2009 (Table 5.1), changes to velocities and basal shear stresses in the upper areas of SE1/2 are relatively small. The terminus region is subject to a much larger acceleration; in the mid-1990s, velocities barely exceed 10 m $a^{-1}$, but these increase to an average of >40 m $a^{-1}$ during the surge (Table 5.1). However, the fall in $\tau_b$ is surprisingly small given that the lower regions transitioned from largely cold-based to warm-based (Fig. 5.2C/D). The relatively small change is instead viewed as inaccuracy in the model, an assumption supported by the large errors in this region (Fig. 5.8).

*Table 5.1 Changes in A) $\tau_b$ (kPa) and B) basal velocity (m a $^{-1}$) for the sliding area of each major glacier over time. Glaciers are located in Figure 2.2. * indicates that there was poor velocity data coverage for that year, with some data filled from the nearest year; for East5 Glacier in 2012, no velocity data were available. † indicates that there was a very small sliding area, with statistics calculated from relatively few data points. ‡ indicates situations where the basal velocities did not exceed 20 m a$^{-1}$ (i.e. there was no basal sliding), so an area similar to other years was selected to provide statistics for comparison.*

| Glacier | Year | | | | |
|---|---|---|---|---|---|
| | **Mid-1990s** | **2009** | **2012** | **2013** | **2014** |
| Belcher | 73.17±54.42 | 60.88±57.96 | 63.21±65.17 | 62.37±62.43 | 65.82±61.37 |
| Belcher Terminus | 19.74±18.20 | 58.90±49.20 | 64.01±65.97 | 69.47±119.71 | 55.53±70.87 |
| Eastern | 72.98±48.12 | 86.94±52.82 | 87.93±40.61* | 96.57±47.58 | 95.42±66.62 |
| Fitzroy | 46.44±34.63 | 43.23±68.15 | 47.21±59.69 | 48.07±24.03 | 48.16±46.40 |
| East7 | 51.21±38.90* | 34.70±19.61 | 42.38±18.28 | 48.74±24.03 | 42.63±14.91 |
| East5 | 52.48±13.22† | 39.33±23.22 | No Data | 49.01±10.38† | 73.47±24.17‡ |
| SE1 | 44.68±27.06 | 35.20±21.33 | 46.63±27.30 | 47.35±27.03 | 45.29±27.59 |
| SE2 | 46.59±36.83 | 42.65±21.04 | 51.88±22.22 | 43.67±17.94 | 40.48±17.37 |
| SE1/2 Termini | 42.91±14.84‡ | 28.63±10.59 | 41.07±18.72 | 31.64±18.11 | 36.73±22.60 |
| NCB | 65.14±50.30 | 62.61±53.31 | 85.20±49.62 | 83.19±55.03 | 83.42±54.84 |
| SCB | 36.22±36.87 | 50.43±34.75 | 64.76±32.81 | 60.71±34.77 | 56.67±41.40 |

**A)**

| Glacier | Year | | | | |
|---|---|---|---|---|---|
| | **Mid-1990s** | **2009** | **2012** | **2013** | **2014** |
| Belcher | 69.68±45.79 | 70.41±38.72 | 66.28±43.15 | 66.90±47.68 | 63.58±45.30 |
| Belcher Terminus | 90.94±70.36 | 59.61±62.26 | 94.41±80.30 | 118.05±89.09 | 98.98±86.29 |
| Eastern | 46.51±14.45 | 39.23±16.30 | 40.68±14.35* | 36.84±15.38 | 35.77±17.15 |
| Fitzroy | 46.51±30.64 | 57.90±30.69 | 55.86±37.60 | 42.95±35.37 | 52.11±37.28 |
| East7 | 59.48±34.02* | 66.15±28.31 | 47.17±18.79 | 52.30±19.62 | 47.44±13.14 |
| East5 | 25.26±5.14† | 81.08±41.92 | No Data | 28.54±3.12† | 12.96±2.44‡ |
| SE1 | 34.92±12.42 | 40.39±12.45 | 32.52±8.58 | 31.21±8.89 | 31.09±7.63 |
| SE2 | 29.99±5.94 | 41.41±18.06 | 38.49±17.02 | 38.00±16.97 | 38.01±14.32 |
| SE1/2 Termini | 7.97±2.63‡ | 39.23±7.43 | 42.78±17.86 | 53.17±24.30 | 39.92±15.59 |
| NCB | 71.88±42.45 | 74.09±31.17 | 33.21±9.91 | 30.98±8.15 | 38.31±10.48 |
| SCB | 88.23±56.44 | 77.58±39.71 | 67.59±26.68 | 66.45±26.51 | 83.70±40.63 |

**B)**

## 5.4 Basal Melting/Freezing Rates

### *5.4.1 Spatial Patterns*

Determining the basal heat budget using outputs from the numerical model allows the calculation of expected melting/freezing rates (Section 4.4.1). However, these values display a large amount of spatial variation even under different parts of the same glacier (Fig. 5.5), yielding high standard deviations on mean values (Table 5.2). Errors on these calculations are difficult to quantify, but are likely to be reasonably large, so only clear trends will be treated as accurate.

Freezing is widespread beneath Fitzroy Glacier in all years (Fig. 5.5C; Table 5.2). This is probably a result of a high basal temperature gradient promoting freezing, alongside the low basal drag producing little frictional heating despite rapid flow velocities (Table. 5.1). Conversely, the bed of Belcher Glacier is subject to net melting in nearly all years (Table 5.2). This might seem unusual considering that is also has high basal temperature gradients (Fig. 5.1A), but both velocities and $\tau_b$ are substantially higher on Belcher Glacier (Table 5.1), increasing the frictional component. The patch of high $\tau_b$ located near to the point when the northern arm of the glacier joins may also be partly responsible for increasing the mean, as this is underlain by an area of intense melting (Fig. 5.5C).

Melt rates beneath SCB vary signficantly over its length; in the upper region, melting dominates, but near the terminus there are substantial amounts of freezing (Fig. 5.5D). Although NCB is almost entierly subject to melt at the bed, this pattern is still visible to some extent. Ths drop downstream may be a result of reduced basal drag towards the terminus as the glacier bed falls below sea level (Fig. 5.3), leading to a drop in frictional heating. Differences between the upper regions of SE1 and SE2 are also present; whereas SE1 is dominated by melting, SE2 is on average consistently freezing (Table 5.1).

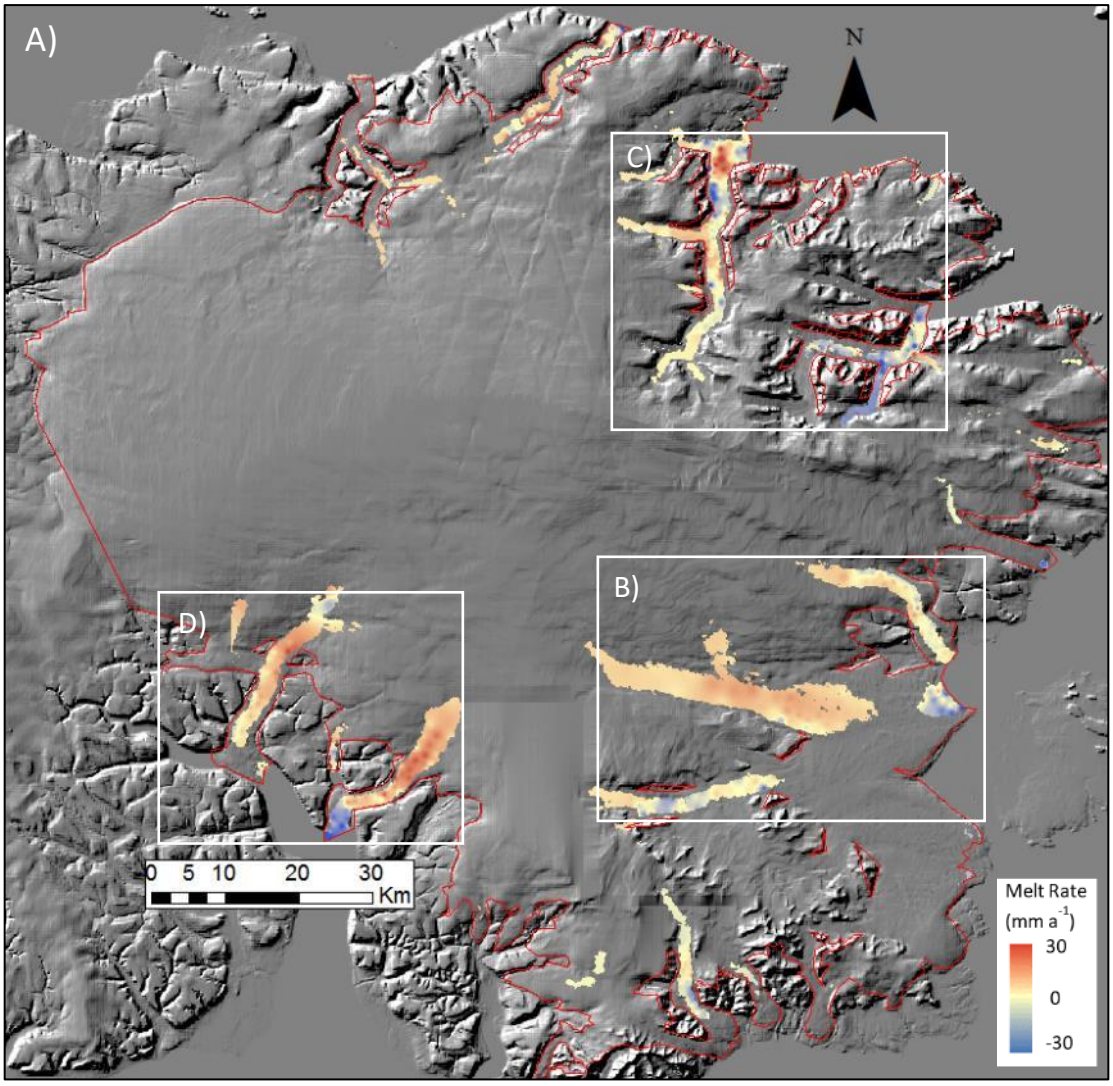
A)
N
C)
B)
D)
0 5 10 20 30
Km
Melt Rate
(mm a-1)
30
0
-30

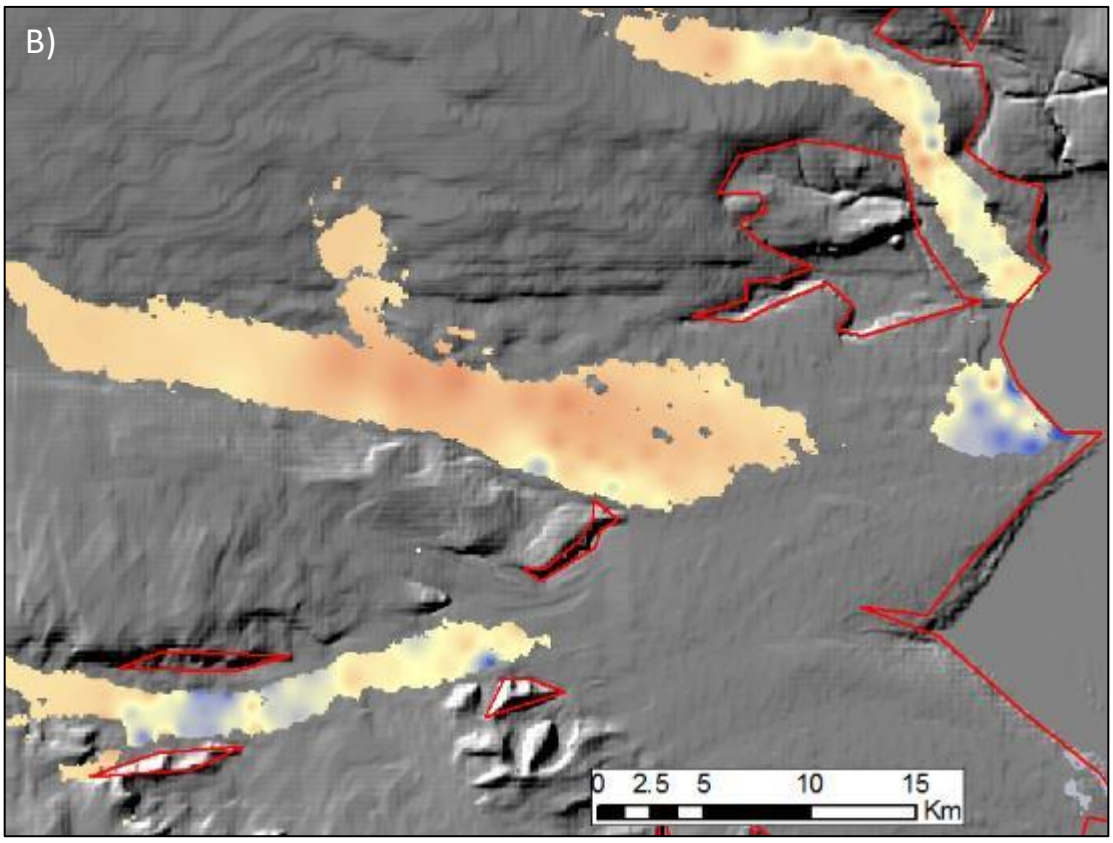
B)
0 2.5 5 10 15
Km

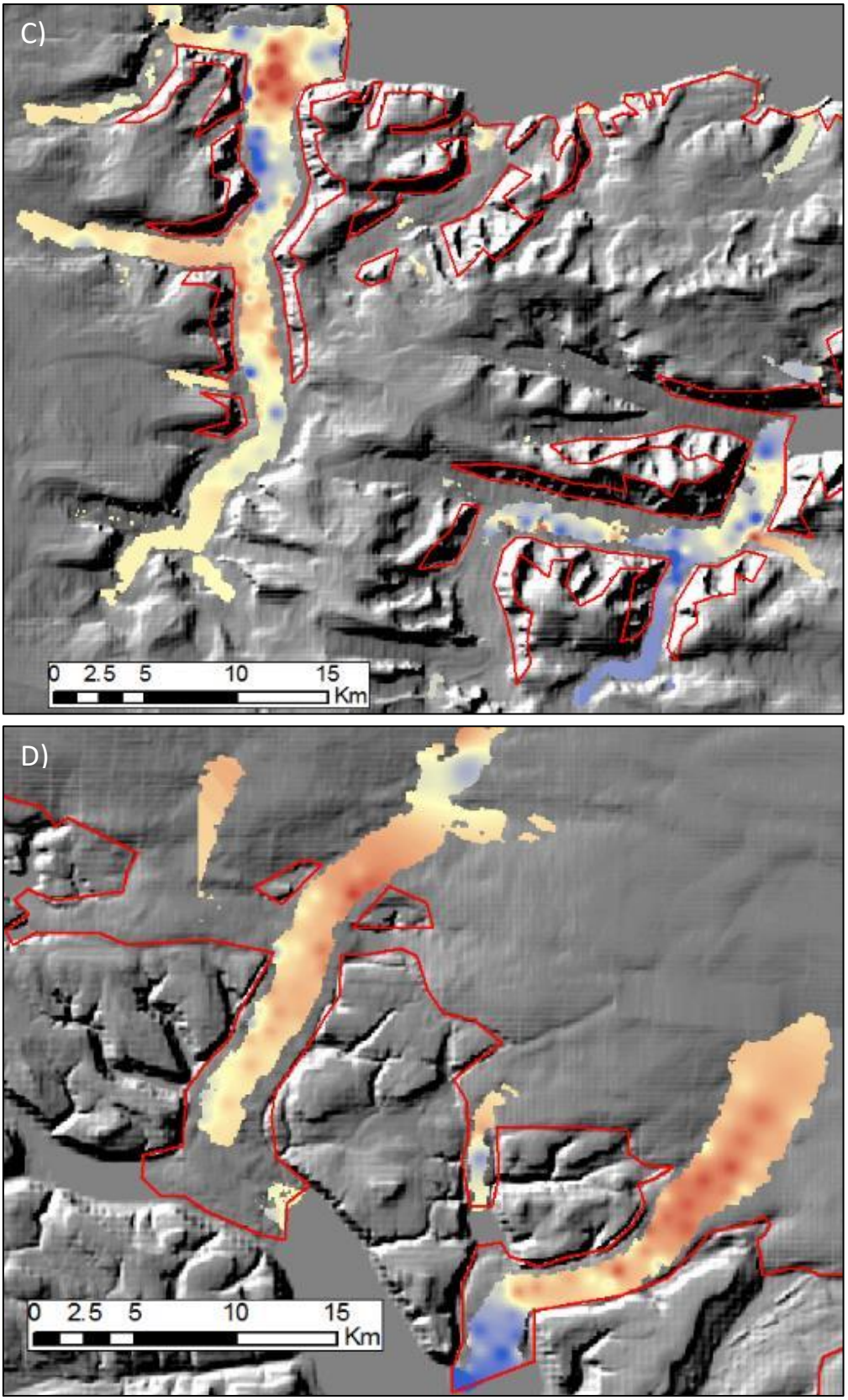


*Figure 5.5. A) Basal melting/freezing rates interpolated from reliable data points beneath the sliding area of the ice cap in 2013, overlaid on a hillshade of the surface DEM. Boxes B), C) and D) are located in A). B) Shows SE1, SE2 and East7 Glacier, C) Belcher Glacier and Fitzroy Glacier and D) The Croker Bay Glaciers. A) Indicates the position of B), C) and D). The red line indicate the model domain.*

*Table 5.2. Basal melting/freezing rates beneath the sliding areas of each glacier in each year, given as a mean ± one standard deviation. If the sliding area changes substantially, the approximate maximum extent was used. * indicates that there was poor velocity data coverage, with some data filled from the nearest year; for East5 Glacier in 2012, no velocity data were available. † indicates that there was a very small sliding area, with statistics calculated from relatively few data points. ‡ indicates situations where the basal velocities did not exceed 20 m $a^{-1}$ (i.e. there was no definite basal sliding), so an area similar to other years was selected to provide statistics for comparison.*

| **Glacier** (Fig. 2.2) | **Sliding Area ($km^2$)** | **Parameter** | **Year** | | | | |
|---|---|---|---|---|---|---|---|
| | | | **Mid-1990s** | **2009** | **2012** | **2013** | **2014** |
| Belcher | 56.0 | Mean Melt rate (mm $a^{-1}$) | -0.72 ± 28.07 | 4.02 ± 18.76 | 7.08 ± 15.96 | 3.69 ± 24.84 | 1.18 ± 16.84 |
| | | Water Volume Equivalent ($10^3$ $m^3$ $a^{-1}$) | -40.32 | 225.12 | 396.48 | 206.64 | 66.08 |
| Belcher Terminus | 4.1 | Mean Melt rate (mm $a^{-1}$) | 0.78 ± 12.78 | 2.03 ± 9.55 | 4.15 ± 9.77 | -1.92 ± 10.88 | -2.97 ± 10.82 |
| | | Water Volume Equivalent ($10^3$ $m^3$ $a^{-1}$) | 3.18 | 8.28 | 16.93 | -7.83 | -12.12 |
| Eastern | 7.6 | Mean Melt rate (mm $a^{-1}$) | 3.82 ± 13.79 | 2.78 ± 17.07 | -3.02 ± 21.68* | -0.61 ± 25.13 | 1.41 ± 17.66 |
| | | Water Volume Equivalent ($10^3$ $m^3$ $a^{-1}$) | 29.03 | 21.13 | -22.95* | -4.64 | 10.72 |
| Fitzroy | 40.6 | Mean Melt rate (mm $a^{-1}$) | -7.12 ± 23.39 | -9.50 ± 18.46 | -6.74 ± 20.68 | -6.13 ± 17.95 | -4.47 ± 19.89 |
| | | Water Volume Equivalent ($10^3$ $m^3$ $a^{-1}$) | -289.07 | -385.70 | -273.64 | -248.88 | -181.48 |
| East7 | 41.9 | Mean Melt rate (mm $a^{-1}$) | 0.96 ± 18.06* | -1.07 ± 9.22 | 2.50 ± 7.46 | 1.16 ± 9.19 | -0.48 ± 9.29 |
| | | Water Volume Equivalent ($10^3$ $m^3$ $a^{-1}$) | 40.22* | -44.83 | 104.75 | 48.60 | -20.11 |
| East5 | 19.5 | Mean Melt rate (mm $a^{-1}$) | 0.60 ± 9.03† | 1.46 ± 9.64 | No Data | 0.33 ± 6.40† | 4.03 ± 2.91‡ |
| | | Water Volume Equivalent ($10^3$ $m^3$ $a^{-1}$) | 11.70† | 28.47 | No Data | 6.44† | 78.59‡ |
| SE1 | 31.2 | Mean Melt rate (mm $a^{-1}$) | -2.47 ± 15.59 | -2.88 ± 10.57 | -1.10 ± 11.78 | -3.16 ± 10.86 | -2.86 ± 10.37 |
| | | Water Volume Equivalent ($10^3$ $m^3$ $a^{-1}$) | -77.06 | -89.86 | -34.32 | -98.59 | -89.23 |
| SE2 | 108.8 | Mean Melt rate (mm $a^{-1}$) | -0.25 ± 11.17 | 5.19 ± 6.62 | 8.14 ± 3.47 | 6.16 ± 4.73 | 4.95 ± 6.10 |
| | | Water Volume Equivalent ($10^3$ $m^3$ $a^{-1}$) | -27.20 | 564.67 | 885.63 | 670.21 | 538.56 |
| SE1/2 Termini | 30.5 | Mean Melt rate (mm $a^{-1}$) | 2.24 ± 0.83‡ | -0.50 ± 9.52 | -3.40 ± 14.39 | -6.56 ± 18.80 | -1.53 ± 13.74 |
| | | Water Volume Equivalent ($10^3$ $m^3$ $a^{-1}$) | 68.32‡ | -15.25 | -103.70 | -200.08 | -46.67 |
| NCB | 53.2 | Mean Melt rate (mm $a^{-1}$) | 4.93 ± 20.63 | 7.41 ± 11.92 | 7.05 ± 9.11 | 5.17 ± 9.01 | 7.02 ± 10.93 |
| | | Water Volume Equivalent ($10^3$ $m^3$ $a^{-1}$) | 262.28 | 394.21 | 375.06 | 275.04 | 373.46 |
| SCB | 41.5 | Mean Melt rate (mm $a^{-1}$) | -3.31 ± 20.72 | 7.02 ± 12.17 | 9.80 ± 12.96 | 3.50 ± 19.22 | 9.55 ± 16.52 |
| | | Water Volume Equivalent ($10^3$ $m^3$ $a^{-1}$) | -137.37 | 291.33 | 406.70 | 145.25 | 396.33 |

### *5.4.2 Temporal Variation*

Temporal changes in the modelled basal melting/freezing rates are difficult to identify, potentially because the large spatial variation obscures smaller changes over time. Notable exceptions include the terminus region of SE1/2, which appears to switch from melting to freezing as it enters the active phase of the surge, and East7 Glacier and Fitzroy Glacier, which see peak freezing rates in 2009 (Table 5.2), coinciding with the highest velocities and weakest beds during their pulses (Table 5.1). It also appears that the acceleration of Belcher Glacier near the terminus has led to a switch from melting to freezing in this lowermost portion.

### *5.4.3 Controls on the Calculated Melting/Freezing Rates*

To investigate the key controls on the calculated melting/freezing rates, linear regressions based on results for the entire sliding area with thicknessses >30 m in 2013 were performed. For each variable in Equation 4.10, a stronger correlation (i.e. the nearer $R^2$ is to one) implies it has had a greater the impact on the calculated basal melting/freezing rates.

*Table 5.3. Results of linear regression of key parameters used to calculate basal melting/freezing rates using data for the entire sliding area of the ice cap in 2013. The points used are the verticies of the elements in the mesh, giving an n = 559. The other parameters are considered to be constants, so are not analysed here.*

| **Parameter** | **$R^2$ Value** |
|---|---|
| Basal temperature gradient ($\theta_b$) | 0.8431 |
| Thermal Conductivity of Ice ($K$) | 0.1595 |
| Total Conductive Component ($K\theta_b$) | 0.8545 |
| Basal Velocity ($u_b$) | 0.0106 |
| Basal Shear Stress ($\tau_b$) | 0.2055 |
| Total Frictional Component ($u_b\tau_b$) | 0.1118 |

The results of this suggest that the basal temperature gradient, thus the rate heat is conducted away from the bed, is a far more important control on the basal melting/freezing rate than frictional heating (Table 5.3). The dominance of $\theta_b$ implies that the distribution of englacial temperatures is very important to the spatial distribution of melting/freezing at

the base. This could help explain the frequent lack of trends in the melt rate calculations, as minor errors in the englacial temperatures could be obscuring more subtle changes to the frictional contribution through time. It is also interesting to note that the basal shear stress is considerably more influential than the velocity; this could explain why freezing rates tend to be elevated when $\tau_b$ falls and velocities rise when flow is faster (Christoffersen et al., 2014; Cook, 2016).

## 5.3 Till Strength and Water Storage

As described in Section 4.4.2, the basal shear stress can be used to estimate the void ratio of the till, and thus the water stored in the pore spaces. These calculations assume that the sediment shear strength is equal to the basal drag, which is likely to be the case for the sliding areas of the ice cap. However, in the terminus region of SE1/2 and East5 Glacier, this assumption breaks down as the trunk became entierly stangnant and frozen to the bed in quiescent years. As this is when the greatest changes in water storage are expected to occur, statisitics were still calculated in the areas where sliding was assumed to occur in other years, but should be treated with caution.

*Table 5.4. Water storage, including the change from the previous year data was available, for the glaciers of greatest interest. Error is given as ± two thirds based on till thicknesses of 0.3 ± 0.2 m.*

| **Glacier** (Fig. 2.2) | **Parameter** | **Year** | | | | |
|---|---|---|---|---|---|---|
| | | **Mid-1990s** | **2009** | **2012** | **2013** | **2014** |
| East5 | Void Ratio | 0.353 ± 0.010 | 0.368 ± 0.023 | - | 0.355 ± 0.007 | - |
| | Water Storage ($10^3$ $m^3$) | 1525 ± 1016 | 1570 ± 1047 | - | 1530 ± 1020 | - |
| | Change Since Previous ($10^3$ $m^3$) | - | 45 ± 30 | - | -41 ± 27 | - |
| SE1/2 Termini | Void Ratio | 0.362 ± 0.022 | 0.377 ± 0.027 | 0.364 ± 0.020 | 0.372 ± 0.017 | 0.369 ± 0.023 |
| | Water Storage ($10^3$ $m^3$) | 2429 ± 1619 | 2500 ± 1667 | 2439 ± 1626 | 2478 ± 1652 | 2465 ± 1643 |
| | Change Since Previous ($10^3$ $m^3$) | - | 71 ± 47 | -61 ± 41 | 39 ± 26 | -13 ± 9 |
| NCB | Void Ratio | 0.357 ± 0.031 | 0.356 ± 0.024 | 0.342 ± 0.019 | 0.344 ± 0.020 | 0.344 ± 0.021 |
| | Water Storage ($10^3$ $m^3$) | 4189 ± 2792 | 4183 ± 2789 | 4067 ± 2711 | 4081 ± 2721 | 4085 ± 2723 |
| | Change Since Previous ($10^3$ $m^3$) | - | -5 ± 3 | -116 ± 77 | 14 ± 9 | 4 ± 2 |
| SCB | Void Ratio | 0.381 ± 0.036 | 0.358 ± 0.054 | 0.350 ± 0.019 | 0.356 ± 0.026 | 0.359 ± 0.026 |
| | Water Storage ($10^3$ $m^3$) | 3428 ± 2285 | 3317 ± 2212 | 3229 ± 2153 | 3263 ± 2175 | 3285 ± 2190 |
| | Change Since Previous ($10^3$ $m^3$) | - | -111 ± 74 | -88 ± 59 | 33 ± 22 | 22 ± 15 |
| East7 | Void Ratio | 0.361 ± 0.023 | 0.368 ± 0.015 | 0.362 ± 0.019 | 0.358 ± 0.016 | 0.360 ± 0.011 |
| | Water Storage ($10^3$ $m^3$) | 3332 ± 2221 | 3381 ± 2254 | 3342 ± 2228 | 3314 ± 2209 | 3327 ± 2218 |
| | Change Since Previous ($10^3$ $m^3$) | - | 49 ± 33 | -39 ± 26 | -28 ± 19 | 13 ± 8 |

Assuming a till depth of 0.3 m, the active phase of the pulse of East5 Glacier and East7 Glacier led to approximately 5 x $10^4$ and 4.5 x $10^4$ $m^3$ of water entering the till, respectively. Changes during the surge of SE1/2 are less clear, although there does appear to be an increase of ~7 x $10^4$ $m^3$ compared to the quiescent state. The most dramatic changes in till water storage are seen beneath the Croker Bay glaciers, especially between 2009 and 2012. This is probably because the sliding areas (Table 5.2) and changes to $\tau_b$ (Table 5.1) are both relatively large.

## 5.5 Transects

To visualise the trends down the central flowline of the glaciers of most interest, transects were extracted spanning years when substantial change to flow patterns occurred. However, problems with the 1 km resolution and interpolated ice thicknesses are apparent in the transects of glaciers East5 Glacier and East7 Glacier; for East5 Glacier, as the bed does not appear to dip below sea level, and for both there should be substantial bedrock bumps (Van Wychen et al., 2017) which are not present (Fig. 5.6). Furthermore, the large drops in velocity near the terminus of East5 Glacier in 2009 and SE2 in 2009 should be ignored, as they are far smaller in the original data (Van Wychen et al., 2012, 2017).

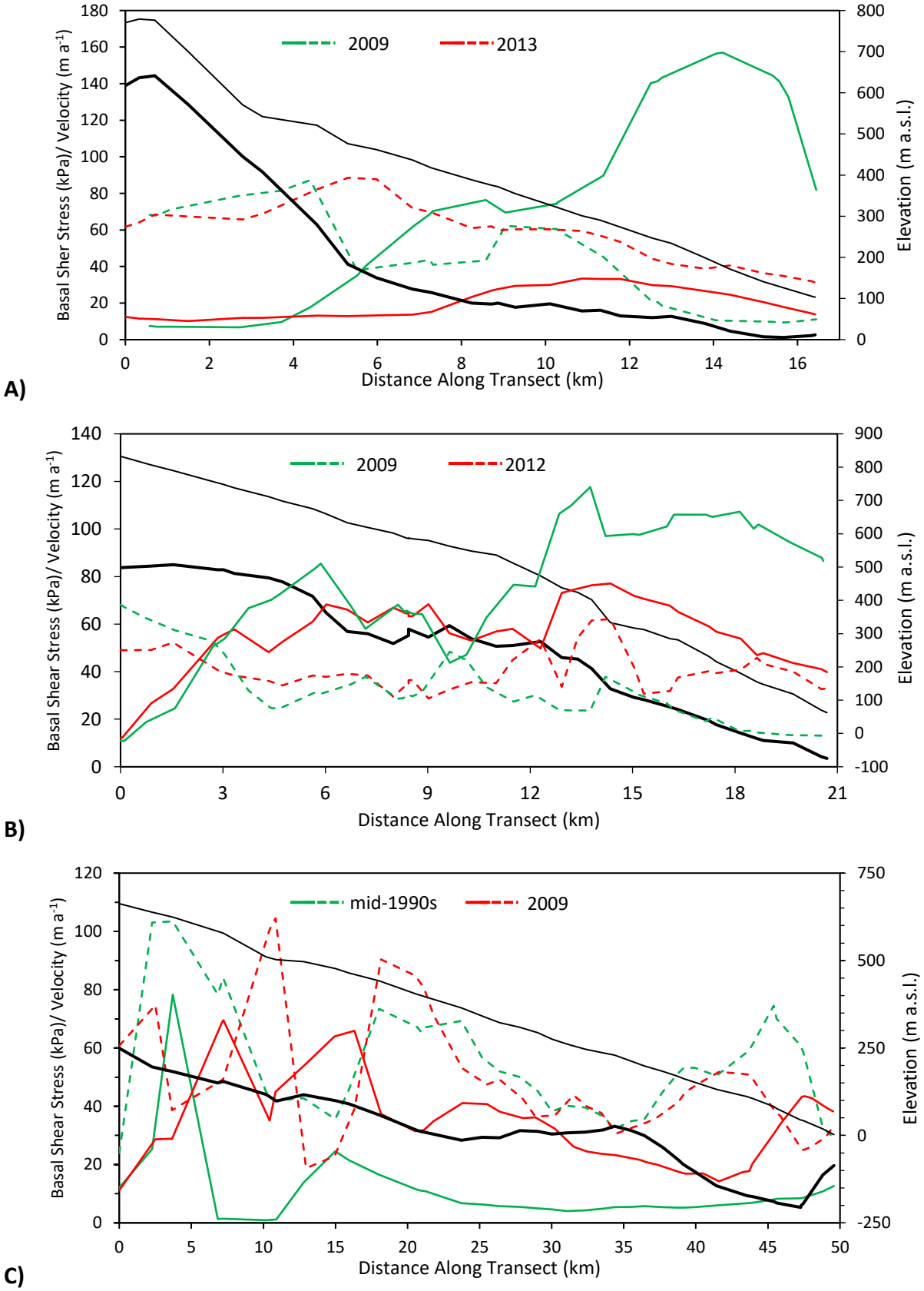


*Figure 5.6 Modelled basal velocity (solid line) and shear stress (dashed line) profiles for A) Glacier East 5 in 2009 (green) and 2013 (red), B) Glacier East 7 in 2009 (green) and 2012 (red), and C) Glacier SE2 in the mid-1990s (green) and 2009 (red). The terminus is located at the right of the profiles. The thin black line indicates the model ice surface topography and the thick line the bed topography.*

For East5 Glacier, very little change in both $\tau_b$ and velocity occurs in the 5 km furthest inland (Fig. 5.6A). Downsteam of this point, the ice thickens rapidly and a trend of increasing velocity and decreasing $\tau_b$ is observed, with basal shear stress significantly lower and velocities far higher during the pulse (Fig. 5.6A). However, in the area between 9 and 11 km, the difference during the pulse is subdued, with lower velocities and virtually no change in $\tau_b$. This is located where a bedrock bump has been recorded by ice-penetrating radar (Dowdeswell et al., 2004; Van Wychen et al., 2017), which, although not present at the resolution used here, will have lowered input velocities leading to a higher basal drag in the inversion. A similar drop in velocity and rise in $\tau_b$ at around 10 km in the profile of East7 Glacier may again be linked to a poorly-resolved bedrock bump (Fig. 5.6B).

For SE2, the slow flow in the upper area in the mid-1990s is not consistent with the input data (Burgess et al., 2005; Van Wychen et al., 2012), so should be ignored. The two areas of faster flow seperated by an area of slower flow are, however, clear in 2009. Basal shear stress appears to be fairly consistent between years in the upper areas, but is noticably lower during the surge in the few kilometres nearest the terminus.

A transect was also taken along Belcher Glacier to investigate the patch of high basal drag, which can be seen as a spike at around 35 km (Fig. 5.7). The location seems to correspond with an overdeepening before a sill (Van Wychen et al., 2017). Downstream of this, $\tau_b$ becomes very low and velocities very high, suggesting little resistance to flow is being provided by the bed. This transition is located approximately where Burgess et al. (2005) noted a change from flow regime 2 to flow regime 3.

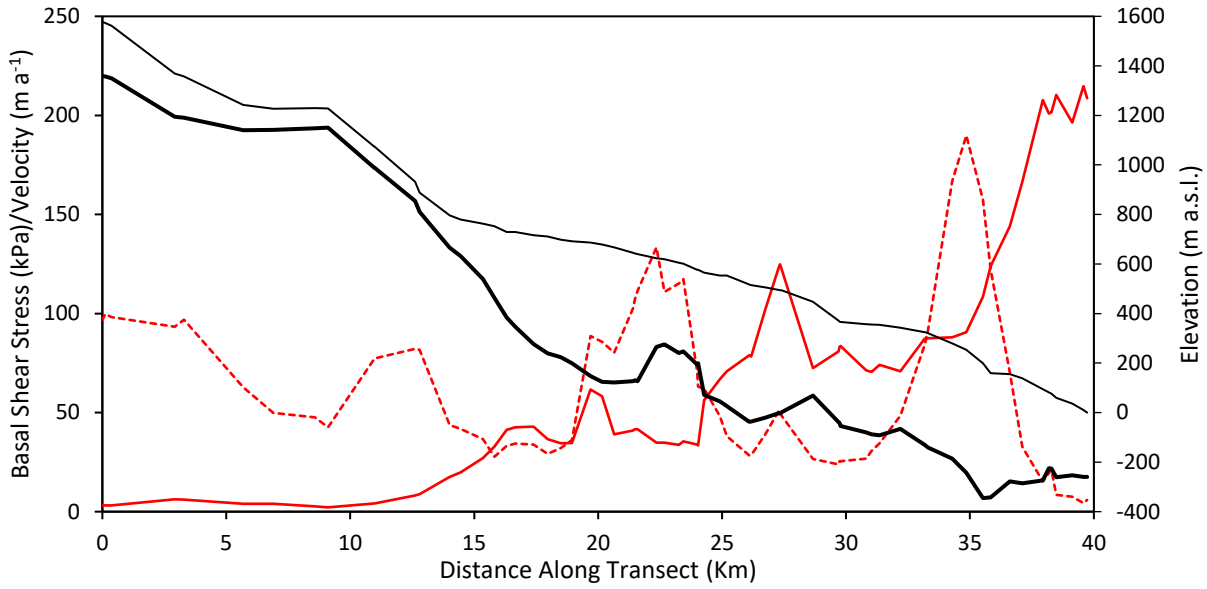


*Figure 5.7 Bed (thick black line) and surface (thin black line) topography, as well as basal velocity (solid red line) and basal shear stress (dashed red line) along a profile of Belcher Glacier in 2013.*

## 5.6 Errors

Errors in the input data will be propagated through the inversion modelling into the results. It is therefore important to attempt to distinguish between actual results and model inaccuracies, despite the inherent difficulty of quantifying of errors. A key issue is uncertainty in the bed topography, which can have a large impact on the results of the inversion. In an area of erronious ice thickness, modelled surface velocities would be substantially different from observed velocities as the mass flux must be consistent. The inversion procedure would seek to reduce this discrepancy by altering the value of $\beta$. The interpolation used to produce ice thicknesses in this study seems to have produced quite large discrepancies with reality. This is illustrated by the summit borehole profile depth (Fig. 5.1B) and the transects (Fig. 5.6), where there are discrepancies in the order of tens of metres. The mountainous topography of eastern Devon Island may make this problem particularly noticeable, as topographic features between flight lines will not be accounted for.

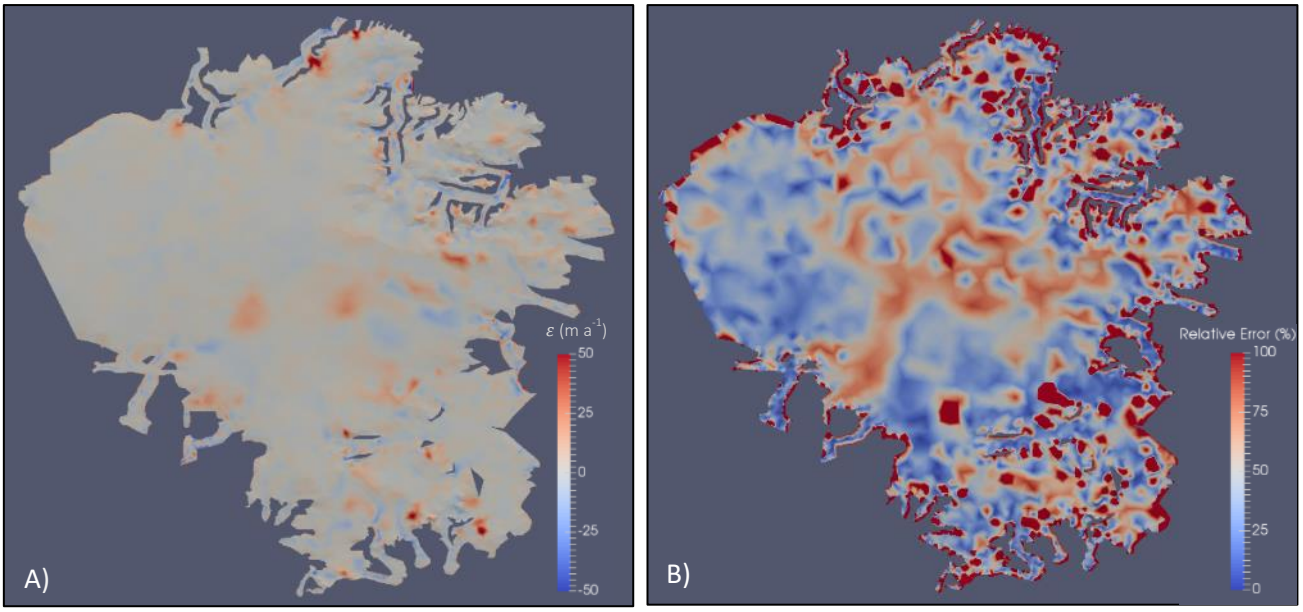


*Figure 5.8. Absolute (A) and relative (B) errors between the modelled and observed surface velocities for the 2013 data.*

The high relative error around the margins, especially where the velocities had to be forced to zero, are probably a result of the very low calculated velocities leading to a greater relative discrepancy. Elsewhere, the relative errors are often fairly low, although they increase again towards the ice cap centre, again probably a result of low velocities. As results have been limited to areas where ice thicknesses are greater than 30 m, many of these marginal areas have been excluded. Furthermore, in the centres of the tidewater glaicers, the relative errors are generally very low. The results from these areas are therefore likely to be reasonably accurate.

# 6. Discussion

This chapter discusses potential insights this study has given into the causes of the changing dynamics of the Devon Ice Cap. The most likely source of the unaccounted-for heat/meltwater reaching the bed is first identified, as this has implications for all the behaviours mentioned subsequently. The glaciers experiencing changes to dynamics which are likely to be closely linked to climate are then considered, before those suggested to be experiencing cyclic variations in velocity (pulsing and surging) are discussed.

## 6.1 Unaccounted Heat Source

In areas with observed surface velocities above 30 m $a^{-1}$, it can be assumed that basal slip is occurring, thus temperatures at the ice-bed interface must reach the PMP. However, as described in Section 3.3.1, this condition was not always met by the model, requiring a boundary condition forcing the bed to the upper temperature limit when surface velocities exceed the 30 m $a^{-1}$ threshold. The disparity between the temperatures produced without the boundary condition and those produced with it therefore represents a source of heat or meltwater to the bed that is unaccounted for in the numerical modelling (Fig. 6.1). The dominance of basal freezing beneath some glaciers is consistent with this hypothesis, as without additional heat or water reaching the bed in these areas, sustained fast flow would not be possible.

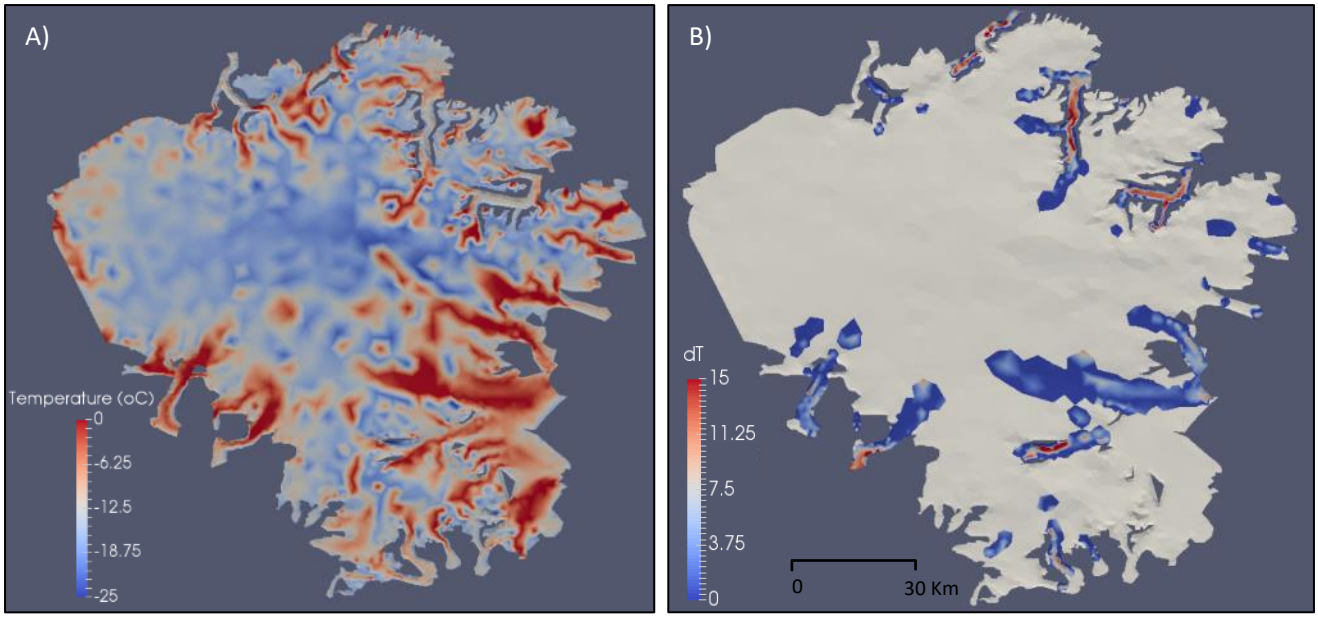


*Figure 6.1. The effect of forcing temperature to the upper limit when basal sliding is likely to be occurring. A) Shows the temperature for 2012 calculated without this condition and B) the difference between this and the temperatures once the boundary condition has been applied for the sliding areas. See Fig. 5.2C for the 2012 temperature distribution with the temperature boundary condition.*

Using a similar approach, modelling of the Flade Isblink ice cap in NE Greenland by Cook (2016) also found that an additional source of heat/meltwater was required for the beds of some sliding areas to reach the PMP. Possible sources of this additional water/heat were suggested to be: (i) withdrawal from a till aquifer, (ii) basal water flow from inland, (iii) error in the geothermal heat flux, or (iv) cryo-hydraulic warming. Christoffersen et al. (2014) found (i) and (ii) to be dominant contributors beneath the Siple Coast ice streams of Antarctica. For an Arctic ice cap, however, (ii) is unlikely as there is no obvious source of basal water in the frozen interior and (i) would lead to rapid depletion of the aquifer, preventing continuous sliding (Cook, 2016). Similarly, the geothermal heat flux is unlikely to be sufficiently high to provide the missing heat.

It therefore seems likely that the penetration of surface meltwater produced during summer melting and the accompanying heat transfer – cryo-hydraulic warming (Phillips et al., 2010) - allows the beds of the major tidewater glaciers of the Devon Ice Cap to reach the PMP. Surface melting occurs over much of Devon Ice Cap (Dowdeswell et al., 2004; Burgess et al., 2005; Clason et al., 2012) and the amount of this water reaching the bed has been linked to the distribution of flow regimes on Devon Ice Cap, supporting this hypothesis (Wyatt and Sharp, 2015). The necessity of including refreezing surface meltwater as an

additional heat source to explain borehole temperature profiles and surface velocities is also similar to the Vestfonna ice cap in eastern Svalbard (Schafer et al., 2014), although unlike Vestfonna, the close match with modelled and observed surface velocities near the summit of Devon Ice Cap (Section 5.1) suggests that meltwater has little effect at this elevation.

## 6.2 Dynamic Change on Devon Ice Cap Outlet Glaciers

### *6.2.1 Croker Bay Glaciers*

The deceleration of both Croker Bay Glaciers (located in Fig. 2.2) post-2009 was accompanied by a drop in basal drag (Table 5.1). This is most pronounced on NCB, which is unsurprising given the dramatic change in observed velocities (Van Wychen et al., 2017). However, there is no clear link between basal melt rates and flow velocities. Although the spatial variation is pronounced (Fig. 5.5D), the beds of both Croker Bay Glaciers are subject to net melting in virtually all years (Table 5.3). Combined with the model's prediction that both glaciers remain consistently warm-based, this suggests that the changes to ice dynamics are not linked to thermal processes. Furthermore, the changes occurred on both glaciers approximately simultaneously, which would not be expected if an internal mechanism was responsible. These findings therefore support Van Wychen et al.'s (2017) suggestion of a control linked to the regional climate.

The results of this study suggest that both glaciers are to some extent reliant on an unaccounted-for heat input in the model to reach the PMP at the bed (Fig. 6.1). Annually variable amounts surface meltwater reach the bed in this region (Clason et al., 2012), thus surface meltwater could potentially influence till strength and cause changes to the dynamics. Assuming the till is 0.3 m thick, the calculated change in water storage in the deforming till layer between 2009 and 2012 is ~$2 \times 10^5$ $m^3$ (Table 5.2) - a value far smaller than the annual changes in meltwater delivery to the bed that Clason et al. (2012) predict are occurring ($2.6 \times 10^8$ in 2004 vs $7.6 \times 10^8$ $m^3$ in 2006).

A mechanism at least partly driven by surface meltwater is therefore feasible, even assuming that <10 % of the meltwater enters the till (as in Bougamont et al., 2014) and

Clason et al.'s (2012) admission that their estimates of the fraction of meltwater reaching the bed are probably too large. This theory is supported by the peak in summer velocities on both glaciers in 2006 (Van Wychen et al., 2017) when meltwater delivery to the bed is known to be high (Clason et al., 2012), and the link between observed velocities and the degree of meltwater penetration (Wyatt and Sharp, 2015).

However, this theory would not directly explain why there are periods of faster and slower flow lasting several years. It also neglects the potential for changes linked to oceanic influences and water circulation within Croker Bay that might affect these tidewater glaciers. Consequently, additional data would be required to evaluate the impact of surface meltwater, to better explain the exact velocity fluctuations observed and to suggest why these changes were limited to the Croker Bay region (Van Wychen et al., 2017). Ideally, these data would include changes to surface velocity, ocean and air surface temperatures both during and between years.

### *6.2.2 Belcher Glacier*

Belcher Glacier is responsible for more than a third of the calving flux of Devon Ice Cap (Table 2.1), making changes to this glacier of particular interest. Van Wychen et al. (2017) suggest that the acceleration, retreat and thinning of the terminus in recent years (Table 5.1; Fig. 2.4) are consistent with observations of marine-terminating glaciers in the Prince of Wales Ice Field some 250 km to the north on Ellesmere Island (Van Wychen et al., 2016), which are in turn suggested to be comparable with those in parts of Greenland (Howat et al., 2008). Speed-up is therefore suspected to be a result of reduced longitudinal resistive stresses as the terminus thins and retreats due to rising air and ocean temperatures, which must be countered by increased strain rates, thus faster flow velocities (Howat et al., 2008; Joughin et al., 2012). The results of this study support this hypothesis; basal drag appears to be very low near the terminus (Fig. 5.7), suggesting the bed is providing very little resistance and this part of the glacier is approaching floatation. The mean basal drag is not particularly low in most years (Table 5.1), but as it is extremely spatially variable, with much higher values near the margins where errors are greater, the means are not viewed as representative.

As well as changes through time, a consistent feature beneath Belcher Glacier is the patch of high $\tau_b$ and high melt rates located approximately 5 km upstream from the terminus (Fig. 5.7). This sticky spot is visible in all years (Fig. 5.3) and errors appears to be very small (Fig. 5.8), suggesting the low drag is a robust outcome. However, a sticky spot in a bedrock depression is unusual; an accumulation of water and/or weak, unconsolidated sediment offering little resistance to flow is more likley (Cook and Swift, 2012). It is therefore hypothesised that the high basal drag is a result of the flow direction of the glacier turning from north-south to east-west as it meets the slower flowing northern arm, producing longitudinal compressional gradients in this area which are reflected in the basal drag. A similar situation with high drag in an overdeepening where a slower-flowing tributary meets the main trunk was inferred for Daugaard-Jensen Gletscher in East Greenland (Perry, 2014).

## 6.3 The Surge of Southeast1 and Southeast2 Glaciers

The long active phase (>6 years) and relatively slow velocities (only four to seven times those in the quiescent phase (Van Wychen et al., 2017) suggests the surge of SE1/2 Glacier is comparable to those on Svalbard, which are also characterised by relatively small increases in velocity (Mansell et al., 2012) and long durations (Dowdeswell et al., 1991). The subdued nature of this surge is also evident in Landsat imagery from the active phase, which reveals a relatively smooth surface (Fig. 6.2). Consequently, it is suggested that a thermal mechanism is most appropriate - a proposal supported further by the terminus region not reaching the PMP during the quiescent phase, implying a change in the thermal regime (Fig. 5.2). Additionally, extensive areas of SE1/2 are grounded below sea level and likely to be underlain by soft, deformable sediment (Dowdeswell et al., 2004), which is required in the soft-bedded thermal mechanisms favoured for Svalbard tidewater glaciers (Fowler et al., 2001; Murray et al., 2003).

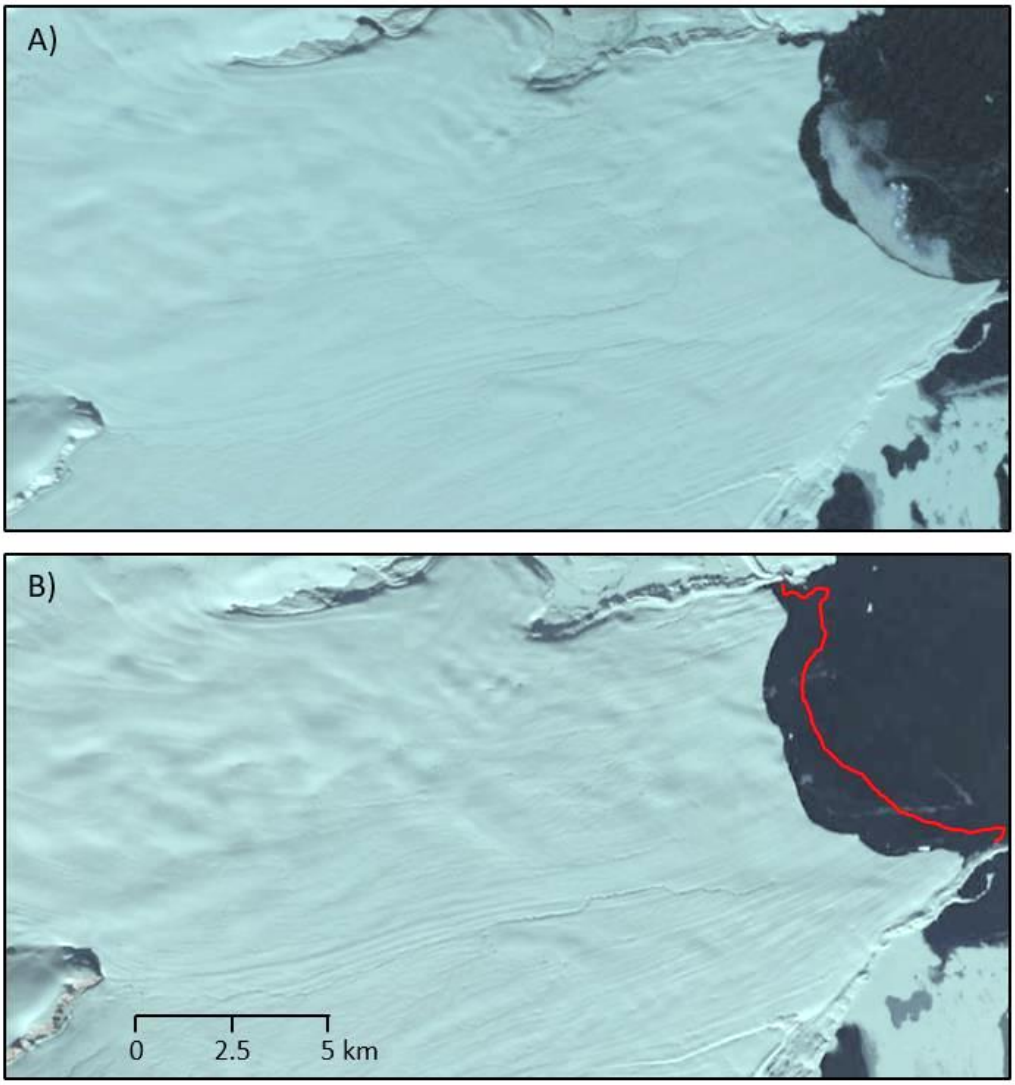


*Figure 6.2. False colour Landsat Image of the shared terminus region of SE1/2. A) Shows the surface prior to its activation on 16th September 2005 and B) the surface approximately seven years after the beginning of the active phase on 30th September 2016. The red line in B) indicates the position of the terminus in A), highlighting the retreat over this interval.*

Following the thermal-switch mechanism (Fowler et al., 2001; Murray et al. 2003), it is suggested that the thickening in the area where the two glaciers meet led to increased basal meltwater production. This weakened the underlying till, which led to dilation and deformation, increasing frictional heating and creating more water at the bed in a positive feedback (Fowler et al., 2001). As additional heat must have reached the bed (Fig. 6.1), this feedback was potentially enhanced by cryo-hydraulic warming as described by Dunse et al. (2015). A closely spaced network of supraglacial streams which sometimes terminate at moulins is visible in the terminus region of the glacier prior to its activation (Dowdeswell et

al., 2004), suggesting surface meltwater does reach the bed in this region. Continued thickening would cause the warm-bedded area to expand, eventually causing the entire bed to reach PMP and fast flow at the terminus to begin. Early in this stage, velocities would be expected to be highest close to the upper end of the zone of thickening (Sund et al., 2009), which appears to be the case (Van Wychen et al., 2012). However, without additional elevation data, it is unknown whether the warm-based area expanded at a faster rate than the area of fast flow, which would help describe the mechanism in further detail.

This propagation downstream is unlike that observed on many tidewater glaciers in Svalbard, which often initiate near the terminus and propagate upstream (e.g. Murray et al., 2003; Mansell et al., 2012). This may be a result of the terminus region of SE1/2 being frozen to the bed in the quiescent phase as it has relatively thin ice, which is unlike large tidewater surging glaciers in Svalbard which are suggested to be entirely warm-bedded (Sevestre et al., 2015). The relatively subdued response of the glacier below the place where the thickening occurred is also unexpected. This is suggested to be a consequence of the increased cross-sectional area as the glaciers enter this piedmont region; mass must be conserved, so flow would slow down, giving limited acceleration (Fig. 5.6C).

The retreat of the terminus of SE1/2 during the active phase of the surge is also unusual (Fig. 6.2). In virtually all other documented surges, the increased ice flux has led to thickening and therefore decreased calving and terminus advance (e.g. Sobota et al., 2016; Dowdeswell and Benham, 2003). The retreat seems to be uniform throughout the surge and predates the activation of the terminus region, suggesting it is climatically driven. Luckman et al. (2015) found that frontal ablation is far more dependent on ocean temperatures than ice dynamics. Consequently, despite flow speeds increasing, it might be the case that the frontal ablation is still capable of outpacing ice flow, potentially helped by the gentle nature of the surge. The channel appears to widen and deepen inland, which could have contributed to this sustained retreat; to conserve mass as the cross-sectional area increases, thinning and retreat will occur (Carr et al., 2014). This was suggested to be the case for Paierlbreen in Svalbard, where a highly-crevassed surface and retreat from a pinning point into deeper water was held responsible for the negligible advance during the surge (Blaszczyk et al., 2013).

The surge of SE1 and SE2 is simultaneous (Fig 2.3), suggesting its timing is controlled by processes acting below the confluence. The beds of the upper fast-flowing units remain at PMP in all years, and although they slow and begin to thicken following the beginning of the active phase, fast flow is maintained (Fig. 2.4). Further evidence for the upper portion of these glaciers having little effect on the surge is found in the calculated melting/freezing rates, which differ greatly between SE1 and SE2. In all years, the sliding area of SE2 is dominated by melting whereas SE1 undergoes freezing (Fig. 5.5B), suggesting that the heat budget beneath the two glaciers is very different. This difference is likely to be a result of a high basal temperature gradient beneath SE1 conducing heat away from the bed rapidly as similar velocities and $\tau_b$ (Table 5.1) suggest the frictional contribution is virtually identical. However, there is a substantial amount of heat from surface meltwater being added to the bed of SE1 (Fig. 6.1), which is likely to be countering this additional freezing and maintaining fast flow.

A deceleration of the terminus region of SE1/2 has not yet been observed, but as the current active phase has lasted for at least 6 years (Van Wychen et al., 2017), a gradual termination in the near future seems probable. As freezing rates increase during the surge, termination could occur as described by Cook (2016). The change to the water volume stored in the till following the beginning of the surge is estimated at ~7 x $10^4$ $m^3$ (Table 5.4), but is highly uncertain. However, the amount appears to be small compared to the rates of freezing (~9 x $10^4$ $m^3$ $a^{-1}$, Table 5.2), suggesting ample water is withdrawn over the length of an active phase to terminate the surge, even accounting for increased amounts of surface meltwater reaching the bed.

Following this theory, conductive heat loss increases as the basal temperature gradient becomes very high when the bed reaches the PMP, exceeding frictional heating during the surge as the increased velocities are accompanied by a drop in $\tau_b$. Fast flow could be maintained despite widespread freezing due to heat and water input from cryo-hydraulic warming, but water would be gradually withdrawn from the till, strengthening it and leading to the eventual cessation of fast flow. Conductive heat loss due to thinning is not excluded by this hypothesis, but it would act on a timescale longer than decades (Gladstone et al., 2014) and the constant geometry used implies this is not essential to explain the termination of a surge (Cook et al., 2016). Cooling due to increased ice advection to the

ocean and hydrological discharge could also contribute, but again would act alongside increased freezing rates (Gladstone et al., 2014).

It is uncertain how long the current active phase will last, but based on surging glaciers in Svalbard, a duration of 10 years is a likely upper bound. However, there is no obvious deceleration after 6 years and the surge is slow (Van Wychen et al., 2017), thus a duration slightly longer than this is possible. The subsequent quiescent phase would be expected to last 50 – 500 years (Dowdeswell et al., 1991). However, climate clearly effects surging (Dowdeswell et al., 1995; Sevestre and Benn, 2015); in a warming climate, it is therefore likely that changes to the nature of surging will occur as the glacier would be unable to rebuild its pre-surge geometry in a warming climate with a likely negative mass balance (Dowdeswell et al., 1995; Murray et al., 2012).

### 6.4 Pulsing Glaciers

Unlike surging glaciers, which also undergo multiannual periods of acceleration then deceleration, pulsing glaciers as defined by Van Wychen et al. (2016) are characterised by propagation of fast flow upstream, and by the acceleration being restricted to areas grounded below sea level (Section 2.5.2). Changes to the elevation and length of the glaciers defined by Van Wychen et al. (2017) as pulsing (East5, East7 and Fitzroy Glaciers) could help suggest the mechanism resulting in the events, but no data regarding elevation change during the pulses of East7 Glacier and Fitzroy Glacier are available. Elevation change during the pulse of East5 Glacier is also largely unknown, but ICESat tracks from 2004-2009 do cover the upper part of the trunk. These laser-altimetric data show thinning of approximately 2.5 m $a^{-1}$ over this interval (Gardener et al., 2011), consistent with ice being displaced downstream.

A systematic examination of terminus location is beyond the scope of this study, but summer Landsat imagery of East5 Glacier appears to show a gradual terminus advance between 2001 and 2011 before retreat in subsequent years, giving a net advance of approximately 400 m between 2000 and 2015 (Van Wychen et al., 2017). This is likely to reflect an increased ice flux, and thus could constrain the duration of the pulse to ~10 years. Although this estimate is highly uncertain, the pulse of Fitzroy Glacier seems to have lasted

from ~2003 to ~2013 (Van Wychen et al., 2017), giving it a similar duration. The length of the quiescent phase is entirely unknown.

Nevertheless, the similar lengths of the events and similar contrasts in velocity between fast and slow flowing periods suggests the mechanism of pulsing may be similar to that of surging. Comparisons with marine-terminating surging glaciers in Svalbard, where propagation of surges up-glacier from starting points at or near the terminus has been observed (Dowdeswell and Benham, 2003; Murray et al., 2003, 2012; Mansell et al., 2012), are likely to be particularly appropriate. For these glaciers, the surge is suggested to begin because of increasing basal shear stress as the lower part of the glacier thins and the terminus retreats during the quiescent phase (Murray et al., 2012). However, this form of surging differs from pulsing in that the velocity variability is not restricted to areas grounded below sea level, which this mechanism would not explain.

A further complication when suggesting a mechanism for pulsing is the differences in the basal conditions of glaciers during a pulse. For example, the beds of East7 Glacier and Fitzroy Glacier consistently reached the PMP, whereas the lower portion of East5 Glacier appears to be frozen except for during the pulse (Fig. 5.2). Furthermore, the pulses of East7 Glacier and Fitzroy Glacier also appear to produce continued terminus retreat during the event, in contrast with the advance of East5 Glacier. Despite this, all pulses do appear to coincide with a reduction in basal drag (Table 5.1). The importance of large-scale bedrock sills and bumps on surface velocities led Van Wychen et al. (2017) to suggest that changes in basal shear stress will modulate the amount of basal motion, which is supported by this finding.

For the pulse of East5 Glacier, the transition from cold-based to warm-based (Fig 5.2) suggests a thermal mechanism is appropriate, potentially operating in a very similar way to thermally-driven surging glaciers as described in Section 6.3 (Fowler et al., 2001; Murray et al., 2003). However, termination resulting from enhanced freezing rates during the pulse of East5 Glacier seems unlikely as freezing rates are not higher during the pulse (Table 5.3). Conversely, for the pulses of East7 Glacier and Fitzroy Glacier, a mechanism driven by a change in thermal regime is not feasible as a cold terminus does not develop during the quiescent period. This is consistent with Sevestre et al.'s (2015) suggestion that large marine-terminating glaciers in Svalbard remain consistently warm-based throughout the

surge cycle. Although no clear mechanism is proposed by Sevestre et al. (2015), production and evacuation of basal meltwater is suggested to be key for these glaciers. The increased freezing rates during the pulses could provide a mechanism for termination comparable to that described in Section 6.3 for the surging glaciers, where frictional heating falls and conductive cooling increases when flow is faster. Assuming the pulse lasted ten years, for East7 Glacier this rate of freezing would withdraw ~4.5 x $10^5$ $m^3$ of water (Table 5.2), which greatly exceeds the ~5 x $10^4$ $m^3$ change in till water storage (Table 5.4). As with the surge of SE1/2, this mechanism could therefore prove sufficient to remove the required volumes of water from the till, even accounting for increased hydrological inputs from enhanced meltwater penetration.

However, it remains unclear why balance velocities appear to be maintained on ice grounded above sea level but are not below it. Van Wychen et al. (2017) suggest marine waters may therefore be influencing the dynamics of these tidewater glaciers; the proximity to the terminus will lead to high basal water pressures, making a slippery bed more likely and reducing the ability of the bed to drain rapidly (Cuffey and Paterson, 2010). Consequently, without additional data constraining the length of the quiescent phases and defining geometric changes during pulses, it remains difficult to suggest a mechanism for pulse-type behaviour with any degree of certainty. For example, it would be interesting to see if the pulse of East5 Glacier was initiated near the terminus despite the cold tongue, as the beginning of the event was not recorded by Van Wychen et al. (2017).

# 7. Conclusions

## 7.1 Main Findings

An adjoint method inversion has provided valuable insights into the basal conditions of the Devon Ice Cap, revealing that it has a base largely frozen to the bed except for beneath the fast-flowing marine-terminating glaciers. However, for many of these glaciers, additional heat/meltwater is required to raise the basal temperatures to the pressure melting point and maintain fast flow despite high rates of basal freezing. It is therefore suggested that cryo-hydraulic warming (Phillips et al., 2010) influences ice flow and the thermal structure of the ice cap.

Consequently, cryo-hydraulic warming may provide a positive feedback during the initiation of the surge of Southest1 Glacier and Southeast2 Glacier (Dunse et al., 2015), where the long duration and the switch of the terminus region from cold-based to warm-based suggest a soft-bedded thermally-regulated mechanism is applicable (Fowler et al., 2001; Murray et al., 2003). However, unlike conventional thermally-regulated surging, freezing rates increase during the active phase. This is a result of steeper basal temperature gradients, thus increased conductive heat loss which is not offset by enhanced frictional heating as the weakened till provides less resistance to flow. The surge could therefore terminate without the need for geometric changes (Cook, 2016). Englacial temperature distributions are very important to the spatial distribution and rates of basal melting/freezing, with the frictional components providing relatively minor controls.

The duration of the pulses and the magnitude of change in velocity between fast and slow flowing periods suggests pulsing behaviour is in some way comparable to marine-terminating glaciers in Svalbard, where surges have been observed to propagate upstream from near the terminus (Murray et al., 2003, 2012; Mansell et al., 2012). However, the thermal conditions at the beds of these glaciers is not consistent; East5 Glacier is subject to a change from warm-based to cold-based, whereas East7 Glacier and Fitzroy Glacier remain warm-based. For the latter two, a thermally regulated mechanism is therefore clearly not appropriate, although the enhanced freezing rates during the pulse could help terminate these events by removing water from the till when flow is faster. These differences, alongside a lack of data regarding geometric changes during the event, make it difficult to

suggest a mechanism for pulse-type behaviour which explains why the variations on velocity are limited to below sea level. A broader concept such as Sevestre and Benn's (2015) enthalpy balance approach might therefore be required to fully explain these phenomena.

For Belcher Glacier, there is relatively little change in the basal conditions as the terminus accelerates, but the very low basal drag near the terminus suggests it is near flotation. The recent acceleration is therefore likely to be a result of climatically-induced thinning and retreat of the terminus, reducing longitudinal resistive stresses and leading to faster flow in a manner similar to that hypothesised for many marine-terminating glaciers in Greenland (Nick et al., 2009). The cause of the changes to the dynamics of the Croker Bay Glaciers is probably also climatically controlled, but understanding the exact responses would require more climatic data and is beyond the scope of this study. Nevertheless, it is suggested that surface meltwater could be reaching the bed and influencing flow, as estimated changes to the volume of water stored in the till are far smaller than the variability in surface meltwater penetration (Clason et al., 2012).

## 7.2 Outlook for Devon Ice Cap

The short-term outlook for Devon Ice Cap is one of continued mass loss with an increasing dynamic contribution. As the thinning, acceleration and retreat of the terminus of Belcher Glacier is probably linked to increased ablation and the glacier approaching flotation, the fast flow is likely to be sustained as its bed lies well below sea level for ~25 km inland. Furthermore, if meltwater is a key influence on the flow of the Croker Bay Glaciers, increased lubrication and the effects of cryo-hydraulic warming could lead to periods faster flow becoming more likely.

The role of cryo-hydraulic warming means surging and pulsing glaciers are also likely to lose increasing volumes of mass through dynamics in the near future. The events may become more frequent as more surface meltwater is likely to be produced and reach the bed, weakening the till and promoting fast flow. Furthermore, continued retreat could potentially lead to sustained fast flow until the terminus retreats above sea level if the thinning led to ungrounding near the terminus, as has been suggested as a possibility for Basin 3 of Austfonna in eastern Svalbard (McMillan et al, 2014). In the coming decades and

centuries, it is likely that this increased dynamic contribution will, however, begin to decline. If Devon Ice Cap continues to lose mass, continued thinning could lead to the glaciers becoming too thin to reach PMP at the bed, possibly decreasing the frequency of the surges and pulses and eventually preventing fast flow all together (Dowdeswell et al., 1995; Sevestre et al., 2015).

## 7.3 Recommendations for Future Study

Analysis was limited by a lack of data regarding the climatic and geometric changes accompanying these events. Consequently, to better understand the changes to the dynamics of Devon Ice Cap, additional data are required. For the surging and pulsing glaciers, it would be particularly useful to determine whether the area of fast flow propagated downstream at a rate slower than the transition between warm and cold based conditions, and whether a surge front was present. For the Croker Bay Glaciers, more climatic data and observations at a sub-annual timescale during a transition between faster and slower flow would prove useful.

A major limitation of the results presented here is the interpolated ice thickness data. To improve upon the interpolated thicknesses used in this study, it would seem sensible to collate all the flight line data available and apply a mass conservation technique (e.g. Morlighem et al., 2011) across the entire ice cap. This could potentially greatly reduce the errors noted in Section 5.6 and allow more confidence in the results. If this was combined with additional computing power, it would also prove useful to increase the maximum model resolution. Although 1 km was sufficient to capture general patterns, the trunks of the major tidewater glaciers terminating in fjords were not well represented.

# References


Ahlkrona, J., Lotstedt, P., Kirchner, N., & Zwinger, T. (2016). Dynamically coupling the non-linear Stokes equations with the shallow ice approximation in glaciology: Description and first applications of the ISCAL method. *Journal of Computational Physics, 308*, 1-19. doi:10.1016/j.jcp.2015.12.025

Alley, R. B., Blankenship, D. D., Bentley, C. R., & Rooney, S. T. (1986). DEFORMATION OF TILL BENEATH ICE STREAM-B, WEST ANTARCTICA. *Nature, 322*(6074), 57-59. doi:10.1038/322057a0

ArcGIS Online (2017). World Imagery basemap. Sources: Esri, DigitalGlobe, Earthstar Geographics, CNES/Airbus DS, GeoEye, USDA FSA, USGS, Getmapping, Aerogrid, IGN, IGP, and the GIS User Community. [01/05/16].

Arthern, R. J., & Gudmundsson, G. H. (2010). Initialization of ice-sheet forecasts viewed as an inverse Robin problem. *Journal of Glaciology, 56*(197), 527-533.

Arthern, R. J., Hindmarsh, R. C. A., & Williams, C. R. (2015). Flow speed within the Antarctic ice sheet and its controls inferred from satellite observations. *Journal of Geophysical Research-Earth Surface, 120*(7), 1171-1188. doi:10.1002/2014jf003239

Bartholomew, I., Nienow, P., Mair, D., Hubbard, A., King, M. A., & Sole, A. (2010). Seasonal evolution of subglacial drainage and acceleration in a Greenland outlet glacier. *Nature Geoscience, 3*(6), 408-411. doi:10.1038/ngeo863

Bekryaev, R. V., Polyakov, I. V., & Alexeev, V. A. (2010). Role of Polar Amplification in Long-Term Surface Air Temperature Variations and Modern Arctic Warming. *Journal of Climate, 23*(14), 3888-3906. doi:10.1175/2010jcli3297.1

Benn, D., & Evans, D. J. (2014). *Glaciers and glaciation*. Routledge.

Bennett, M. R. (2003). Ice streams as the arteries of an ice sheet: their mechanics, stability and significance. *Earth-Science Reviews, 61*(3-4), 309-339. doi:10.1016/s0012-8252(02)00130-7

Berger, S., Favier, L., Drews, R., Derwael, J. J., & Pattyn, F. (2016). The control of an uncharted pinning point on the flow of an Antarctic ice shelf. *Journal of Glaciology, 62*(231), 37-45. doi:10.1017/jog.2016.7

Bernales, J., Rogozhina, I., Greve, R., & Thomas, M. (2017). Comparison of hybrid schemes for the combination of shallow approximations in numerical simulations of the Antarctic Ice Sheet. *Cryosphere, 11*(1), 247-265. doi:10.5194/tc-11-247-2017

Blankenship, D. D., Bentley, C. R., Rooney, S. T., & Alley, R. B. (1986). SEISMIC MEASUREMENTS REVEAL A SATURATED POROUS LAYER BENEATH AN ACTIVE ANTARCTIC ICE STREAM. *Nature, 322*(6074), 54-57. doi:10.1038/322054a0

Blaszczyk, M., Jania, J. A., & Kolondra, L. (2013). Fluctuations of tidewater glaciers in Hornsund Fjord (Southern Svalbard) since the beginning of the 20th century. *Polish Polar Research, 34*(4), 327-352. doi:10.2478/popore-2013-0024

Bliss, L. C. (1977). *Truelove Lowland, Devon Island, Canada: A High Arctic Ecosystem*. University of Alberta.

Boon, S., Burgess, D. O., Koerner, R. M., & Sharp, M. J. (2010). Forty-seven Years of Research on the Devon Island Ice Cap, Arctic Canada. *Arctic, 63*(1), 13-29.

Bougamont, M., Christoffersen, P., Hubbard, A. L., Fitzpatrick, A. A., Doyle, S. H., & Carter, S. P. (2014). Sensitive response of the Greenland Ice Sheet to surface melt drainage over a soft bed. *Nature Communications, 5*, 9. doi:10.1038/ncomms6052

Boulton, G. S. (1996). Theory of glacial erosion, transport and deposition as a consequence of subglacial sediment deformation. *Journal of Glaciology, 42*(140), 43-62.

Boulton, G. S., & Jones, A. S. (1979). Stability of temperate ice caps and ice sheets resting on beds of deformable sediment. *Journal of Glaciology*, *24*(90), 29-43.

Boulton, G. S., & Hindmarsh, R. C. A. (1987). SEDIMENT DEFORMATION BENEATH GLACIERS - RHEOLOGY AND GEOLOGICAL CONSEQUENCES. *Journal of Geophysical Research-Solid Earth and Planets, 92*(B9), 9059-9082. doi:10.1029/JB092iB09p09059

Brinkerhoff, D. J., Meyer, C. R., Bueler, E., Truffer, M., & Bartholomaus, T. C. (2016). Inversion of a glacier hydrology model. *Annals of Glaciology, 57*(72), 84-95. doi:10.1017/aog.2016.3

Burgess, D., & Sharp, M. J. (2008). Recent changes in thickness of the Devon Island ice cap, Canada. *Journal of Geophysical Research-Solid Earth, 113*(B7), 18. doi:10.1029/2007jb005238

Burgess, D. O., & Sharp, M. J. (2004). Recent changes in areal extent of the Devon Ice Cap, Nunavut, Canada. *Arctic Antarctic and Alpine Research, 36*(2), 261-271. doi:10.1657/1523-0430(2004)036[0261:rciaeo]2.0.co;2

Burgess, D. O., Sharp, M. J., Mair, D. W. F., Dowdeswell, J. A., & Benham, T. J. (2005). Flow dynamics and iceberg calving rates of Devon Ice Cap, Nunavut, Canada. *Journal of Glaciology, 51*(173), 219-230. doi:10.3189/172756505781829430

Carr, J. R., Stokes, C., & Vieli, A. (2014). Recent retreat of major outlet glaciers on Novaya Zemlya, Russian Arctic, influenced by fjord geometry and sea-ice conditions. *Journal of Glaciology, 60*(219), 155-170. doi:10.3189/2014JoG13J122

Christoffersen, P., Bougamont, M., Carter, S. P., Fricker, H. A., & Tulaczyk, S. (2014). Significant groundwater contribution to Antarctic ice streams hydrologic budget. *Geophysical Research Letters, 41*(6), 2003-2010. doi:10.1002/2014gl059250

Clarke, G. K. C., Collins, S. G., & Thompson, D. E. (1984). FLOW, THERMAL STRUCTURE, AND SUBGLACIAL CONDITIONS OF A SURGE-TYPE GLACIER. *Canadian Journal of Earth Sciences, 21*(2), 232-240. doi:10.1139/e84-024

Clason, C., Mair, D. W. F., Burgess, D. O., & Nienow, P. W. (2012). Modelling the delivery of supraglacial meltwater to the ice/bed interface: application to southwest Devon Ice Cap, Nunavut, Canada. *Journal of Glaciology, 58*(208), 361-374. doi:10.3189/2012JoG11J129

Cohen, J., Screen, J. A., Furtado, J. C., Barlow, M., Whittleston, D., Coumou, D., . . . Jones, J. (2014). Recent Arctic amplification and extreme mid-latitude weather. *Nature Geoscience, 7*(9), 627-637. doi:10.1038/ngeo2234

Colgan, W., & Sharp, M. (2008). Combined oceanic and atmospheric influences on net accumulation on Devon ice cap, nunavut, Canada. *Journal of Glaciology, 54*(184), 28-40. doi:10.3189/002214308784409044

Cook, S. (2016). *Blink and You'll Miss It: An Investigation into Surging on Flade Isblink, Greenland* (unpublished MPhil dissertation). University of Cambridge, Cambridge.

Cook, S. J., & Swift, D. A. (2012). Subglacial basins: Their origin and importance in glacial systems and landscapes. *Earth-Science Reviews, 115*(4), 332-372. doi:10.1016/j.earscirev.2012.09.009

Copland, L., Sharp, M. J., & Dowdeswell, J. A. (2003a). The distribution and flow characteristics of surge-type glaciers in the Canadian High Arctic. *Annals of Glaciology, Vol 36, 36*, 73-81. doi:10.3189/172756403781816301

Copland, L., Sharp, M. J., & Dowdeswell, J. A. (2003b). The distribution and flow characteristics of surge-type glaciers in the Canadian High Arctic. *Annals of Glaciology, Vol 36, 36*, 73-81. doi:10.3189/172756403781816301

Cuffey, K. M., & Paterson, W. S. B. (2010). *The physics of glaciers*. Academic Press.

Dowdeswell, J. A., Bassford, R. P., Gorman, M. R., Williams, M., Glazovsky, A. F., Macheret, Y. Y., . . . Miller, H. (2002). Form and flow of the Academy of Sciences Ice Cap, Severnaya Zemlya, Russian High Arctic. *Journal of Geophysical Research-Solid Earth, 107*(B4), 16. doi:10.1029/2000jb000129

Dowdeswell, J. A., & Benham, T. J. (2003). A surge of Perseibreen, Svalbard, examined using aerial photography and ASTER high resolution satellite imagery. *Polar Research, 22*(2), 373-383. doi:10.1111/j.1751-8369.2003.tb00118.x

Dowdeswell, J. A., Benham, T. J., Gorman, M. R., Burgess, D., & Sharp, M. J. (2004). Form and flow of the Devon Island Ice Cap, Canadian Arctic. *Journal of Geophysical Research-Earth Surface, 109*(F2), 14. doi:10.1029/2003jf000095

Dowdeswell, J. A., & Collin, R. L. (1990). FAST-FLOWING OUTLET GLACIERS ON SVALBARD ICE CAPS. *Geology, 18*(8), 778-781. doi:10.1130/0091-7613(1990)018<0778:ffogos>2.3.co;2

Dowdeswell, J. A., Hamilton, G. S., & Hagen, J. O. (1991). THE DURATION OF THE ACTIVE PHASE ON SURGE-TYPE GLACIERS - CONTRASTS BETWEEN SVALBARD AND OTHER REGIONS. *Journal of Glaciology, 37*(127), 388-400.

Dowdeswell, J. A., Hodgkins, R., Nuttall, A. M., Hagen, J. O., & Hamilton, G. S. (1995). MASS-BALANCE CHANGE AS A CONTROL ON THE FREQUENCY AND OCCURRENCE OF GLACIER SURGES IN SVALBARD, NORWEGIAN HIGH ARCTIC. *Geophysical Research Letters, 22*(21), 2909-2912. doi:10.1029/95gl02821

Dunse, T., Schellenberger, T., Hagen, J. O., Kaab, A., Schuler, T. V., & Reijmer, C. H. (2015). Glacier-surge mechanisms promoted by a hydro-thermodynamic feedback to summer melt. *Cryosphere, 9*(1), 197-215. doi:10.5194/tc-9-197-2015

Echelmeyer, K., & Wang, Z. X. (1987). DIRECT OBSERVATION OF BASAL SLIDING AND DEFORMATION OF BASAL DRIFT AT SUB-FREEZING TEMPERATURES. *Journal of Glaciology, 33*(113), 83-98.

Eisen, O., Harrison, W. D., Raymond, C. F., Echelmeyer, K. A., Bender, G. A., & Gorda, J. L. D. (2005). Variegated Glacier, Alaska, USA: a century of surges. *Journal of Glaciology, 51*(174), 399-406. doi:10.3189/172756505781829250

Fowler, A. C., Murray, T., & Ng, F. S. L. (2001). Thermally controlled glacier surging. *Journal of Glaciology, 47*(159), 527-538. doi:10.3189/172756501781831792

Furst, J. J., Durand, G., Gillet-Chaulet, F., Merino, N., Tavard, L., Mouginot, J., . . . Gagliardini, O. (2015). Assimilation of Antarctic velocity observations provides evidence for uncharted pinning points. *Cryosphere, 9*(4), 1427-1443. doi:10.5194/tc-9-1427-2015

Gagliardini, O., Zwinger, T., Gillet-Chaulet, F., Durand, G., Favier, L., de Fleurian, B., . . . Thies, J. (2013). Capabilities and performance of Elmer/Ice, a new-generation ice sheet model. *Geoscientific Model Development, 6*(4), 1299-1318. doi:10.5194/gmd-6-1299-2013

Gardner, A. S., Moholdt, G., Cogley, J. G., Wouters, B., Arendt, A. A., Wahr, J., . . . Paul, F. (2013). A Reconciled Estimate of Glacier Contributions to Sea Level Rise: 2003 to 2009. *Science, 340*(6134), 852-857. doi:10.1126/science.1234532

Gardner, A. S., Moholdt, G., Wouters, B., Wolken, G. J., Burgess, D. O., Sharp, M. J., . . . Labine, C. (2011). Sharply increased mass loss from glaciers and ice caps in the Canadian Arctic Archipelago. *Nature, 473*(7347), 357-360. doi:10.1038/nature10089

Gardner, A. S., & Sharp, M. (2007). Influence of the arctic circumpolar vortex on the mass balance of Canadian High Arctic glaciers. *Journal of Climate, 20*(18), 4586-4598. doi:10.1175/jcli4268.1

Gardner, A. S., & Sharp, M. (2009). Sensitivity of net mass-balance estimates to near-surface temperature lapse rates when employing the degree-day method to estimate glacier melt. *Annals of Glaciology, 50*(50), 80-86.

Gilbert, A., Flowers, G. E., Miller, G. H., Rabus, B. T., Van Wychen, W., Gardner, A. S., & Copland, L. (2016). Sensitivity of Barnes Ice Cap, Baffin Island, Canada, to climate state and internal dynamics. *Journal of Geophysical Research-Earth Surface, 121*(8), 1516-1539. doi:10.1002/2016jf003839

Gilbert, J. C., & Lemarechal, C. (1989). SOME NUMERICAL EXPERIMENTS WITH VARIABLE-STORAGE QUASI-NEWTON ALGORITHMS. *Mathematical Programming, 45*(3), 407-435. doi:10.1007/bf01589113

Gillet-Chaulet, F., Durand, G., Gagliardini, O., Mosbeux, C., Mouginot, J., Remy, F., & Ritz, C. (2016). Assimilation of surface velocities acquired between 1996 and 2010 to constrain the form of the basal friction law under Pine Island Glacier. *Geophysical Research Letters, 43*(19), 10311-10321. doi:10.1002/2016gl069937

Gillet-Chaulet, F., Gagliardini, O., Seddik, H., Nodet, M., Durand, G., Ritz, C., . . . Vaughan, D. G. (2012). Greenland ice sheet contribution to sea-level rise from a new-generation ice-sheet model. *Cryosphere, 6*(6), 1561-1576. doi:10.5194/tc-6-1561-2012

Gladstone, R., Schafer, M., Zwinger, T., Gong, Y., Strozzi, T., Mottram, R., . . . Moore, J. C. (2014). Importance of basal processes in simulations of a surging Svalbard outlet glacier. *Cryosphere, 8*(4), 1393-1405. doi:10.5194/tc-8-1393-2014

Glen, J. W. (1955). THE CREEP OF POLYCRYSTALLINE ICE. *Proceedings of the Royal Society of London Series a-Mathematical and Physical Sciences, 228*(1175), 519-538. doi:10.1098/rspa.1955.0066

Golub, G. H., Hansen, P. C., & O'Leary, D. P. (1999). Tikhonov regularization and total least squares. *Siam Journal on Matrix Analysis and Applications, 21*(1), 185-194. doi:10.1137/s0895479897326432

Gong, Y., Zwinger, T., Cornford, S., Gladstone, R., Schafer, M., & Moore, J. C. (2017). Importance of basal boundary conditions in transient simulations: case study of a surging marine-terminating glacier on Austfonna, Svalbard. *Journal of Glaciology, 63*(237), 106-117. doi:10.1017/jog.2016.121

Greve, R. (1997). Application of a polythermal three-dimensional ice sheet model to the Greenland Ice Sheet: Response to steady-state and transient climate scenarios. *Journal of Climate, 10*(5), 901-918. doi:10.1175/1520-0442(1997)010<0901:aoaptd>2.0.co;2

Habermann, M., Truffer, M., & Maxwell, D. (2013). Changing basal conditions during the speed-up of Jakobshavn Isbrae, Greenland. *Cryosphere, 7*(6), 1679-1692. doi:10.5194/tc-7-1679-2013

Hansen, P. C. (1999). *The L-curve and its use in the numerical treatment of inverse problems*. IMM, Department of Mathematical Modelling, Technical University of Denmark.

Herdes, E., Copland, L., Danielson, B., & Sharp, M. (2012). Relationships between iceberg plumes and sea-ice conditions on northeast Devon Ice Cap, Nunavut, Canada. *Annals of Glaciology, 53*(60), 1-9. doi:10.3189/2012AoG60A163

Hock, R., de Woul, M., Radic, V., & Dyurgerov, M. (2009). Mountain glaciers and ice caps around Antarctica make a large sea-level rise contribution. *Geophysical Research Letters, 36*, 5. doi:10.1029/2008gl037020

Hooke, R. L. (1981). FLOW LAW FOR POLYCRYSTALLINE ICE IN GLACIERS - COMPARISON OF THEORETICAL PREDICTIONS, LABORATORY DATA, AND FIELD-MEASUREMENTS. *Reviews of Geophysics, 19*(4), 664-672.

Howat, I. M., Joughin, I., Fahnestock, M., Smith, B. E., & Scambos, T. A. (2008). Synchronous retreat and acceleration of southeast Greenland outlet glaciers 2000-06: ice dynamics and coupling to climate. *Journal of Glaciology, 54*(187), 646-660. doi:10.3189/002214308786570908

Jay-Allemand, M., Gillet-Chaulet, F., Gagliardini, O., & Nodet, M. (2011). Investigating changes in basal conditions of Variegated Glacier prior to and during its 1982-1983 surge. *Cryosphere, 5*(3), 659-672. doi:10.5194/tc-5-659-2011

Jiskoot, H., Murray, T., & Boyle, P. (2000). Controls on the distribution of surge-type glaciers in Svalbard. *Journal of Glaciology, 46*(154), 412-422. doi:10.3189/172756500781833115

Joughin, I., Alley, R. B., & Holland, D. M. (2012). Ice-Sheet Response to Oceanic Forcing. *Science, 338*(6111), 1172-1176. doi:10.1126/science.1226481

Kamb, B. (1991). RHEOLOGICAL NONLINEARITY AND FLOW INSTABILITY IN THE DEFORMING BED MECHANISM OF ICE STREAM MOTION. *Journal of Geophysical Research-Solid Earth, 96*(B10), 16585-16595. doi:10.1029/91jb00946

Kamb, B., Raymond, C. F., Harrison, W. D., Engelhardt, H., Echelmeyer, K. A., Humphrey, N., . . . Pfeffer, T. (1985). GLACIER SURGE MECHANISM - 1982-1983 SURGE OF VARIEGATED GLACIER, ALASKA. *Science, 227*(4686), 469-479. doi:10.1126/science.227.4686.469

Kavanaugh, J. L., & Clarke, G. K. C. (2006). Discrimination of the flow law for subglacial sediment using in situ measurements and an interpretation model. *Journal of Geophysical Research-Earth Surface, 111*(F1), 20. doi:10.1029/2005jf000346

Keeler, C. M. (1964). *Relationship between climate, ablation, and run-off on the Sverdrup Glacier: 1963, Devon Island, NWT* (No. 27). Arctic Institute of North America.

Khazendar, A., Borstad, C. P., Scheuchl, B., Rignot, E., & Seroussi, H. (2015). The evolving instability of the remnant Larsen B Ice Shelf and its tributary glaciers. *Earth and Planetary Science Letters, 419*, 199-210. doi:10.1016/j.eps1.2015.03.014

Koerner, R., & Russell, R. D. (1979). DELTA-O-18 VARIATIONS IN SNOW ON THE DEVON ISLAND ICE CAP, NORTHWEST-TERRITORIES, CANADA. *Canadian Journal of Earth Sciences, 16*(7), 1419-1427. doi:10.1139/e79-126

Koerner, R. M. (1966). Accumulation on the Devon Island ice cap, Northwest Territories, Canada. *Journal of Glaciology*, *6*(45), 383-392.

Koerner, R. M. (1977). Devon Island ice cap: core stratigraphy and paleoclimate. *Science*, *196*(4285), 15-18.

Koerner, R. M. (2005). Mass balance of glaciers in the Queen Elizabeth Islands, Nunavut, Canada. *Annals of Glaciology, Vol 42, 2005, 42*, 417-423. doi:10.3189/172756405781813122

Konovalov, Y. V., & Nagornov, O. V. (2015). Two-dimensional prognostic experiments for fast-flowing ice streams from the Academy of Sciences Ice Cap: future modeled histories obtained for the reference surface mass balance. *Earth System Dynamics Discussions*, *6*(2).

Krabill, William B. (2014), updated 2016. *IceBridge ATM L4 Surface Elevation Rate of Change*, [Canada]. Boulder, Colorado USA: NASA DAAC at the National Snow and Ice Data Center. http://dx.doi.org/10.5067/BCW6CI3TXOCY. [20/05/16].

Lenaerts, J. T. M., van Angelen, J. H., van den Broeke, M. R., Gardner, A. S., Wouters, B., & van Meijgaard, E. (2013). Irreversible mass loss of Canadian Arctic Archipelago glaciers. *Geophysical Research Letters, 40*(5), 870-874. doi:10.1002/grl.50214

Lliboutry, L. (1968). General theory of subglacial cavitation and sliding of temperate glaciers. *Journal of Glaciology*, *7*(49), 21-58.

Luckman, A., Murray, T., & Strozzi, T. (2002). Surface flow evolution throughout a glacier surge measured by satellite radar interferometry. *Geophysical Research Letters, 29*(23), 4. doi:10.1029/2001gl014570

Macayeal, D. R. (1992). THE BASAL STRESS-DISTRIBUTION OF ICE STREAM-E, ANTARCTICA, INFERRED BY CONTROL METHODS. *Journal of Geophysical Research-Solid Earth, 97*(B1), 595-603. doi:10.1029/91jb02454

Macayeal, D. R. (1993). A TUTORIAL ON THE USE OF CONTROL METHODS IN ICE-SHEET MODELING. *Journal of Glaciology, 39*(131), 91-98.

Mair, D., Burgess, D., & Sharp, M. (2005). Thirty-seven year mass balance of Devon Ice Cap, Nunavut, Canada, determined by shallow ice coring and melt modeling. *Journal of Geophysical Research-Earth Surface, 110*(F1), 13. doi:10.1029/2003jf000099

Majorowicz, J. A., & Embry, A. F. (1998). Present heat flow and paleo-geothermal regime in the Canadian Arctic margin: analysis of industrial thermal data and coalification gradients. *Tectonophysics, 291*(1-4), 141-159. doi:10.1016/s0040-1951(98)00036-5

Mansell, D., Luckman, A., & Murray, T. (2012). Dynamics of tidewater surge-type glaciers in northwest Svalbard. *Journal of Glaciology, 58*(207), 110-118. doi:10.3189/2012JoG11J058

Markham, Clements R. *The Voyages of William Baffin, 1612-1622* (Vol. 63). London: Printed for The Hakluyt Society.

McMillan, M., Shepherd, A., Gourmelen, N., Dehecq, A., Leeson, A., Ridout, A., . . . Strozzi, T. (2014). Rapid dynamic activation of a marine-based Arctic ice cap. *Geophysical Research Letters, 41*(24), 8902-8909. doi:10.1002/2014gl062255

Millan, R., Mouginot, J., & Rignot, E. (2017). Mass budget of the glaciers and ice caps of the Queen Elizabeth Islands, Canada, from 1991 to 2015. *Environmental Research Letters*, *12*(2), 024016.

Mills, W. J. (2003). *Exploring polar frontiers: a historical encyclopedia* (Vol. 1). ABC-CLIO.

Minchew, B., Simons, M., Bjornsson, H., Palsson, F., Morlighem, M., Seroussi, H., . . . Hensley, S. (2016). Plastic bed beneath Hofsjokull Ice Cap, central Iceland, and the sensitivity of ice flow to surface meltwater flux. *Journal of Glaciology, 62*(231), 147-158. doi:10.1017/jog.2016.26

Moholdt, G., Heid, T., Benham, T., & Dowdeswell, J. A. (2012). Dynamic instability of marine-terminating glacier basins of Academy of Sciences Ice Cap, Russian High Arctic. *Annals of Glaciology, 53*(60), 193-201. doi:10.3189/2012AoG60A117

Morlighem, M., Rignot, E., Seroussi, H., Larour, E., Ben Dhia, H., & Aubry, D. (2010). Spatial patterns of basal drag inferred using control methods from a full-Stokes and simpler models for Pine Island Glacier, West Antarctica. *Geophysical Research Letters, 37*, 6. doi:10.1029/2010gl043853

Morlighem, M., Rignot, E., Seroussi, H., Larour, E., Ben Dhia, H., & Aubry, D. (2011). A mass conservation approach for mapping glacier ice thickness. *Geophysical Research Letters, 38*, 6. doi:10.1029/2011gl048659

Mosbeux, C., Gillet-Chaulet, F., & Gagliardini, O. (2016). Comparison of adjoint and nudging methods to initialise ice sheet model basal conditions. *Geoscientific Model Development, 9*(7), 2549-2562. doi:10.5194/gmd-9-2549-2016

Murray, T. (1997). Assessing the paradigm shift: Deformable glacier beds. *Quaternary Science Reviews, 16*(9), 995-1016. doi:10.1016/s0277-3791(97)00030-9

Murray, T., James, T. D., Macheret, Y., Lavrentiev, I., Glazovsky, A., & Sykes, H. (2012). Geometric Changes in a Tidewater Glacier in Svalbard during its Surge Cycle. *Arctic Antarctic and Alpine Research, 44*(3), 359-367. doi:10.1657/1938-4246-44.3.359

Murray, T., & Porter, P. R. (2001). Basal conditions beneath a soft-bedded polythermal surge-type glacier: Bakaninbreen, Svalbard. *Quaternary International, 86*, 103-116. doi:10.1016/s1040-6182(01)00053-2

Murray, T., Strozzi, T., Luckman, A., Jiskoot, H., & Christakos, P. (2003). Is there a single surge mechanism? Contrasts in dynamics between glacier surges in Svalbard and other regions. *Journal of Geophysical Research-Solid Earth, 108*(B5), 15. doi:10.1029/2002jb001906

Murray, T., Stuart, G. W., Miller, P. J., Woodward, J., Smith, A. M., Porter, P. R., & Jiskoot, H. (2000). Glacier surge propagation by thermal evolution at the bed. *Journal of Geophysical Research-Solid Earth, 105*(B6), 13491-13507. doi:10.1029/2000jb900066

Nick, F. M., Vieli, A., Howat, I. M., & Joughin, I. (2009). Large-scale changes in Greenland outlet glacier dynamics triggered at the terminus. *Nature Geoscience, 2*(2), 110-114. doi:10.1038/ngeo394

Nickling, W. G., & Bennett, L. (1984). THE SHEAR-STRENGTH CHARACTERISTICS OF FROZEN COARSE GRANULAR DEBRIS. *Journal of Glaciology, 30*(106), 348-357.

Nye, J. F. (1957). THE DISTRIBUTION OF STRESS AND VELOCITY IN GLACIERS AND ICE-SHEETS. *Proceedings of the Royal Society of London Series a-Mathematical and Physical Sciences, 239*(1216), 113-133. doi:10.1098/rspa.1957.0026

Nye, J. F. (1976). Water flow in glaciers: jökulhlaups, tunnels and veins. *Journal of Glaciology*, *17*(76), 181-207.

O'Leary, M., & Christoffersen, P. (2013). Calving on tidewater glaciers amplified by submarine frontal melting. *Cryosphere, 7*(1), 119-128. doi:10.5194/tc-7-119-2013

Paterson, W. S. B. (1977). SECONDARY AND TERTIARY CREEP OF GLACIER ICE AS MEASURED BY BOREHOLE CLOSURE RATES. *Reviews of Geophysics, 15*(1), 47-55. doi:10.1029/RG015i001p00047

Paterson, W. S. B., & Clarke, G. K. C. (1978). COMPARISON OF THEORETICAL AND OBSERVED TEMPERATURE PROFILES IN DEVON ISLAND ICE CAP, CANADA. *Geophysical Journal of the Royal Astronomical Society, 55*(3), 615-632. doi:10.1111/j.1365-246X.1978.tb05931.x

Paterson, W. S. B., Koerner, R. M., Fisher, D., Johnsen, S. J., Clausen, H. B., Dansgaard, W., . . . Oeschger, H. (1977). AN OXYGEN-ISOTOPE CLIMATIC RECORD FROM DEVON ISLAND ICE CAP, ARCTIC CANADA. *Nature, 266*(5602), 508-511. doi:10.1038/266508a0

Pattyn, F. (2003). A new three-dimensional higher-order thermomechanical ice sheet model: Basic sensitivity, ice stream development, and ice flow across subglacial lakes. *Journal of Geophysical Research-Solid Earth, 108*(B8), 15. doi:10.1029/2002jb002329

Pattyn, F., Perichon, L., Aschwanden, A., Breuer, B., de Smedt, B., Gagliardini, O., . . . Zwinger, T. (2008). Benchmark experiments for higher-order and full-Stokes ice sheet models (ISMIP-HOM). *Cryosphere, 2*(2), 95-108. doi:10.5194/tc-2-95-2008

Perry, T. (2014). *Flow Characteristics, Setting, and Basal Boundary Condition of North Greenland Outlet Glaciers* (unpublished MPhil dissertation). University of Cambridge, Cambridge.

Petra, N., Martin, J., Stadler, G., & Ghattas, O. (2014). A COMPUTATIONAL FRAMEWORK FOR INFINITE-DIMENSIONAL BAYESIAN INVERSE PROBLEMS, PART II: STOCHASTIC NEWTON MCMC WITH APPLICATION TO ICE SHEET FLOW INVERSE PROBLEMS. *Siam Journal on Scientific Computing, 36*(4), A1525-A1555. doi:10.1137/130934805

Petra, N., Zhu, H. Y., Stadler, G., Hughes, T. J. R., & Ghattas, O. (2012). An inexact Gauss-Newton method for inversion of basal sliding and rheology parameters in a nonlinear Stokes ice sheet model. *Journal of Glaciology, 58*(211), 889-903. doi:10.3189/2012JoG11J182

Pfeffer, W. T., Arendt, A. A., Bliss, A., Bolch, T., Cogley, J. G., Gardner, A. S., . . . Randolph, C. (2014). The Randolph Glacier Inventory: a globally complete inventory of glaciers. *Journal of Glaciology, 60*(221), 537-552. doi:10.3189/2014JoG13J176

Pfeffer, W. T., Harper, J. T., & O'Neel, S. (2008). Kinematic constraints on glacier contributions to 21st-century sea-level rise. *Science, 321*(5894), 1340-1343. doi:10.1126/science.1159099

Phillips, T., Rajaram, H., Colgan, W., Steffen, K., & Abdalati, W. (2013). Evaluation of cryo-hydrologic warming as an explanation for increased ice velocities in the wet snow zone, Sermeq Avannarleq, West Greenland. *Journal of Geophysical Research-Earth Surface, 118*(3), 1241-1256. doi:10.1002/jgrf.20079

Phillips, T., Rajaram, H., & Steffen, K. (2010). Cryo-hydrologic warming: A potential mechanism for rapid thermal response of ice sheets. *Geophysical Research Letters, 37*, 5. doi:10.1029/2010gl044397

Radic, V., & Hock, R. (2010). Regional and global volumes of glaciers derived from statistical upscaling of glacier inventory data. *Journal of Geophysical Research-Earth Surface, 115*, 10. doi:10.1029/2009jf001373

Radic, V., & Hock, R. (2011). Regionally differentiated contribution of mountain glaciers and ice caps to future sea-level rise. *Nature Geoscience, 4*(2), 91-94. doi:10.1038/ngeo1052

Raper, S. C. B., & Braithwaite, R. J. (2006). Low sea level rise projections from mountain glaciers and icecaps under global warming. *Nature, 439*(7074), 311-313. doi:10.1038/nature04448

Raymond, M. J., & Gudmundsson, G. H. (2009). Estimating basal properties of ice streams from surface measurements: a non-linear Bayesian inverse approach applied to synthetic data. *Cryosphere, 3*(2), 265-278. doi:10.5194/tc-3-265-2009

Rinne, E., Shepherd, A., Muir, A., & Wingham, D. (2011). A Comparison of Recent Elevation Change Estimates of the Devon Ice Cap as Measured by the ICESat and EnviSAT Satellite Altimeters. *Ieee Transactions on Geoscience and Remote Sensing, 49*(6), 1902-1910. doi:10.1109/tgrs.2010.2096472

Röthlisberger, H. (1972). Water pressure in intra-and subglacial channels. *Journal of Glaciology*, *11*(62), 177-203.

Schafer, M., Gillet-Chaulet, F., Gladstone, R., Pettersson, R., Pohjola, V. A., Strozzi, T., & Zwinger, T. (2014). Assessment of heat sources on the control of fast flow of Vestfonna ice cap, Svalbard. *Cryosphere, 8*(5), 1951-1973. doi:10.5194/tc-8-1951-2014

Schafer, M., Moller, M., Zwinger, T., & Moore, J. C. (2015). Dynamic modelling of future glacier changes: mass-balance/elevation feedback in projections for the Vestfonna ice cap, Nordaustlandet, Svalbard. *Journal of Glaciology, 61*(230), 1121-1136. doi:10.3189/2015JoG14J184

Schafer, M., Zwinger, T., Christoffersen, P., Gillet-Chaulet, F., Laakso, K., Pettersson, R., . . . Moore, J. C. (2012). Sensitivity of basal conditions in an inverse model: Vestfonna ice cap, Nordaustlandet/Svalbard. *Cryosphere, 6*(4), 771-783. doi:10.5194/tc-6-771-2012

Schoof, C. (2010). Ice-sheet acceleration driven by melt supply variability. *Nature, 468*(7325), 803-806. doi:10.1038/nature09618

Seroussi, H., Morlighem, M., Rignot, E., Larour, E., Aubry, D., Ben Dhia, H., & Kristensen, S. S. (2011). Ice flux divergence anomalies on 79north Glacier, Greenland. *Geophysical Research Letters, 38*, 5. doi:10.1029/2011gl047338

Sevestre, H., & Benn, D. I. (2015). Climatic and geometric controls on the global distribution of surge-type glaciers: implications for a unifying model of surging. *Journal of Glaciology, 61*(228), 646-662. doi:10.3189/2015j0g14j136

Sevestre, H., Benn, D. I., Hulton, N. R. J., & Baelum, K. (2015). Thermal structure of Svalbard glaciers and implications for thermal switch models of glacier surging. *Journal of Geophysical Research-Earth Surface, 120*(10), 2220-2236. doi:10.1002/2015jf003517

Shannon, S. R., Payne, A. J., Bartholomew, I. D., van den Broeke, M. R., Edwards, T. L., Fettweis, X., . . . Zwinger, T. (2013). Enhanced basal lubrication and the contribution of the Greenland ice sheet to

future sea-level rise. *Proceedings of the National Academy of Sciences of the United States of America, 110*(35), 14156-14161. doi:10.1073/pnas.1212647110

Shapero, D. R., Joughin, I. R., Poinar, K., Morlighem, M., & Gillet-Chaulet, F. (2016). Basal resistance for three of the largest Greenland outlet glaciers. *Journal of Geophysical Research-Earth Surface, 121*(1), 168-180. doi:10.1002/2015jf003643

Sharp, M. (1988). SURGING GLACIERS - BEHAVIOR AND MECHANISMS. *Progress in Physical Geography, 12*(3), 349-370. doi:10.1177/030913338801200302

Sharp, M., Burgess, D. O., Cogley, J. G., Ecclestone, M., Labine, C., & Wolken, G. J. (2011). Extreme melt on Canada's Arctic ice caps in the 21st century. *Geophysical Research Letters, 38*, 5. doi:10.1029/2011gl047381

Shepherd, A., Du, Z. J., Benham, T. J., Dowdeswell, J. A., & Morris, E. M. (2007). Mass balance of Devon ice cap, Canadian arctic. *Annals of Glaciology, Vol 46, 2007, 46*, 249-+. doi:10.3189/172756407782871279

Sobota, I., Weckwerth, P., & Nowak, M. (2016). Surge dynamics of Aavatsmarkbreen, Svalbard, inferred from the geomorphological record. *Boreas, 45*(2), 360-376. doi:10.1111/bor.12160

Sund, M., Eiken, T., Hagen, J. O., & Kaab, A. (2009). Svalbard surge dynamics derived from geometric changes. *Annals of Glaciology, 50*(52), 50-60.

Sundal, A. V., Shepherd, A., Nienow, P., Hanna, E., Palmer, S., & Huybrechts, P. (2011). Melt-induced speed-up of Greenland ice sheet offset by efficient subglacial drainage. *Nature*, *469*(7331), 521-524.

Tikhonov, A. N., & Arsenin, V. I. (1977). *Solutions of ill-posed problems* (Vol. 14). Washington, DC: Winston.

Todd, J., & Christoffersen, P. (2014). Are seasonal calving dynamics forced by buttressing from ice melange or undercutting by melting? Outcomes from full-Stokes simulations of Store Glacier, West Greenland. *Cryosphere, 8*(6), 2353-2365. doi:10.5194/tc-8-2353-2014

Tulaczyk, S., Kamb, W. B., & Engelhardt, H. F. (2000a). Basal mechanics of Ice Stream B, West Antarctica 1. Till mechanics. *Journal of Geophysical Research-Solid Earth, 105*(B1), 463-481. doi:10.1029/1999jb900329

Tulaczyk, S., Kamb, W. B., & Engelhardt, H. F. (2000b). Basal mechanics of Ice Stream B, West Antarctica 2. Undrained plastic bed model. *Journal of Geophysical Research-Solid Earth, 105*(B1), 483-494. doi:10.1029/1999jb900328

Turrin, J. B., Forster, R. R., Sauber, J. M., Hall, D. K., & Bruhn, R. L. (2014). Effects of bedrock lithology and subglacial till on the motion of Ruth Glacier, Alaska, deduced from five pulses from 1973 to 2012. *Journal of Glaciology, 60*(222), 771-781. doi:10.3189/2014JoG13J182

van der Veen, C. J. (2002). Calving glaciers. *Progress in Physical Geography, 26*(1), 96-122. doi:10.1191/0309133302pp327ra

van Pelt, W. J. J., Oerlemans, J., Reijmer, C. H., Pettersson, R., Pohjola, V. A., Isaksson, E., & Divine, D. (2013). An iterative inverse method to estimate basal topography and initialize ice flow models. *Cryosphere, 7*(3), 987-1006. doi:10.5194/tc-7-987-2013

Van Wychen, W., Burgess, D. O., Gray, L., Copland, L., Sharp, M., Dowdeswell, J. A., & Benham, T. J. (2014). Glacier velocities and dynamic ice discharge from the Queen Elizabeth Islands, Nunavut, Canada. *Geophysical Research Letters, 41*(2), 484-490. doi:10.1002/2013gl058558

Van Wychen, W., Copland, L., Burgess, D. O., Gray, L., & Schaffer, N. (2015). Glacier velocities and dynamic discharge from the ice masses of Baffin Island and Bylot Island, Nunavut, Canada. *Canadian Journal of Earth Sciences, 52*(11), 980-989. doi:10.1139/cjes-2015-0087

Van Wychen, W., Copland, L., Gray, L., Burgess, D., Danielson, B., & Sharp, M. (2012). Spatial and temporal variation of ice motion and ice flux from Devon Ice Cap, Nunavut, Canada. *Journal of Glaciology, 58*(210), 657-664. doi:10.3189/2012JoG11J164

Van Wychen, W., Davis, J., Burgess, D. O., Copland, L., Gray, L., Sharp, M., & Mortimer, C. (2016). Characterizing interannual variability of glacier dynamics and dynamic discharge (1999-2015) for the ice masses of Ellesmere and Axel Heiberg Islands, Nunavut, Canada. *Journal of Geophysical Research-Earth Surface, 121*(1), 39-63. doi:10.1002/2015jf003708

Van Wychen, W., Davis, J., Copland, L., Burgess, D. O., Gray, L., Sharp, M., ... & Benham, T. J. (2017). Variability in ice motion and dynamic discharge from Devon Ice Cap, Nunavut, Canada. *Journal of Glaciology*, *63*(239), 436-449.

Van der veen, C. J., & Whillans, I. M. (1989). FORCE BUDGET .1. THEORY AND NUMERICAL-METHODS. *Journal of Glaciology, 35*(119), 53-60. doi:10.3189/002214389793701581

van der Vorst, H. A. (1992). BI-CGSTAB - A FAST AND SMOOTHLY CONVERGING VARIANT OF BI-CG FOR THE SOLUTION OF NONSYMMETRIC LINEAR-SYSTEMS. *Siam Journal on Scientific and Statistical Computing, 13*(2), 631-644. doi:10.1137/0913035

Walder, J. S. (1986). HYDRAULICS OF SUBGLACIAL CAVITIES. *Journal of Glaciology, 32*(112), 439-445.

Weertman, J. (1957). On the sliding of glaciers. *Journal of Glaciology*, *3*(21), 33-38.

Weertman, J. (1973). CLOSURE RATES EXPECTED FOR A ROSS ICE-SHELF DRILL HOLE AT 166 DEGREES 82 DEGREES 30'S. *Antarctic Journal of the United States, 8*(5), 310-310.

Weertman, J. (1983). CREEP DEFORMATION OF ICE. *Annual Review of Earth and Planetary Sciences, 11*, 215-240. doi:10.1146/annurev.ea.11.050183.001243

Wyatt, F. R., & Sharp, M. J. (2015). Linking surface hydrology to flow regimes and patterns of velocity variability on Devon Ice Cap, Nunavut. *Journal of Glaciology, 61*(226), 387-399. doi:10.3189/2015JoG14J109

Zhang, S. X., Mirza, K., & Barnes, C. R. (2016). Upper Ordovician - Upper Silurian conodont biostratigraphy, Devon Island and southern Ellesmere Island, Canadian Arctic Islands, with implications for regional stratigraphy, eustasy, and thermal maturation. *Canadian Journal of Earth Sciences, 53*(9), 931-949. doi:10.1139/cjes-2016-0002

Zwally, H. J., Abdalati, W., Herring, T., Larson, K., Saba, J., & Steffen, K. (2002). Surface melt-induced acceleration of Greenland ice-sheet flow. *Science, 297*(5579), 218-222. doi:10.1126/science.1072708

Zwinger, T., & Moore, J. C. (2009). Diagnostic and prognostic simulations with a full Stokes model accounting for superimposed ice of Midtre Lovenbreen, Svalbard. *Cryosphere, 3*(2), 217-229.